

https://dspace.org/

An investigation into high gear and low gear propulsion in human gait and its relation to metatarsal diaphyseal geometric cross-sectional properties

Reyneker, Mark Brenden

2023-06
University of the Witwatersrand, Johannesburg
https://hdl.handle.net/10539/41904

Reyneker, Mark Brenden. (2023). An investigation into high gear and low gear propulsion in human gait and its relation to metatarsal diaphyseal geometric cross-sectional properties. [Master's dissertation, University of the Witwatersrand, Johannesburg]. https://hdl.handle.net/10539/41904

Downloaded from a DSpace repository. https://dspace.org/



An investigation into high gear and low gear propulsion in human gait and its relation to metatarsal diaphyseal geometric cross-sectional properties.

by

Mark B. Reyneker

(1588048)

Dissertation

Submitted in fulfilment of the requirements for the degree

MSc in **Palaeontology**

in the Faculty of Science, University of the Witwatersrand, Johannesburg, South Africa

Supervisor:

Dr. Bernhard Zipfel

Co-supervisor:

Prof. Kristian J. Carlson

October 2022

ABSTRACT

This study investigates the relationship between metatarsal bone form, as quantified by cross-sectional geometric properties, and its relationship to high (medial forefoot loading) versus low gear (lateral forefoot loading) push-off during the propulsion phase of the gait cycle. The objective being to assess whether forefoot loading may be variable or whether high gear loading occurs in higher frequencies, as depicted in theoretical foot function models. The study sample (n=53), made up of three broad groups, include Later Stone Age southern Africans, post-industrial individuals from South Africa, and the Jomon of Japan. Metatarsals 1-5 cross-sectional geometric properties (CSA, I_x, I_y, I_{min}, I_{max}, Z_x, Z_y, Z_p, Z_{min}, Z_{max}) taken from CT scans at 25%, 35%, 50% and 65% metatarsal diaphyseal biomechanical lengths are grouped into high gear (metatarsal 1-2) and low gear (metatarsal 2-5) for comparison. The combined population analysis reveals that the high gear metatarsal diaphysis exhibit significantly higher strength and rigidity driven mainly by the post-industrial individuals from South Africa and the Later Stone Age southern Africans. In contrast, the Jomon of Japan, exhibit no significant differences between high and low gear metatarsals except for CSA, $I_{max,}$ and Z_{max}. Furthermore, metatarsal 1 and 5 differ far less in cross-sectional geometric properties in the Jomon of Japan compared to the other populations except for medial-lateral strength (Zy) and torsional and average bending strength (Zp) where metatarsal 5 is significantly higher. The study findings indicate that forefoot loading demonstrates variability during the propulsion phase of gait, while also suggesting a higher frequency of occurrence for high gear push-off. This challenges current theoretical models of foot function that emphasise high gear push-off as typical and normal for striding bipedalism.

DECLARATION

I, Mark B. Reyneker, declare that this dissertation, titled an investigation into high gear and low gear propulsion in human gait and its relation to metatarsal diaphyseal geometric cross-sectional properties, submitted for the degree of Masters of Palaeontology at the University of the Witwatersrand, is entirely my original work, except where otherwise acknowledged. I affirm that this work has not been submitted in whole or in part for any other degree or qualification at this or any other university.

I further declare that:

- Any external sources of information used in this thesis, including text, figures, tables, or data, have been appropriately acknowledged and referenced.
- All contributions made by other individuals or organizations to this research have been duly acknowledged.
- There was no conflict of interest, to my knowledge, that may have influenced the research or its outcomes.
- All ethical guidelines and protocols for human samples have been followed during this research.

Signed: 

Mark B. Reyneker Date: 26 June 2023

ACKNOWLEDGEMENTS

I acknowledge the unwearied support of my supervisors Dr Bernhard Zipfel and Prof. Kristian J. Carlson through all the struggles that the COVID-19 pandemic created. The sympathy displayed by the Post-graduate Supervisory Committee of the Evolutionary Studies Institute, University of the Witwatersrand, South Africa, by allowing me extra time to complete my dissertation. Dr Tea Jashashvili for kindly teaching me how to use the Avizo software. Dr Jean-Sebastien Gounot of the Genome Institute of Singapore for his assistance with the statistical analysis. Dr Brendon Billings of the School of Anatomical Sciences, University of the Witwatersrand for access to The Raymond A. Dart Collection. Dr Gen Suwa of The Department of Anthropology and Prehistory at The University Museum, The Museum Tokyo, for access to skeletal material belonging to the Jomon populations of Japan. The National Museum of Bloemfontein for access to the Late Stone Age southern African skeletal material in the Archaeological Human Skeletal Collection. The National Research Foundation (NRF) for making it possible for my supervisor Dr Bernhard Zipfel to visit and approve of my research facility in Malaysia. I am grateful to the African Origins Platform (grant number AOP150926143039 through K. Carlson and B. Zipfel) for funding the acquisition of the Japanese human remains. Most importantly, my wife Shiori and daughter Skyla who never objected to me working late at night and while on holiday.

TABLE OF CONTENTS

ABSTRACT ii
DECLARATION vi
ACKNOWLEDGEMENTS iviii
LIST OF ABBREVIATIONS viii

CHAPTER 1 – INTRODUCTION 1
1.1 Bone form 1
1.2 Cross-sectional bone geometry 5
1.3 High gear and low gear push-off 6
1.4 Objectives 14
1.5 Hypothesis 14
CHAPTER 2 – MATERIALS AND METHODS 15
2.1 Materials 15
2.1.1 The metatarsal sample 15
2.1.1.1 Post-industrial individuals from South Africa 16
2.1.1.2 Later Stone Age southern Africans 18
2.1.1.3 The Jomon of Japan 20
2.1.2 Computed Tomography (CT) scanning equipment 23
2.1.3 Bone 3D rendering and alignment software 23
2.1.4 Bone cross section analyses software 24
2.2 Methods 24
2.2.1 Computed tomography (CT) scanning 24
2.2.2 Metatarsal three-dimensional rendering and alignment 25
2.3 Analyses 32
2.3.1 Standardisation procedures 32
2.3.2 Statistical analyses 32
CHAPTER 3 – RESULTS 34
3.1 Combined population metatarsal diaphyseal CSGPs 34
3.2 High gear and low gear metatarsal diaphyseal CSGPs 36
3.3 Individual metatarsal diaphyseal CSGPs 39
3.3.1 Metatarsal diaphyseal rigidity 39
3.3.2 Metatarsal diaphyseal strength 39
3.3.3 Metatarsal diaphyseal shape ratio 40
CHAPTER 4 – DISCUSSION AND CONCLUSIONS 42
4.1 Discussion 42
4.2 Conclusions 48

REFERENCE LIST 49
APPENDIX A – METATARSAL SAMPLE BIOMECHANICAL LENGTHS 66
APPENDIX B – METATARSAL CROSS-SECTIONAL GEOMETRIC PROPERTY SOURCE DATA 72
APPENDIX C – METATARSAL SAMPLE CROSS-SECTIONAL OUTLINES 74

LIST OF TABLES

Table 2. 1: Description of the post-industrial humans from South Africa. 17
Table 2. 2: Post-industrial humans from South Africa 18
Table 2. 3: LSA foragers from South Africa 19
Table 2. 4: Description of the LSA Southern Africans 20
Table 2. 5: Description of the Jomon of Japan 21
Table 2. 6: The Jomon of Japan derived geographically from the Pacific Coast of Honshu 22
Table 2. 7: Description of cross-sectional geometric properties. 31

LIST OF FIGURES

Figure 1. 1. An example of bone cross section reshaping by modelling resulting in an increase in bending stiffness……. 2
Figure 1. 2. An example of bone cross section reshaping by modelling due to menopausal bone loss rather than altered mechanical loading. 3
Figure 1. 3. A Force-Time graph of a modern human gait cycle demonstrating vertical ground reaction forces, in Newtons, and time in percentage of a single leg gait cycle. 7
Figure 1. 4. Illustrates the transverse metatarsal axis (solid line) formed by MH1 and MH2 and the oblique axis (dotted line) formed by MH2 to MH5. 8
Figure 1. 5. Schematic windlass mechanism superimposed on a cadaveric specimen displaying the windlass phenomenon……..……11
Figure 2. 1. Materials and methods workflow summary. 15
Figure 2. 2. MT1 diaphyseal cross section displayed in the Avizo software 3D viewer (left) with the completed module components displayed in a hierarchical tree view in the project view panel (right)……. 23

Figure 2. 3. Human right hallucal MT displaying landmark positioning and standardized spatial alignment…… 25

Figure 2. 4. Screen captures from the Avizo software displaying the final alignment of the MT 1-5 proximal articular surface renderings.. 26

Figure 2. 5. Biomechanical length and cross section slices along the diaphysis of a metatarsal.....28

Figure 2. 6. Lateral view of an idealized metatarsal illustrating representative cross sections and their locations for 25%, 35%, 50% and 65% regions of interest.. 28

Figure 2. 7. Left hallucal metatarsal cross sections at the 65% region of interest (ROI) from an individual in the post-industrial South African sample……..... 29

Figure 2. 8. Workflow for identifying trabeculae and intracortical porosities.. 30

Figure 2. 9. Left hallucal metatarsal cross section at the 65% ROI from an individual in the post-industrial South African sample……...30

Figure 3. 1. Boxplots (median, quartile, and range) of high gear (MT1 and 2) and low gear (MT2, 3, 4 and 5) mean MT CSGPs for the combined post-industrial individuals of South Africa, LSA Southern Africans and the Jomon of Japan..... 35

Figure 3. 2. Boxplots (median, quartile, and range) of high gear (MT1 and 2) and low gear (MT2, 3, 4 and 5) mean MT CSGPs for the post-industrial individuals of South Africa, LSA foragers of South Africa and the Jomon of Japan……..38

Figure 3. 3. Line plots of the mean CSGPs for MTs 1-5 of the post-industrial individuals of South Africa, Later Stone Age Southern Africans and the Jomon of Japan.. 41

Figure 4. 1. Pedography using the Novel-emed ® system and kinematic video gait analyses of a modern human's unshod feet displaying low gear push-off……46

Figure 4. 2. Seiza or Japanese style kneel sitting. 47

LIST OF ABBREVIATIONS

MT	Metatarsal
MH	Metatarsal head
MTP	Metatarsal-phalangeal
B.P.	Before Present
ROI	Region of interest
CSGP	Cross-sectional geometric property
SMA	Second moments of area
LSA	Later Stone Age

CHAPTER 1 – INTRODUCTION

There are four categories of studies that evaluate the relationship between bone form and its biomechanical function: joint form and pathology, trabecular architecture, histology, and cross-sectional geometry (Pearson and Lieberman, 2004). This study investigates the relationship between metatarsal bone form, as quantified by cross-sectional geometric properties, and its possible relationship to high versus low gear push-off during the propulsion phase of the gait cycle.

1.1 Bone form

Bone is a term used to describe both the organ and the material it is made of (Sharir et al., 2008). Increased mechanical loading of bone can lead to changes in its form (Carlson, 2005; Carlson and Marchi, 2014; Chirchir et al., 2015; Duncan et al., 2002; Jashashvili et al., 2015; Laskey et al., 2010; Lieberman and Crompton, 1998; Lieberman et al., 2003; Marchi, 2005; Martin et al., 2015; Pearson, 2000; Ruff, 1987; Ruff et al., 1993; Ruff et al., 2006; Shaw and Stock, 2009). Increased strain stimulates deposition of new bone tissue when exceeding a modelling threshold, which strengthens the bone in the direction of deformations and reduces strain to its original level (Lieberman and Crompton, 1998; Lieberman et al., 2003; Ruff, 2018). Modelling describes the process of paired or unpaired bone formation and/or resorption of periosteal and/or endosteal surfaces resulting in bone cross section reshaping (Barak, 2019). An example of modelling occurring with paired bone deposition and resorption is when bone is deposited on the outer perimeter (periosteal surface) while bone resorption occurs on the inner perimeter (endosteal surface) leading to an increase in the outer radius and a concomitant expansion in the inner radius of the medullary cavity (Fig. 1.1). The result on the bone's cross-sectional geometry is an increase in bending stiffness (Sharir et al., 2008).

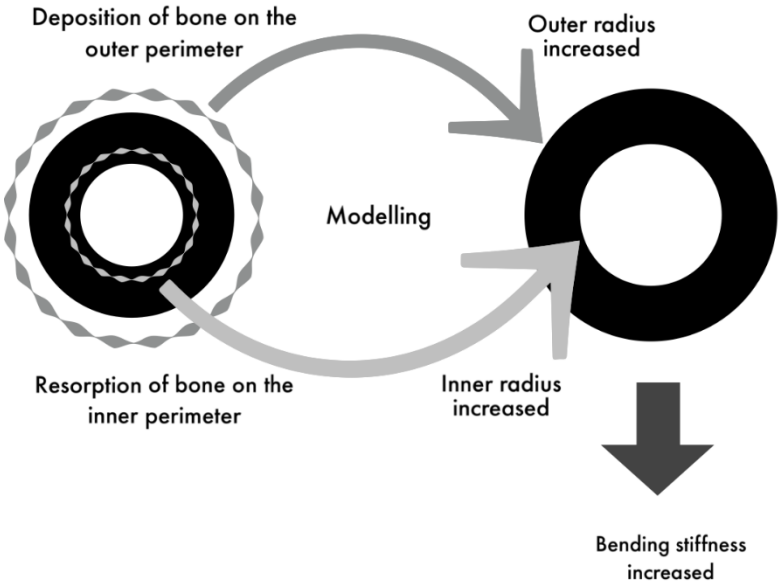


Figure 1.1. An example of bone cross section reshaping by modelling resulting in an increase in bending stiffness. Adapted from Sharir, A., Barak, M.M. and Shahar, R. (2008) 'Whole bone mechanics and mechanical testing', *The Veterinary Journal*, 177(1), pp.13.

This adaptive response of bone to its loading regime is commonly referred to as bone functional adaptation and can be used to infer mobility patterns in past populations (Carlson and Marchi, 2014; Ruff et al., 2006). It is important to note however, that other factors such as bone disease, sex, foot pathologies, menopause, age, diet are biological factors that along with behavioural factors may affect bone structure (Bae et al., 2012; Carlson and Marchi, 2014; Duncan et al., 2002; Ferretti et al., 1996; Groll et al., 1999; Högler et al., 2003; Laskey et al., 2010; Martin et al., 2015; Pathria et al., 2016; van Rietbergen et al., 2002; Wehrli et al., 2006). An example of modelling occurring independent of mechanical loading is found in post-menopausal women, where endocortical bone resorption increases and outpaces periosteal bone deposition, which slows or ceases due to physiological changes, ultimately leading to decreased bone mass with a reduction in bending stiffness (Fig. 1.2).

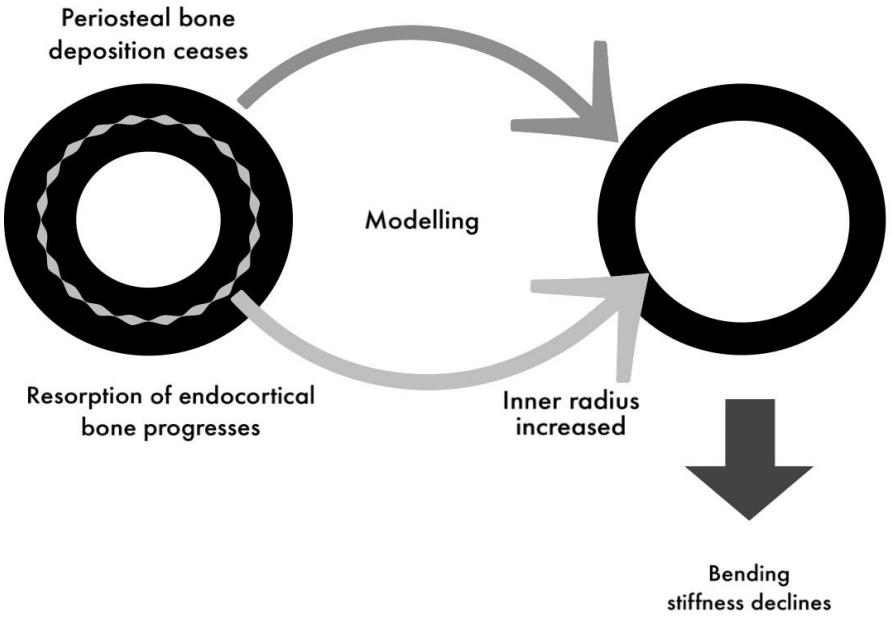


Figure 1.2. An example of bone cross section reshaping by modelling due to menopausal bone loss rather than altered mechanical loading. Adapted from Sharir, A., Barak, M.M. and Shahar, R. (2008) 'Whole bone mechanics and mechanical testing', *The Veterinary Journal*, 177(1), pp.13.

Supporting evidence for these relationships can be found in experimental studies. For example, in comparing diaphyseal femoral shape of mice engaged in linear versus turning locomotion, Carlson and Judex (2007) found evidence that turning altered distribution of bone mass and hence cross-sectional shape compared to the linear and control groups. Lieberman et al. (2001) compared epiphyses of exercised and sedentary sheep and concluded that subchondral articular surface area did not increase in response to mechanical loading, but that the diaphyseal geometric cross-sectional properties (I_{max}, I_{min}, I_{max}/I_{min}, J, CA) did increase.

Because of the relationship between loading regimes and bone form, skeletal variation has been used to explain activity patterns in past and present populations (Ruff, 2018). Murray Valley aboriginal people are described as having engaged in a lifestyle that imposed little muscular and bone stress because their femoral and humeral diaphysis and articular surfaces were found to be gracile in comparison to other modern human

populations (Collier, 1989; Pearson, 2000). Confirmation of these patterns can be found in studies of modern athletes, representing among the most active individuals living today. Shaw and Stock (2009) observed tibial cross-sectional diaphyseal properties (I_{max}, I_{min}, I_{max}/I_{min}, J, %CA) of a group of adolescent runners and field hockey players to be different, particularly stronger, compared to a control group of similarly aged individuals. In an investigation into the bone geometry of the distal radius of long-term tennis players, Ducher et al. (2005) found that the dominant radius had a marked increase in bone size and a slight increase in volumetric bone mineral density. Modern human adults, however, who became active after a sedentary phase during childhood retain the potential to slow the rate of endosteal resorption, but they are unable to add significant amounts of new sub-periosteal bone (Ericksen, 1976; Lazenby, 1990).

The response of bone to mechanical loading is also used for characterizing broader evaluations of activities in different groups of humans through time or even species level differences. For example, the conclusion that the Tianyuan 1 femora belonged to physically active Pleistocene hunter-gatherers was reached because of the elevated femoral shaft bending strength measured (Wei et al., 2017). The Jomon of Japan are said to have been highly mobile in comparison to modern industrial-era Japanese because of high metatarsal (MT) diaphyseal strength (Z_p) in the former (Hagihara and Nara, 2018). Furthermore, postcranial robusticity comparisons between Neandertals and the earliest anatomically modern humans have been used to differentiate their activity levels (Pearson, 2000).

Given the above, it is reasonable to ask whether lateral MT (MT2-5) diaphysis may have higher bone rigidity (second moments of area) or strength (section moduli) if they are loaded more than the medial MT (MT1-2) diaphysis during low gear push-off. Conversely, medial MT diaphysis may have higher bone rigidity (second moments of area) or strength (section moduli) if they are loaded more than lateral MT diaphysis during high gear push-off.

1.2 Cross-sectional bone geometry

Applying the engineering theory of beam mechanics, strength of a bone is a function of the amount of cortical bone present in the cross section, and its distribution around the centroid of the cross section (Laskey et al., 2010; Lieberman et al., 2004; Martin et al., 2015). The ability of a bone to resist structural failure (fracture) due to bending and torsion is referred to as strength, whereas its ability to resist deformation from the same forces is referred to as rigidity (Ruff, 2018). Cross-sectional properties known as second moments of area are proportional to bending and torsional rigidity, while bending and torsional strength are proportional to a property known as section moduli (Ruff, 1987; Ruff, 2018). These cross-sectional properties are used for the structural analysis of long bone cortices.

Cross-sectional geometric studies have been successfully used to quantify diaphyseal structure of long bones allowing inferences to be made on activity patterns, such as mobility levels (Carlson and Judex, 2007; Carlson and Marchi, 2014; Davies and Stock, 2014; Duncan et al., 2002; Griffin et al., 2008; Jashashvili et al., 2015; Laskey et al., 2010; Marchi, 2005; Ruff, 1987; Ruff 2008a; Ruff and Larsen, 2014; Shaw and Stock, 2009; Shaw et al., 2014). Early techniques required manually measuring bone length and circumferences either directly from bones or from radiographic images limiting structural bone interpretations and resulting in imprecise indicators of biological adaptation (Lovejoy et al., 1976; Ruff, 1987). As a result, long bone cross-sectional geometry has become an important means to evaluate mechanical properties to reconstruct locomotor behaviour among fossil hominins (Ruff et al., 2020). On the contrary, Wescott (2014) advised against using bone geometry as a sole indicator for interpreting mobility, but to look at the data in a biological and archaeological context since there may be other non-ambulatory habitual activities influencing bone diaphyseal shape. Mobility impairment due to neurological disease, secular changes such as an increase in stature and body mass, habitual activities such as hoeing, raking, and sitting postures are examples of non-ambulatory habitual activities than can influence cross-sectional bone strength and shape (Wescott, 2014). However, since humans are habitually bipedal and rarely use their feet directly for non-ambulatory activities, metatarsal bone geometry will be minimally affected by these types of other habitual activities.

Modern human and hominin studies utilizing cross-sectional bone geometry have often been conducted on the femur and tibia (Carlson et al., 2007; Davies and Stock, 2014; Duncan et al., 2002; Högler et al., 2003; Kontulainen et al., 2008; Laskey et al., 2010; Manske et al., 2006; Ruff, 1987; Ruff, 2009; Ruff and Larsen, 2014; Shaw et al., 2014; Wescott, 2014; Woodhead et al., 2001), or on the humerus and ulna (Bass et al., 2002; Carlson et al., 2007; Ducher et al., 2005; Ruff, 2009). Griffin and Richmond (2005) "were the first to examine cross-sectional geometric properties of human MTs and their relationship to external loads during walking and running". While generally less attention has been devoted to investigating cross-sectional geometry of MTs than other long bones (Griffin et al., 2008), it is worth noting that Hagihara and Nara (2018) drew conclusions about forefoot loading patterns between Jomon hunter-gatherers and modern Japanese people using the cross-sectional geometry of their MTs. Other studies of MT diaphysis have examined cortical thickness and second moments of area along entire shafts and shown important distinctions between groups of human, hominin, chimpanzee and gorilla first metatarsals (Jashashvili et al., 2015) and fifth metatarsals (Dowdeswell et al., 2017).

1.3 High gear and low gear push-off

Stance phase has an initial peak in vertical forces at 15% and a second peak between 45-50% of the human gait cycle (Fig. 1.3) (Hayafune et al., 1999). The beginning of the terminal stance phase is marked by heel rise, which typically coincides with the beginning of the second force peak during which the forefoot carries peak load (Hayafune et al., 1999; Whittle, 2014). During this late phase of the gait cycle, a forefoot propulsive mechanism occurs along a transverse or oblique metatarsal axis, or successively low gear first followed by high gear (Kelikian and Sarrafian, 2011; Vogler and Bojsen-Møller, 2000).

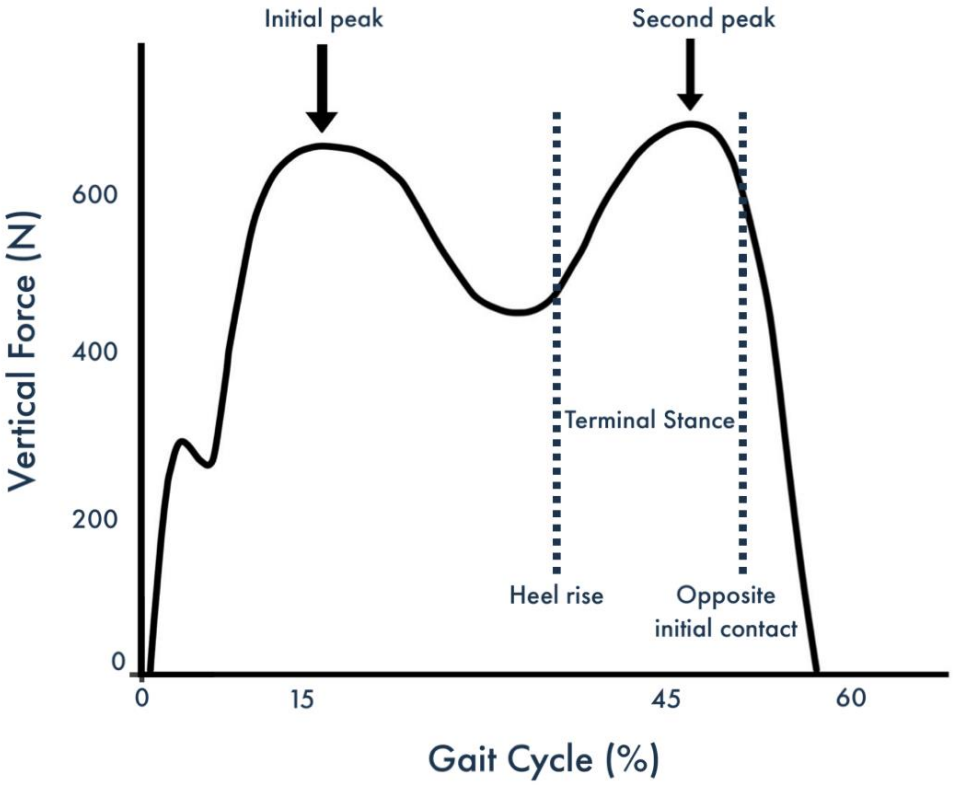


Figure 1.3. A Force-Time graph of a modern human gait cycle demonstrating vertical ground reaction forces, in Newtons, and time in percentage of a single leg gait cycle. (Adapted from Hayafune, N., Hayafune, Y. and Jacob, H.A.C., 1999. Pressure and force distribution characteristics under the normal foot during the push-off phase in gait. *The foot*, *9*(2), pp.90.)

"The transverse axis or 'high gear' is formed by metatarsal heads one (MH1) and two (MH2), while the oblique axis or 'low gear' is formed by MH 2-5" (Bojsen-Møller, 1979). The term high gear push-off describes a weight transfer over the forefoot from the lateral to the medial side; low gear push-off describes lateral loading of the forefoot without the medialward weight transfer (Bojsen-Møller, 1979). Weight transfer over the forefoot from the lateral to the medial side for a high gear push-off is considered typical in humans although variation in this pattern may occur based on speed of gait (Aiello et al., 1990; Bojsen-Møller and Lamoreux, 1979; Haile-Selassie et al., 2012).

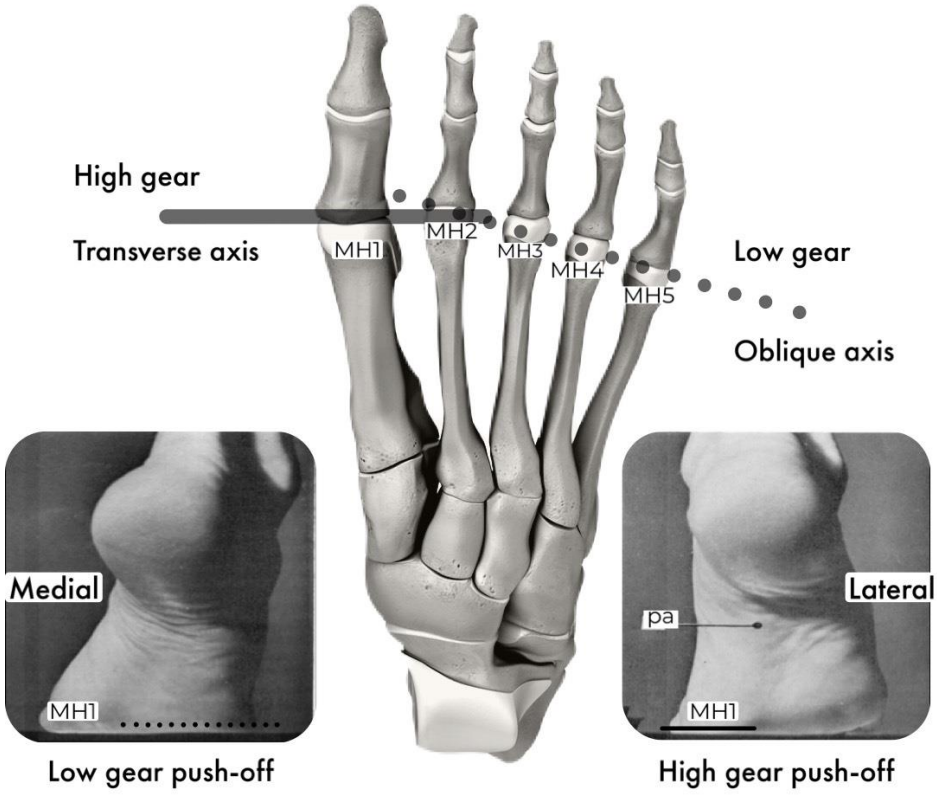


Figure 1.4. Illustrates the transverse metatarsal axis (solid line) formed by MH1 and MH2 and the oblique axis (dotted line) formed by MH2 to MH5. High gear push-off occurs when propulsion during terminal stance phase utilises the transverse axis resulting in the visible appearance of the plantar aponeurosis (pa) in the plantar view of the foot. Low gear push-off occurs when propulsion during terminal stance phase utilises the oblique axis and a taut plantar aponeurosis is not visible (Adapted from Bojsen-Møller, F.,1979. 'Calcaneocuboid joint and stability of the longitudinal arch of the foot at high and low gear push off.', *Journal of Anatomy*, 129(Pt 1), pp. 170.)

Bojsen-Møller (1979) investigated high and low gear toe-off in an experiment as follows: A glass plate with an underlying mirror and camera were inserted into a walkway to capture foot contact area during propulsion. Video and still images were used to visually estimate foot function during the propulsion phase of gait. If the plantar aponeurosis was visibly taut and the foot appeared to have most of its pressure on the plantar medial aspect, it was deemed high gear propulsion (Fig. 4). If the plantar aponeurosis was not visible, and the foot appeared to have most of its weight laterally distributed, then it was deemed low gear push-off. The study concluded that high gear toe-off occurred when the windlass

mechanism was activated, and forefoot weight transfer was from lateral to medial. Low gear push-off occurred when the windlass mechanism was only partially, or not at all activated, and forefoot weight was distributed laterally. This experiment was repeated by Aquino and Payne (2001), who reported that only 66.7% of their subjects (n=39) displayed a visibly taut plantar aponeurosis at push-off. If a taut plantar aponeurosis at push-off is a reliable indicator for windlass activation, and thus high gear push-off, then the other subjects were possibly pushing-off in low gear.

In recent years, more modern techniques using peak plantar pressures have been used to investigate weight transfer during propulsion. Collectively, plantar pressure studies do not provide a consistent pattern in reporting forefoot loading at push-off. For example, in samples numbering less than 55 subjects, the highest pressures for the forefoot have been shown to occur under MH2 then MH3 followed by the hallux (Bryant et al., 2000; Maetzler et al., 2010; Putti et al., 2008). In contrast, Hayafune et al. (1999) evaluated pressure and force distribution under the foot, specifically at the push-off phase of stance, and found an incredibly wide range of plantar peak pressures among 84 subjects, including mean peak pressures that were highest under hallucal phalanges rather than MH2 or MH1. D'Aout and colleagues (2009) examined peak plantar pressures in a shod western population and shod and unshod Indian populations and found mean peak forefoot pressure to be under MH2 and MH3. Using a foot pressure-sensing treadmill, body surface markers and high-speed cameras, Bates et al. (2013) observed medial forefoot propulsion (high gear) when the arch was stiffened (taut plantar aponeurosis). Crompton and colleagues (2010) cited an example of a clinically normal individual displaying plantar peak pressures on the lateral mid-foot, and MH2-4 and hallux with no lateral-to-medial movement of the centre of pressure. This peak plantar pressure pattern suggests a flexible lateral column of the foot with no weight transfer to the hallux at push-off. This is contrary to what was described by Bojsen-Møller (1979). Interestingly, in evaluating the Laetoli footprints, Crompton and colleagues (2012) concluded that there was a lateral-to-medial force transfer resulting in a medial or high gear push-off.

On the other hand, theoretical models of foot function appear to emphasize medial weight transfer mainly to the first metatarsal-phalangeal (MTP) joint and hallucal phalangeal joints to stabilize the foot through the windlass mechanism (Dananberg, 2000; Durrant and Chockalingam, 2009 Fuller, 2000; Harradine and Bevan, 2009; Hicks, 1954). The

windlass mechanism (Fig. 1.5) accounts for how the foot is converted from a flexible structure into a stiffened lever by predominantly loading the hallux (high gear) in the propulsive phase of gait as the heel rises and the plantar aponeurosis tenses (Bojsen-Møller, 1979; Hicks, 1954; Bojsen-Møller and Flagstad, 1976; Vogler and Bojsen-Møller, 2000). Deviating from lateral to medial weight transfer preceding push-off, to activate the windlass mechanism, is identified as a pathological state in modern humans caused by conditions such as functional hallux limitus and hallux rigidus (Clough, 2005; Dananberg, 2000; Van Gheluwe et al., 2006). Hallux limitus is described as a limitation of first metatarsophalangeal joint motion during closed-kinetic-chain exercises, but normal joint motion during open-kinetic-chain exercises, i.e., the condition is only detectable with videography and plantar pressure studies as a momentary blockade of sagittal plane motion of the first MTP joint (Clough, 2005; Dananberg, 2000; Fuller, 2000; Payne et al., 2002). Payne et al. (2002) found that a total of 53 of 86 normal feet tested positive for hallux limitus leading the authors to advise that clinicians make the test for functional hallux limitus a routine examination. While functional hallux limitus manifests no symptoms at the joint itself, it is recognised as a pathology that through compensatory mechanisms like excessive supination at push-off, causes achilles tendinopathy, knee pain and lower back pain (Clough, 2005; Dananberg, 2000; Fuller, 2000; Payne et al., 2002). Given the insipid diagnostics and potentially high prevalence of hallux limitus, it is possible that what is perceived as a disorder of the first MTP is in fact variation attributable to a higher than appreciated occurrence of low gear push-off in the human population.

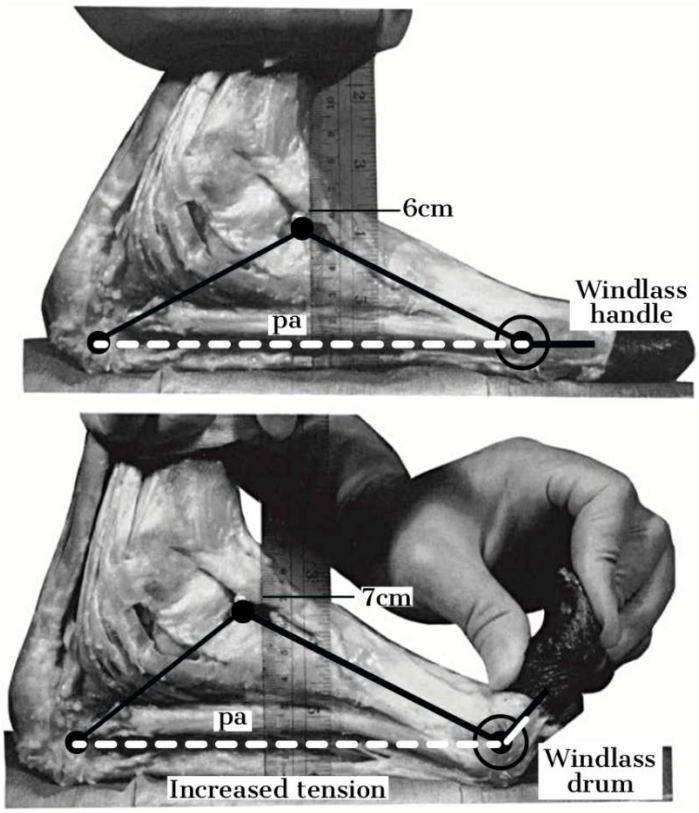


Figure 1.5. Schematic windlass mechanism superimposed on a cadaveric specimen displaying the windlass phenomenon. This mechanism is initiated when the hallux is passively dorsiflexed causing the longitudinal arch to rise, the rearfoot to supinate, the leg to externally rotate, and the plantar aponeurosis (dashed line) to tense up resulting in a stiffened foot. This phenomenon is analogous to the winding of a cable (plantar aponeurosis) by pulling a handle (proximal phalanx of the hallux) around the drum of a windlass (first metatarsophalangeal joint). (Adapted from Kelikian, A.S. and Sarrafian, S.K. eds., 2011. *Sarrafian's anatomy of the foot and ankle: descriptive, topographic, functional*. Lippincott Williams & Wilkins, pp 592.)

Song and Geyer (2011) indicate that feet utilising the windlass mechanism during walking save 15% more energy than feet without a windlass mechanism because the former stiffens the foot to allow for more energy efficient weight transfer (high gear) during propulsion. Griffin and colleagues (2015) then hypothesized that the windlass mechanism was selectively advantageous in our ancestors to increase speed while also promoting energy conservation during bipedal gait. It is, however, unknown as to when during hominin evolution this mechanism emerged since components that make up the windlass mechanism are poorly preserved in the fossil record (Griffin et al., 2015).

Furthermore, Fuller (2000) postulated that a malfunctioning windlass mechanism may lead to foot pathologies such as plantar fasciitis, hallux abducto-valgus and hallux limitus in humans. Hicks (1954) reported that the arch-raising action of the plantar aponeurosis almost disappeared when it was transected on a cadaveric specimen. Similarly in a literature review, Tweed and colleagues (2009) found that plantar fasciotomy may lead to a loss of stability in the medial longitudinal arch and gait abnormalities since the plantar fascia functions to passively resist flattening of the longitudinal arch during mid-stance. In contrast, Welte and co-workers (2018) point out that the windlass mechanism only occurs as described by Hicks (1954) in static positions and not during dynamic foot loading. Additionally, Kirby (2017) reported that due to the unique morphological configuration of the bone and soft tissue of the human foot, an increase in Achilles tendon tension due to dynamic foot loading automatically increases foot longitudinal arch stiffness before late midstance. According to Pataky et al. (2008) the prevention of arch collapse (or conversely increase in arch height), usually attributed as a function of the windlass mechanism at push-off, begins in early stance phase due to increased plantar aponeurosis tension caused by muscular activity.

The role of intrinsic muscular contributions to arch stiffening was dismissed by Hicks (1954). However, Kelly et al. (2012), using ultrasound guided bi-polar fine-wire electromyography inserted into the abductor hallucis, flexor digitorum brevis and quadratus plantae muscles, demonstrated that the plantar intrinsic muscles are recruited to stiffen the longitudinal arch when it is loaded during single leg and double leg support. Ultimately, medial longitudinal arch stiffening that occurs during stance phase is not only reliant on the plantar fascia but instead depends on a load sharing system of the osseus elements of the arch, the Achilles tendon, and plantar ligaments in addition to the plantar fascia and intrinsic foot muscles (Fauth et al., 2004; Kelly et al., 2014; Kelly et al., 2012; Kirby, 2017). Consequently, any theoretical model of foot function that only emphasizes medial longitudinal arch stiffening through the windlass mechanism activated upon high gear push-off requires closer review.

In contrast to many theoretical models, numerous studies of hominin postcranial fossils indicate that there were a variety of terrestrial bipedal gait kinematics exhibited by hominins (DeSilva et al., 2013; DeSilva et al., 2019; Dowdeswell et al., 2017; Haile-Selassie et al., 2012; Harcourt-Smith et al., 2015; Su and Carlson, 2017; Zipfel et al.,

2011). Increased mid-tarsal mobility and the absence of a longitudinal arch in *Australopithicus sediba* suggests that the development of bipedal adaptations in the hominin lineage evolved in a non-linear pattern and that there may have been various kinematic solutions for being a bipedal hominin (DeSilva et al., 2013; Prang, 2015; Zipfel et al. 2011). Variation is further illustrated when comparing the distal hallucal phalanx of hominins. According to Trinkaus and colleagues (2021), the known Late and Middle Pleistocene Atapuerca-SH exhibit a hallucal distal phalanx resembling recent humans – laterally deviated due to the toeing-out pedal position during striding bipedal gait. Whereas "the known distal phalanges of australopiths, Early Pleistocene *Homo* and the Middle Pleistocene Dinaledi sample exhibit minimal lateral deviation of the hallucal distal phalanx" (Trinkaus et al., 2021). It is plausible that high and low gear push-off could be responsible for the variation seen in hallucal distal phalanges. In comparing MT5 fossil hominin second moments of area, Dowdeswell and co-workers (2017) observed that *A. africanus* (StW114/115)*, H. habilis* (OH8) *and P. robustus* (SKX33380) had human-like dorsoplantar rigidity whereas *H. erectus* (D4058) *and H. naledi* (UW.101-1439, UW.101-518) exhibited a more African ape-like uniform rigidity along the diaphysis. This led the authors to conclude that evolution of human bipedalism, at least from the perspective of the foot, was a process that involved a number of experiments in hominin foot loading patterns along the way (Dowdeswell et al., 2017).

Evidence for kinematic variation in the bipedal gait of hominins is present in the varied pedal fossils represented in the fossil record. Haile-Selassie and colleagues (2012) suggested that there was "more than one hominin locomotor adaption at the beginning of the Late Pliocene" since BRT-VP-w/73 was a facultative biped with an abducted hallux while contemporaneous *A. afarensis* was a striding terrestrial biped with an adducted hallux. The Dmanisi hominin foot was described as having an arch and a human-like talus for improved locomotor economy (Pontzer et al., 2010), but interestingly, it has ape-like, MT internal structure (Dowdeswell et. al., 2017). *Australopithecus sediba* was a biped, yet it exhibited evidence of a mid-tarsal break (e.g., presumably high peak lateral loading) and a foot that hyper-pronated lowering the arch as the foot prepared for propulsion (DeSilva et al., 2013). An unstable lateral column suggests that *A. sediba* may have had a low gear toe-off. Bates and colleagues (2013) also found lateral mid-foot compliance to be inversely proportional to the pressure exerted by the MT1 and the hallucal phalanges,

but the authors attributed this to a ubiquitous soft tissue coupling mechanism rather than an osseous locking mechanism. Another example of varied push-off is *Ardipithecus ramidus*, which is believed to have performed fulcrimation (push-off) on the lateral metatarsal heads in the presence of an abducted first ray (Lovejoy et al., 2009).

Accordingly, if the bipedal hominin foot evolved in such a mosaic fashion, then it is likely that it did not exhibit one consistent pattern of forefoot loading during propulsion. Low gear push-off may not be a pathological state but rather a variable locomotor adaptation observable in non-trivial frequencies in modern humans.

1.4 Objectives

The aim of this study is to investigate whether lateral forefoot loading, inferred from higher strength and rigidity of MT2-5 (low gear MTs) in relation to MT1-2 (high gear MTs), may have occurred at push-off in selected human populations. The objective being to assess whether forefoot loading may be variable or whether high gear loading occurs in high frequencies, as depicted in theoretical foot function models.

1.5 Hypothesis

High gear push-off, indicated by relative strength and rigidity of MT1-2, occurs in higher frequency than low gear push-off, indicated by relative strength and rigidity of MT2-5 in humans.

CHAPTER 2 – MATERIALS AND METHODS

The purpose of this chapter is to introduce the research materials used and the methodology employed for this quantitative study regarding the intraspecific differences in metatarsal (MT) bone cross-sectional geometry related to high gear and low gear push off. Workflow is summarised in Fig. 2.1.

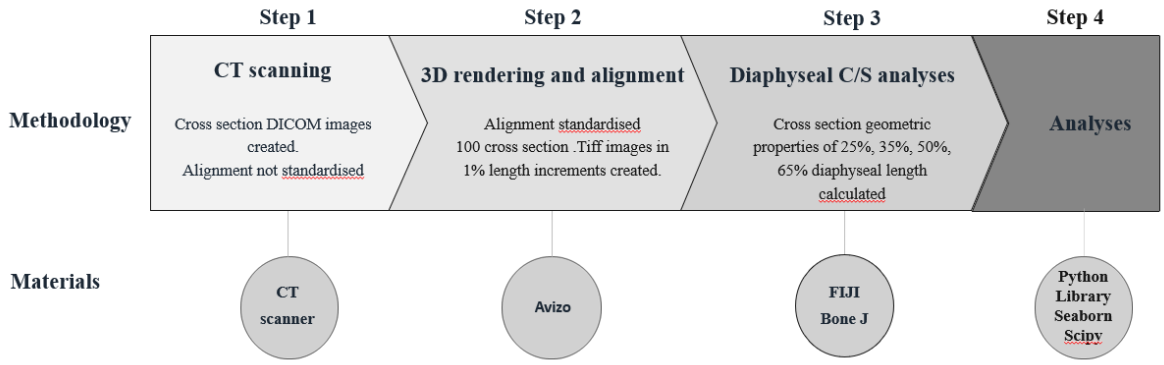


Figure 2.1. Materials and methods workflow summary.

2.1 Materials

The materials used in this study include a metatarsal sample, computed tomography scanning equipment, bone 3D rendering and alignment software and bone cross section analyses software.

2.1.1 The metatarsal sample

The metatarsals used in the current study were obtained from three sources. Ethical approval was obtained for each of the three populations. The Raymond A. Dart Collection of Human Skeletons (Human Research Ethics Committee (Medical) Clearance Certificate: W-CBP-220504-01), the National Museum Bloemfontein Archaeological Human Skeletal Collection and the University Museum (Approval Reference Number:

NMB ECC 2015/05), The University Tokyo (UMUT), Jomon Collection (Approved by Dr. G. Suwa from the Department of Anthropology and Prehistory at UMUT).

The entire sample is comprised of three broad groups: Later Stone Age southern Africans (i.e., Khoesan), post-industrial individuals from South Africa, and the Jomon of Japan. The sample incorporates a variety of lifestyles, including partially shod and unshod, highly mobile and sedentary individuals who lived on diverse terrain.

All five MTs from each individual's left foot were utilised. Where the left MTs were incomplete, missing, or damaged, right MTs were substituted. However, MTs from different sides were not mixed. All sets of left and right MTs were maintained as such and were not substituted for each other. MTs with an external surface that appeared pathological were excluded. Only MTs with fused epiphyses were included. Sex and age of individuals were obtained from collection records and only adults were included. Individuals with MTs that showed evidence of healed traumatic pathologies, such as bone callus or deformity, as a result of a fracture, were excluded. MTs that exhibited minor, partial post-depositional destruction of one of the articular surfaces, but an intact diaphysis, were included to ensure sufficient sample size. However, MTs with either distal or proximal articular surface post-depositional destruction were excluded since the alignment process in step 2 (Fig 2.1) depended on the articular surfaces.

2.1.1.1 Post-industrial individuals from South Africa

The post-industrial individuals in this sample are from rural and urban ethnic populations. They consist of various black South African linguistic groups (i.e., Xhosa, Zula, and Sotho) that are considered to be one homogenous group (Dayal et al., 2008). Males and females are equally represented and have an age range of 25-30 years old. They were migrant laborers (e.g., miners) (Dayal et al., 2009) who are presumed to have been shod. However, living urban adult females in South Africa reported being unshod or partially shod as children and continued to engage in unshod leisure behaviour (Thompson and Zipfel, 2005). Since these individuals grew up in rural areas but moved to Johannesburg to find work as adults (Carlson et al., 2007), it is likely that they were partially shod as

children and shod as adults. Table 2.1 summarizes the details of the modern post-industrial sample.

Table 2.1: Description of the post-industrial individuals from South Africa.

Lifestyle	Terrain	Climate	Shod/Unshod	Specimen	n
Sedentary	Modern flat, hard surfaces	Warm	Partially shod	Complete MT 1-5	14

The sample is curated in The Raymond A. Dart Collection of Human Skeletons. The human specimens in this collection were prepared from unclaimed bodies from Transvaal hospital sources, archaeological excavations, mine disasters and accidents (Dayal et al., 2009; Tal and Tau, 1983). The sex and tribe/race recorded by hospital administrative staff is believed to be accurate but the age less reliable with 25% of specimens differing by more than 10 years from the estimated age (Dayal et al., 2009; Tal and Tau, 1983). In 1959, a flood submerged the collection, and many bones were mixed with each other and never rectified (Tobias, 2005). The sample selected does not form part of the mixed bones since they are from less than four decades ago. The individual, population group, collection accession number, age and sex are summarized in Table 2.2.

Table 2.2: Post-industrial humans from South Africa curated in The Raymond A. Dart Collection of Human Skeletons

Collection Accession Number	Population group	Age	Sex
A8	Sotho	30	M
A9	Venda	20	M
A13	Pondo	30	M
A14	Zulu	25	M
A17	Sotho	26	M
A163	Sotho	25	M
A170	Sotho	29	M
A22	Xhosa	30	F
A209	Sotho	25	F
A218	Sotho	25	F
A458	Sotho	24	F
A883	Sotho	27	F
A1285	Sotho	29	F
A3060	Sotho	29	F

2.1.1.2 Later Stone Age southern Africans

Later Stone Age (LSA) southern Africans, referred to collectively as the Khoesan, are the indigenous hunter-gatherer peoples of Southern Africa (Schuster et al., 2010). Nevertheless, the term Khoesan does not signify one unified identity since peoples speaking Khoesan languages are linguistically and culturally dissimilar and each has their own history (Pakendorf and Stoneking, 2021). The LSA southern African sample in this study inhabited or utilised the Matjes River Rock Shelter from almost 8,000 B.P. to 2,000 B.P. (L'Abbé et al., 2008; Sealy and Pfeiffer, 2000; Stock and Pfeiffer, 2001). Although individuals in this sample are believed to have been active until death (Stock and Pfeiffer, 2001), they were not necessarily walking long distances all the time. There is evidence of a diverse dietary (marine and terrestrial protein) history suggesting that journeys were made to visit other groups, with a different diet, further away on occasion (Sealy and Pfeiffer, 2000). However, given that their marine and terrestrial food supply was near to their coastal settlements, their daily activity may have been relatively low ranging (Sealy and Pfeiffer, 2000).

The Khoesan individuals in this group were discovered in the Eastern Cape, Matjes River Rock Shelter (L'Abbé et al., 2008; Morris, 1992), except for one individual who is from the Aughrabies site. They lived in a warm climate wearing minimal clothing and are presumed to have been habitually unshod (Stock and Pfeiffer, 2001). They negotiated rugged terrain while foraging for terrestrial and marine resources (Stock and Pfeiffer, 2001). The Matjes River Rock Shelter site was excavated in the 1920's and 1950's. Excavations have been criticized for having commingled skeletal remains and using poor excavation techniques making it difficult to associate individuals with specific layers or cultures. (L'Abbé et al., 2008; Morris, 1992; Rightmire, 1978; Sealy et al., 2006). Fortunately, the collection has been improved by many authors sorting through the data found in the 'Catalogue of Holocene Skeletons in South Africa' by Morris (1992) and various field notes by Hoffman (Jenkins et al., 2007; L'Abbé et al., 2008; Sealy et al., 2006; Sealy and Pfeiffer, 2000; Stock and Pfeiffer, 2001). The individuals from Matjes River Rock Shelter form part of the Archaeological Human Skeletal Collection at the National Museum of Bloemfontein (Morris, 1992). The individual accession number, sex and site of discovery are summarized in Table 2.3.

Table 2.3: LSA foragers from South Africa curated in the Archaeological Human Skeletal Collection at the National Museum of Bloemfontein

Collection Accession Number	Site	Sex
MRN4Wilton	Undetermined	F
NMB not acc MSk2	Matjies River Rock Shelter	F
NMB not acc SS2	Matjies River Rock Shelter	F
NMB not acc SS1	Matjies River Rock Shelter	M
NMB not acc SS3	Matjies River Rock Shelter	M
NMB MSk5	Matjies River Rock Shelter	Undetermined
NMB 1231 - 1	Matjies River Rock Shelter	Undetermined
NMB 1231 - 2	Matjies River Rock Shelter	Undetermined
NMB 1231 - 4	Matjies River Rock Shelter	Undetermined
NMB 1231 - 5	Matjies River Rock Shelter	Undetermined
NMB 1231 - 9	Matjies River Rock Shelter	Undetermined
NMB 1231 - 11	Matjies River Rock Shelter	Undetermined
NMB 1231 - 12	Matjies River Rock Shelter	Undetermined
NMB 1231 - 14	Matjies River Rock Shelter	Undetermined
NMB 1420	Aughrabies	Undetermined

LSA southern Africans are well-suited for investigating relationships between habitual behaviour (high gear or low gear push off) and bone structure (cross-sectional geometry) because variables affecting bone geometry are already known; it is assumed that all individuals were active life-long and had high lower limb loading, there was gender-based division of labour, less task specialisation, they were long time inhabitants of their respective environments, they were genetically homogenous, lived in a warm climate and presumably had no age-related bone changes given their short life expectancy relative to modern standards. (Sealy and Pfeiffer, 2000; Stock and Pfeiffer, 2001; Wollmann and Cameron, 2022). Table 2.4 summarizes details of the LSA southern Africans.

Table 2.4: Description of the LSA southern Africans

Lifestyle	Terrain	Climate	Shod/Unshod	Specimen	n
Presumed sedentary coupled with seasonal extensive travelling	Coastal rugged and inland	Warm	Presumed unshod	Complete sets of MT 1-5	15

2.1.1.3 The Jomon of Japan

Jomon is the name given to the prehistoric period (ca. 13,000 – 2,000 BP) in Japan which starts after the Palaeolithic period and precedes the Yayoi Period (Habu, 1996). The Jomon of Japan population were a homogenous group whose subsistence depended on hunting, fishing, collecting and possibly the use of cultivated plants (Akazawa, 1999; Habu and Junko, 2004). This active lifestyle made them physically agile with relatively high muscle mass (Yamaguchi, 1982). The Jomon of Japan people were highly mobile, as evidenced by their metatarsals being more robust than those of modern-day Japanese people (Hagihara and Nara, 2018). They are presumed to have engaged in long distance trade requiring traveling to inland, mountainous regions of Japan in the late to final Jomon phase (Hagihara and Nara, 2018; Underhill and Habu, 2006). Most of the large Jomon settlements were located on the Pacific Coast Honshu where coastal and forest resources were in close proximity (Perri, 2016). The selected sample represents the prefectures of Aichi, Chiba, Fukushima, and Osaka located along the Pacific Coast of Honshu. The Jomon of Japan population was relatively sedentary with likely seasonal occupation of

residential bases during the early, middle, and late Jomon periods (Habu, 1996; Underhill and Habu, 2006).

Japanese islands have a largely mountainous terrain and an extreme north-south orientation that results in a variation of climatic conditions from subarctic to subtropical (Perri, 2016). As a result, different subsistence hunter-gatherer systems existed in different regions (Underhill and Habu, 2006). "Hokkaido and the northern border of Honshu were primarily exploiting marine mammals and fish; south-western Honshu and the southern islands were primarily exploiting plant and marine foods; and north-central Honshu was exploiting a mixture of terrestrial animals, plants, and marine foods" (Perri, 2016). Table 2.5 summarizes details of The Jomon of Japan.

Table 2.5: Description of the Jomon of Japan

Lifestyle	Terrain	Climate	Shod/Unshod	Specimen	n
Relatively sedentary	Uneven	Variable	Partially shod	Complete sets of MT 1-5	24

The Department of Anthropology and Prehistory at The University Museum, The Museum of Tokyo (UMUT), houses the skeletal material belonging to the prehistoric (6000-2300BP) populations of Japan. Micro-CT scans of MTs 1-5 of the left or right foot of 14 individuals were made available on approval by Dr. G. Suwa from the Department of Anthropology and Prehistory at UMUT. Each individual's collection accession number is listed in Table 2.6.

Table 2.6: The Jomon of Japan derived geographically from the Pacific Coast of Honshu. Curated in The Department of Anthropology and Prehistory at The University Museum, The Museum Tokyo (UMUT)

Collection Accession Number	Site, Prefecture	Sex	Jomon subphase*
UMUT130166	Hobi, Aichi	Undetermined	Final
UMUT130242	Hobi, Aichi	M	Final
UMUT130145	Hobi, Aichi	F	Final
UMUT130152	Hobi, Aichi	M	Final
UMUT130195	Hobi, Aichi	F	Final
UMUT130849	Ikawazu, Aichi	M	Late/Final
UMUT130850	Ikawazu, Aichi	M	Late/Final
UMUT130857-2	Ikawazu, Aichi	F	Late/Final
UMUT130860	Ikawazu, Aichi	M	Late/Final
UMUT130861	Ikawazu, Aichi	M	Late/Final
UMUT130867	Ikawazu, Aichi	F	Late/Final
UMUT130868	Ikawazu, Aichi	F	Late/Final
UMUT131086-1	Ko, Osaka	Undetermined	Early to Final indet
UMUT131085-1	Ko, Osaka	M	Early to Final indet
UMUT131096	Ko, Osaka	Undetermined	Early to Final indet
UMUT131098	Ko, Osaka	M	Early to Final indet
UMUT131086-2	Ko, Osaka	Undetermined	Early to Final indet
UMUT131719	Ubayama, Chiba	F	Late middle-middle late
UMUT131061	Ubayama, Chiba	Undetermined	Late
UMUT131067	Ubayama, Chiba	M	Late
UMUT131377	Sanganji, Fukushima	M	Late/Final
UMUT131380-G1	Sanganji, Fukushima	Undetermined	Late/Final
UMUT131380-G2	Sanganji, Fukushima	F	Late/Final
UMUT131376	Sanganji, Fukushima	F	Late/Final

*Early 6,000-5,000 cal BP
Middle 5,000-4,000 cal BP
Late 4,000-3,000 cal BP
Final 3,000-2,300 cal BP

2.1.2 Computed Tomography (CT) scanning equipment

The Philips Brilliance 16P medical CT scanner at the Charlotte Maxeke Johannesburg Academic Hospital (South Africa) was used to CT scan MTs of the post-industrial individuals from South Africa. The SkyScan 1173 high energy micro-CT scanner at The University Museum, The Museum Tokyo (UMUT) was used to scan MTs of the Jomon of Japan. A Nikon Metrology XTH 225/320 LC dual source industrial CT system housed in the Microfocus X-ray Computed Tomography Facility in the Evolutionary Studies Institute of the University of the Witwatersrand was used to scan metatarsals of the Later Stone Age southern Africans.

2.1.3 Bone 3D rendering and alignment software

Thermo Scientific™ Avizo™ software (Waltham, Massachusetts, USA) is a 3D data visualization and analysis software application for analyzing material structure, properties, and performances. The program enables users to interact with data sets displayed in a 3D viewer and a tree view. The 3D viewer displays the data set as an interactive 3D image with a variety of angle views. The tree view is a graphical control element that represents a hierarchical view of the data and module components (Fig. 2.2). Avizo has been used in many fields ranging from life sciences to material sciences and has been used extensively in paleontology and archeological published research.

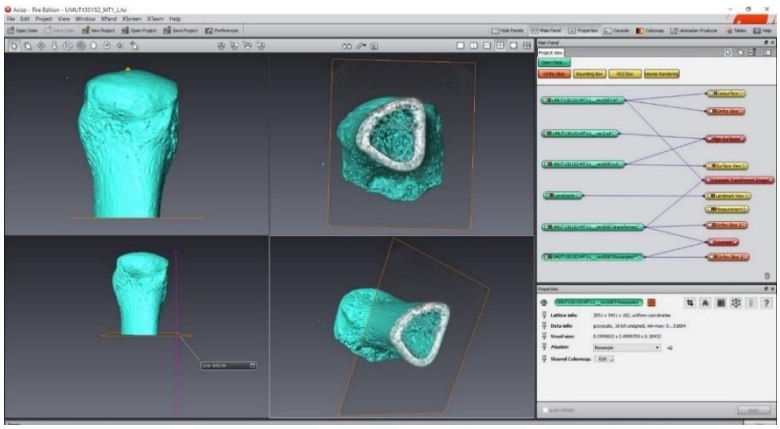


Figure 2. 2. MT1 diaphyseal cross section displayed in the Avizo software 3D viewer (left) with the completed module components displayed in a hierarchical tree view in the project view panel (right).

2.1.4 Bone cross section analyses software

FIJI (ImageJ) is an open-source biological-image processing and analysis software (Schindelin et al., 2012; Schindelin et al., 2015). Bone J is an open-source bone image analysis plugin for FIJI (Doube et al., 2010). FIJI was used to binarise and convert each cross-sectional image to 8-bit, analyse image quality, exclude bone deformity, fill intracortical porosity and remove trabecular struts. The Bone J plugin was used to orientate cross sections within images and to calculate standard cross-sectional properties from these cross sections (Doube et al., 2010).

2.2 Methods

The data collection process consisted of acquiring metatarsal CT-scans that were then rendered into three-dimensional images and positioned following a standardized protocol. This allowed for the extraction of specific diaphyseal slices (e.g., 50% length) for calculating cross-sectional geometric properties.

2.2.1 Computed tomography (CT) scanning

The post-industrial South African metatarsals were CT scanned using the open SKULL U.H.R. 0.5 protocol (Philips Healthcare, Andover, MA, USA). The scanning was performed at 140 kVp with a tube current of 253 mAs, a slice thickness of 0.67 mm, and a reconstruction increment of 0.3 mm. After the acquisition of all raw data, image data for a specimen were reconstructed as 16-bit DICOM images using a bone re-construction algorithm (i.e., a “sharp” kernel).

The Later Stone Age forager’s MTs were micro-CT scanned at 90 kV and 220 µA energy settings using 1000 projections and a 0.5 mm copper filter. All raw data were reconstructed in Inspect-X software, which is Nikon Metrology proprietary software associated with the micro-CT scanner. A beam hardening correction factor preset 2 was applied to optimize image quality. Image volumes were registered as 16-bit pixel .TIF image stacks, with spatial resolutions ranging between 26 and 49 µm.

The MTs of the Jomon of Japan were micro-CT scanned at 130Kv and 40 μA energy settings using a 0.25mm brass filter. A beam hardening correction of 30% was applied. Image volumes were registered as 16-bit pixel .TIF image stacks, with spatial resolutions ranging between 69.9 and 90 um.

The above image stacks were stored in separate folders according to individual collection accession numbers in preparation for the three-dimensional rendering process.

2.2.2 Metatarsal three-dimensional rendering and alignment

Avizo software was used for 3D rendering of the micro-CT scans followed by extraction of cross sections from the diaphysis based on the digital protocol published by Jashashvili and colleagues (2015). The workflow can be described as follows: Landmarks were positioned in the center of the proximal and distal articular surfaces of a given metatarsal. A line linking the two landmarks defined the longitudinal axis of its diaphysis. The longitudinal axis was then aligned parallel to the z-axis and orthogonal to the x-axis of the metatarsal rendering (Fig. 2.3).

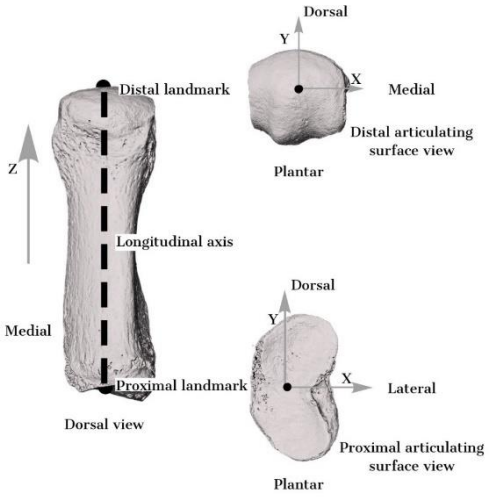


Figure 2.3. Human right hallucal MT displaying landmark positioning and standardized spatial alignment. Dorsal view: distal and proximal articular surfaces of a metatarsal with landmarks positioned in the centers of their respective articular surfaces. The dotted line joining the two landmarks indicates the longitudinal axis of the diaphysis that was aligned parallel to the z-axis and orthogonal to the x-axis in the alignment protocol. The mediolateral axis of the diaphysis is aligned parallel to the x-axis, while the dorsoplantar axis of the diaphysis is aligned parallel to the y-axis.

Each rendering was subsequently rotated about its longitudinal axis until the proximal articular surface of the MT was aligned in the chosen natural anatomical alignment, i.e., with respect to the transverse arch (Fig. 2.4A). Anatomical positions of the MT proximal articular surfaces were based on the description and illustration by Kelikian and Sarrafian (2011) (Fig. 2.4B). This is in contrast with published techniques which align the proximal articular surface parallel to the Y-axis (Dowdeswell et al., 2017) or align the dorsal aspect of the MT base parallel to the x-axis (White et al., 2011). Positioning in anatomical alignment was selected because a goal of the study was to investigate the effect of loading during low and high gear push-off on all the MTs with the entire metatarsus in anatomical position (e.g., with the MT heads plantigrade and the proximal articular surfaces aligned to adjacent MT articular surfaces (Fig. 2.4C).

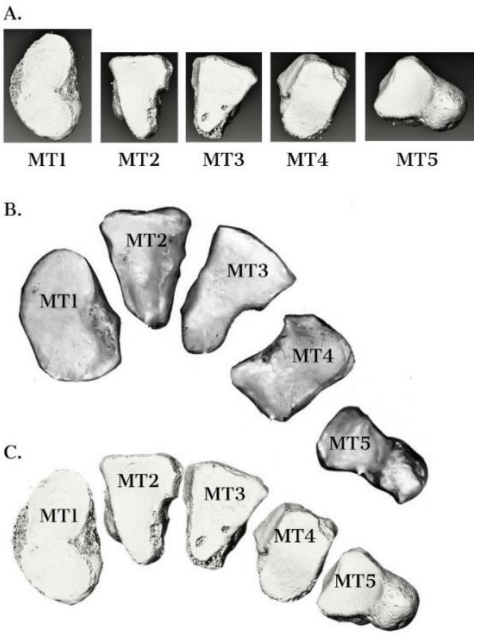


Figure 2.4. A. Screen captures from the Avizo software displaying the final alignment of the MT 1-5 proximal articular surface renderings. B. Proximal MT 1-5 bases illustrated in anatomical alignment and forming a transverse arch that is higher medially and lower laterally (Adapted from Kelikian, A.S. and Sarrafian, S.K. eds., 2011. *Sarrafian's anatomy of the foot and ankle: descriptive, topographic, functional*. Lippincott Williams & Wilkins, pp 101.). C. A composite of the screen captures of the final MT 1-5 alignment (modelled after illustration B) from the Avizo software (A) to illustrate the proximal articular surface alignment to the adjacent MT articulating surfaces creating a transverse arch.

This orientation protocol ensured that reference axes were defined and standardized across bones as accurately as possible because the determination of cross-sectional properties can be sensitive to bone positioning (Carlson, 2005). The result was that each metatarsal rendering (e.g., each MT4) and its cross-sectional slices were comparably oriented in space (i.e., in similar orientations with respect to the x-, y-, and z-axes). Once the orientation protocol was applied, original volume data were resliced in the new alignment to match the new spatial coordinate system. Regions of interest (ROIs) from the diaphysis (i.e., 25%, 35%, 50% and 65% lengths) were selected as the basis of structural comparisons. Each MT was divided into 100 slices along its biomechanical length in an AVIZO protocol (fig. 2.5). In this procedure, slices are spaced at 1% length increments along the longitudinal axis of the metatarsal. All 100 slices were saved in .TIF format and the targeted ROIs (i.e., slices at 25%, 35%, 50% and 65% lengths; (Fig. 2.6) were subjected to further analyses in FIJI (ImageJ) with the Bone J plugin. When modelling long bones as beams, biomechanical length is more appropriate to use as a measure of length than maximum length since the former more accurately reflects the lever arm dimension of a long bone shaft (Carlson, 2005). Biomechanical length of an MT was measured as the distance between the landmarks that were placed on proximal and distal articular surfaces (Fig. 2.5). For MTs compared to other long bones such as the femur, biomechanical length differs little from the maximum length dimension. This mirrors physical measurement of biomechanical length on metatarsals (Marchi, 2005; Marchi, 2010, White et al., 2011).

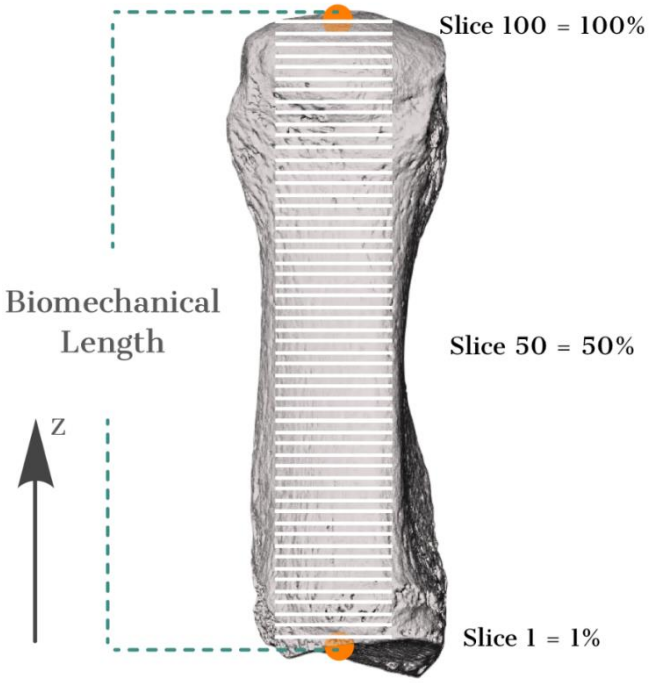


Figure 2.5. Biomechanical length and cross-sectional slices along the diaphysis of a metatarsal. White lines illustrate approximate diaphyseal locations of the 100 slices at regular intervals that were extracted as part of the orientation process (not to scale). Distance between consecutive slices is equivalent to 1% of biomechanical length thereby standardizing locations of ROIs across all metatarsals analyzed.

2.2.3 Metatarsal cross section analyses

Extracted metatarsal cross-sectional slices from 25%, 35%, 50% and 65% ROIs saved as .TIFF formatted files were exported into FIJI software for quantifying structural properties (Fig. 2.5).

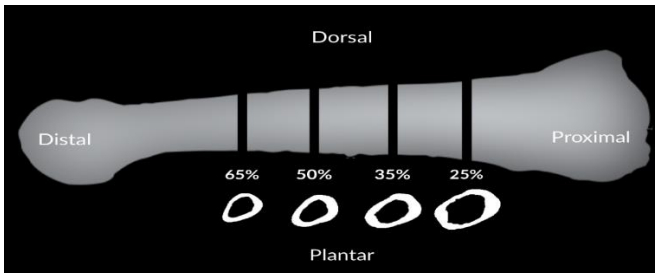
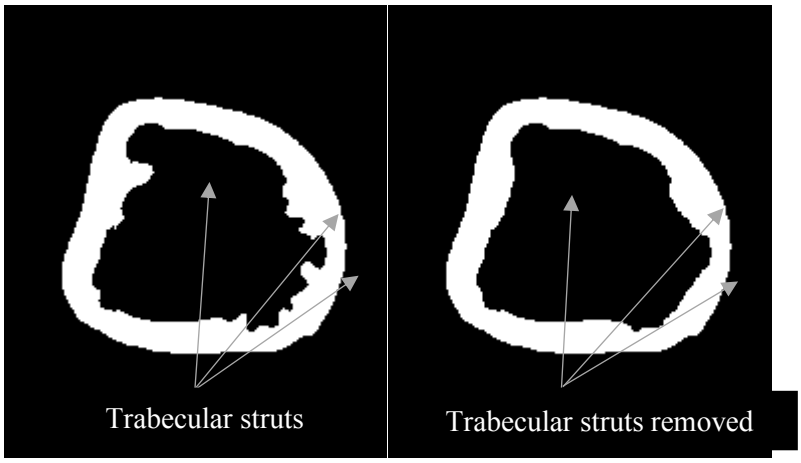


Figure 2.6. Lateral view of an idealized metatarsal illustrating representative cross sections and their locations for 25%, 35%, 50% and 65% regions of interest. The proximal end is towards the right of the image and corresponds to 0% length of the metatarsal while the distal end is towards the left and corresponds to 100% length of the metatarsal.

Once a cross section image was exported to FIJI, it followed a series of standardized steps that enabled calculation of cross-sectional geometric properties. First, the image was converted to an 8-bit image and binarized by setting the threshold to half the maximum grey value exhibited by bone pixels i.e.: 127 (Xing et al., 2018). The paintbrush tool in FIJI was used to remove any obvious trabecular struts from the endosteal border (Fig. 2.7) and to fill any intracortical porosities, e.g., those caused by a nutrient foramen (Carlson, 2005). Trabecular struts do not contribute to diaphyseal bending rigidity but could contribute to bone area. An increase in bone area without an increase in diaphyseal rigidity could create an error in data analyses. While this process of removing struts can be subjective, care was taken to be internally consistent in decision-making throughout the process of digitally removing struts at the endosteal border.



A. B.

Figure 2.7. Left hallucal metatarsal cross sections at the 65% region of interest (ROI) from an individual in the post-industrial South African sample (A) Cross section displaying portions of trabecular struts on the endosteal border. (B) The same cross section as illustrated in (A), but with the 'cleaned' endosteal border displayed after digitally removing trabecular struts using the paintbrush tool in FIJI software.

It is possible to confuse multiple intracortical porosities adjacent to each other at the endosteal border for separate trabeculae. To distinguish between trabeculae versus multiple intracortical porosities, the slice of interest was displayed in 3D on one screen,

as a guide on how much bone to remove from the 2D image on another screen (see Fig. 2.8).

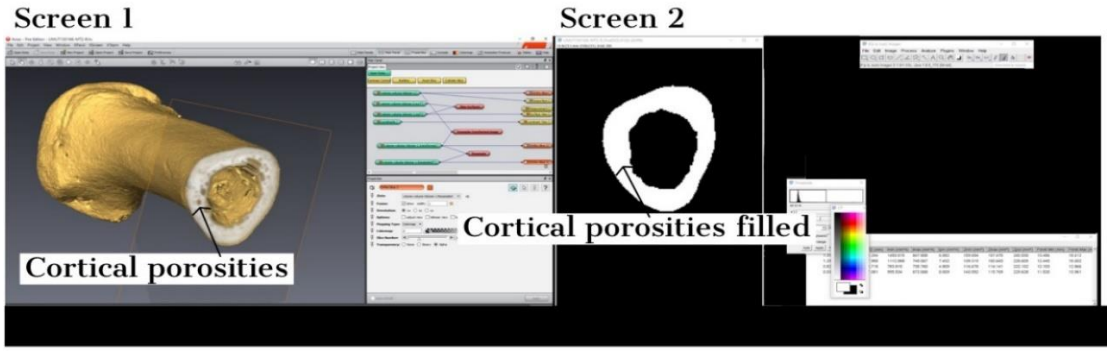


Figure 2.8. Workflow for identifying trabeculae and intracortical porosities. Screen 1 displays the MT rendering (using Avizo software) allowing for the adjacent slices to be viewed in 3D which helps to distinguish between trabecula versus bone partitions separating multiple intracortical porosities. Screen 2 displays an example of a binarized 8-bit 2D image from which trabecular struts are removed along the endosteal border and also an example of an intracortical porosity filled using the paintbrush tool in FIJI software.

Next, the Bone J plugin was used to define anatomical planes in the cross-sectional image. Specifically, the dorsal, plantar, medial and lateral surfaces of the cross section were assigned (Fig. 2.9).

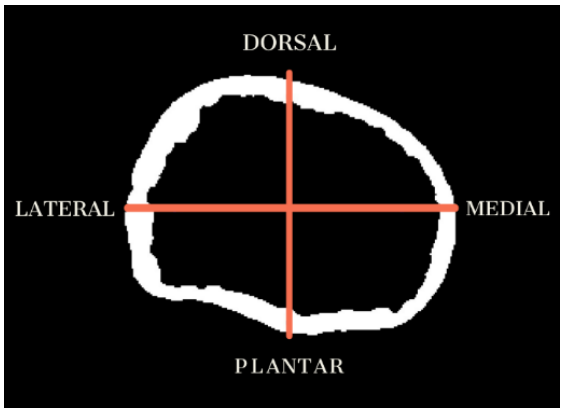


Figure 2.9. Left hallucal metatarsal cross section at the 65% ROI from an individual in the post-industrial South African sample. Image displays locations of dorsal, plantar, medial, and lateral surfaces.

After anatomical planes were defined for a cross section in the Bone J plugin, standard CSGP's were calculated (Doube et al., 2010). These are summarized in Table 2.7. Second moments of area, I_x and I_y, describe the resistance of long bone diaphysis to bending about mediolateral and dorsoplantar planes, respectively (Griffin and Richmond, 2005; Wei et al., 2017). Principle moments of area are calculated about the principal axes of a cross section and denote maximum (I_{max}) and minimum (I_{min}) bending rigidity. "A bone's ability to resist deformation, prior to failure is referred to as rigidity" (Ruff, 2018). Principle moments of area and second moments of area help to describe the directionality of resistance to bending loads within the MT diaphysis (Shaw and Stock, 2009).

The ratio of principle moments of area (I_{max}/I_{min}) provides a measure of cross-sectional shape or shape index (i.e., degree of circularity) of the diaphysis (Carlson, 2005; Saers et al., 2021). Section moduli, Z_x and Z_y describe bending strength of the diaphysis about mediolateral and dorsoplantar planes, respectively. "The strength of a bone is it's ability to resist failure or breaking" (Ruff, 2018).

Table 2.7: Description of cross-sectional geometric properties.

Cross section property	Mechanical relevance
Cross sectional area (CSA)	Correlate of compressive rigidity
Second moments of area about the x-axis (I_x)	Correlate of bending rigidity about the mediolateral axis
Second moments of area about the y-axis (I_y)	Correlate of bending rigidity about the dorsoplantar axis
Maximum second moments of area (I_{max})	Correlate of maximum bending rigidity
Minimum second moments of area (I_{min})	Correlate of minimum bending rigidity
Shape Ratio (I_{max}/I_{min})	Correlate of cross-sectional shape
Section modulus about the x-axis (Z_x)	Correlate of bending strength about the mediolateral axis in the elastic range
Section modulus about the y-axis (Z_y)	Correlate of bending strength about the dorsoplantar axis in the elastic range
Polar section modulus (Z_p)	Correlated of torsional and twice average bending strength

2.3 Analyses

Metatarsal CSGPs were standardised before conducting statistical analyses. The standardisation procedure employed and the statistical analyses process is discussed below.

2.3.1 Standardisation procedures

The preferable way to scale CSGPs is to standardize second moments of area (SMAs) for long bones to the product of body mass (kg) and bone length^2 (mm^2) and section moduli to the product of body mass (kg) and bone length (mm) (Ruff, 2018; Ruff, 2000; Ruff and Larsen, 2014). This is important since larger individuals would have larger bones that would be absolutely stronger or more rigid relative to smaller individuals. Scaling, therefore, allows one to calculate the strength and rigidity of a bone relative to a unit of standardisation. Unfortunately, estimated body masses of all three populations were not readily available or measurable for standardisation purposes. As a result, the historical scaling procedure of standardizing CSGPs to bone length to create dimensionless variables was utilized (Ruff, 1984). Thus, CSA was standardised to bone length^2; I_{max}, I_{min}, I_x, and I_y were standardised to bone length^4; and Z_{max}, Z_{min}, Z_p, Z_x, and Z_y were standardised to bone length^3 (Ruff, 1984). Values were then scaled for readability by multiplying them by either 10^6 (i.e.: CSA, Z_{max}, Z_{min}, Z_p, Z_x, Z_y x 10^6) or 10^9 (i.e., I_{max}, I_{min}, I_x, and I_y).

2.3.2 Statistical analyses

The forefoot was divided according to the high and low gear axis described by Bojsen-Møller (1979), i.e., high gear consists of MTs 1 and 2 while low gear consists of MTs 2, 3, 4 and 5. ROI's 25%, 35%, 50% and 65% diaphyseal length were selected. The mean of the aggregate of each ROI's CSGP was calculated to create a "whole shaft" CSGP value. For example, the mean of I_x for locations 25%, 35%, 50%, 65% diaphyseal length of MT1 per population was calculated to create a "whole shaft" I_x mean for MT1. This resembles the "whole shaft" approach used by Dowdeswell et al., (2017).

Box plots displaying medians, quartiles, and ranges were used to graphically compare CSGPs of high gear and low gear MTs between populations. Boxplot outliers were based on a default interquartile range value of 1.5. Line plots of the mean CSGPs for MTs 1-5 of each population were plotted for comparative purposes. Males and females were not separated in comparisons because of concerns over small sample sizes. Mann-Whitney U tests (two-sided alternative) were used to evaluate whether there were significant differences between high gear and low gear CSGPs across the three groups. Statistical significance was established with an alpha = 0.05, i.e., p-value < 0.05.

Python 3.10 (Python Software Foundation, USA), a general-purpose programming language with multiple statistics modules, was used for statistical analysis. Graphical plots were generated using the seaborn library (v.0.11.1) in Python. Seaborn is a library package installed in Python for making statistical graphics (Waskom, 2021). Python Scipy (v.1.6.3), an open-sourced software built on the NumPy extension of Python, was used for statistical tests and analyses.

CHAPTER 3 – RESULTS

High gear is formed by metatarsal (MT) heads one and two, while low gear is formed by MT heads two, three, four and five (Bojsen-Møller, 1979) as detailed in chapter 1 and 2. Instead of dividing the forefoot into the anatomical medial (MTs 1, 2 and 3) and lateral column (MTs 3 and 4), for the purpose of this study, the forefoot was divided according to the high and low gear axis, i.e., high gear consists of MTs 1 and 2 while low gear consists of MTs 2, 3, 4 and 5.

The combined population sample results are presented first, followed by the high gear and low gear and finally the individual MT diaphyseal CSGPs.

3.1 Combined population metatarsal diaphyseal CSGPs

When combining all three populations, CSGPs of the high gear MTs were significantly higher than the low gear MTs. This is primarily due to the larger combined population of post-industrial individuals of South Africa and the LSA southern Africans, compared to the Jomon of Japan population, driving the overall pattern (Fig. 3.1)

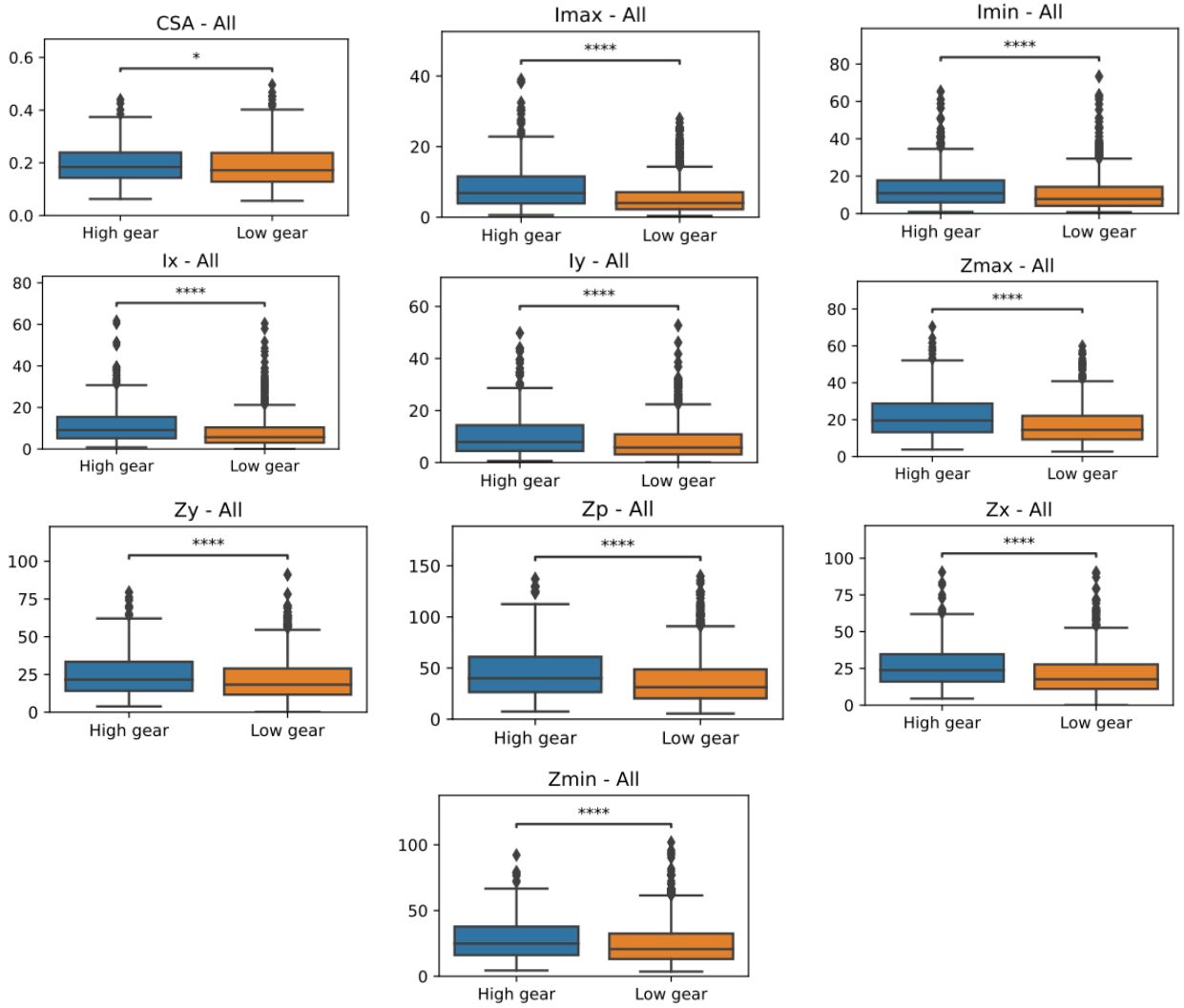


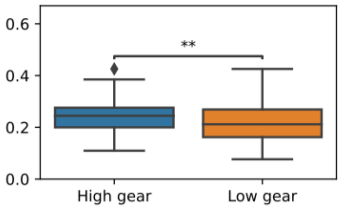
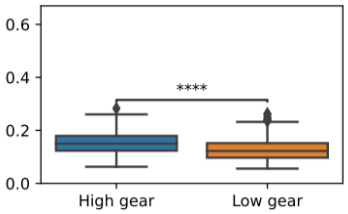
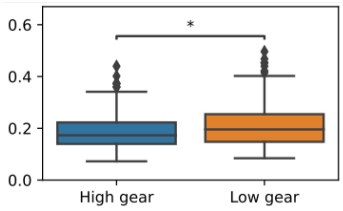
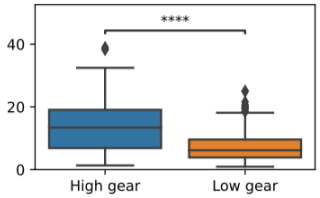
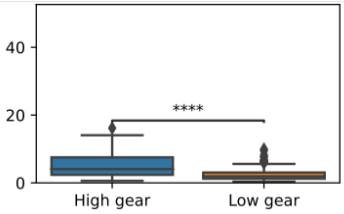
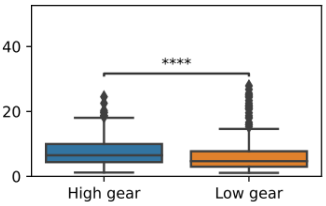
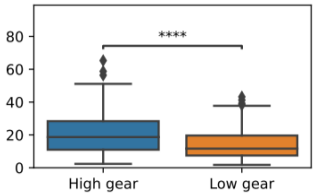
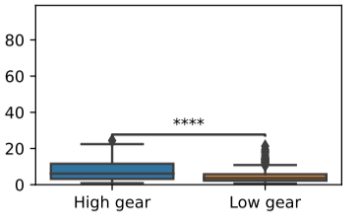
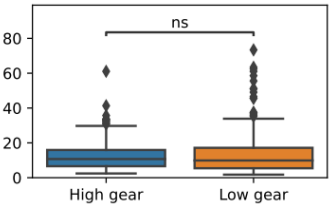
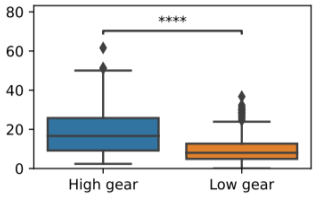
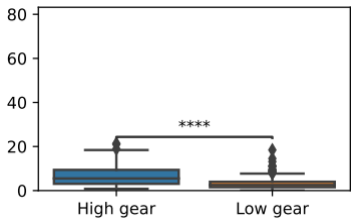
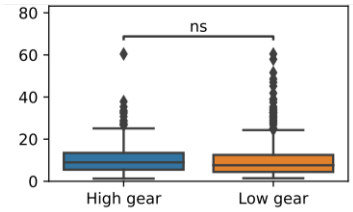
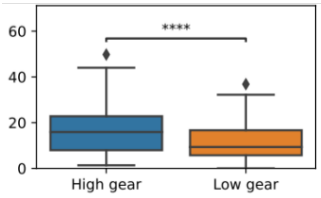
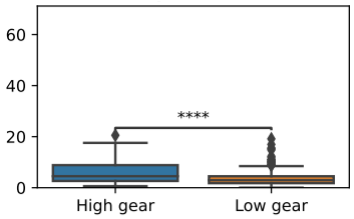
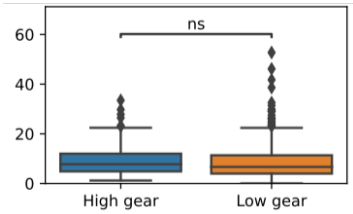
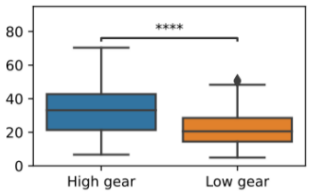
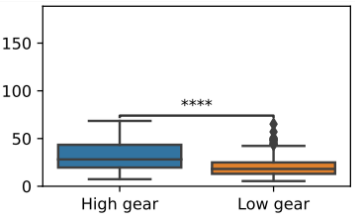
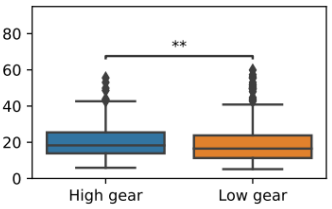
Figure 3.1. Boxplots (median, quartile, and range) of high gear (MT1 and 2) and low gear (MT2, 3, 4 and 5) mean MT CSGPs for the combined post-industrial individuals of South Africa, LSA southern Africans and the Jomon of Japan. Values displayed on the y-axis are dimensionless after standardisation by bone length i.e.: CSA is standardised to bone length^2; I_{max}, I_{min}, I_x, I_y are standardised to bone length^4; and Z_{max}, Z_{min}, Z_p, Z_x, and Z_y are standardised to bone length^3. Boxplot whiskers are based on an interquantile range value set to the default of 1.5. Diamond shaped plots outside of the boxplot whiskers represent the outliers. Stars are linked to the p-value obtained by performing a Mann-Whitney U test two-sided and represent the following:

p-value >= 0.05: 'ns' (not significant), p-value < 0.05: '*', p-value < 0.01: '**', p-value < 0.001: '***', p-value < 0.0001: '****'CSA, cross sectional area; I_x ,Second moments of area about the x-axis; I_y , Second moments of area about the y-axis; I_{max} ,Maximum second moments of area; I_{min}, Minimum second moments of area; I_{max}/I_{min}, Shape Ratio; Z_x , Section modulus about the x-axis.

3.2 High gear and low gear metatarsal diaphyseal CSGPs

The standardised CSGPs for the high gear and low gear MTs of the post-industrial individuals of South Africa, Later Stone Age (LSA) South Africans and the Jomon of Japan are presented in Fig. 3.2. The CSGPs of the high gear MTs (MTs 1 and 2) were significantly higher than those of the low gear MTs (MTs 2, 3, 4 and 5) in the post-industrial individuals of South Africa and the LSA foragers of South Africa.

Except for CSA, I_{max} and Z_{max}, there were no significant differences in CSGPs between high gear and low gear MTs in the Jomon of Japan. The low gear MTs had significantly higher CSA but significantly lower I_{max} and Z_{max} than the high gear MTs in the Jomon of Japan. The CSGPs of the post-industrial individuals and the LSA southern Africans were similar with regards to the significance in differences between the high and low gear MTs. The Jomon of Japan, therefore, displayed a different pattern in diaphyseal structure between high and low gear MTs when compared to the post-industrial individuals and the LSA foragers of South Africa.

CSGP	Post-Industrial individuals of South Africa	Later Stone Age Southern Africans	Jomon of Japan
CSA			
I_{max}			
I_{min}			
I_x			
I_y			
Z_{max}			

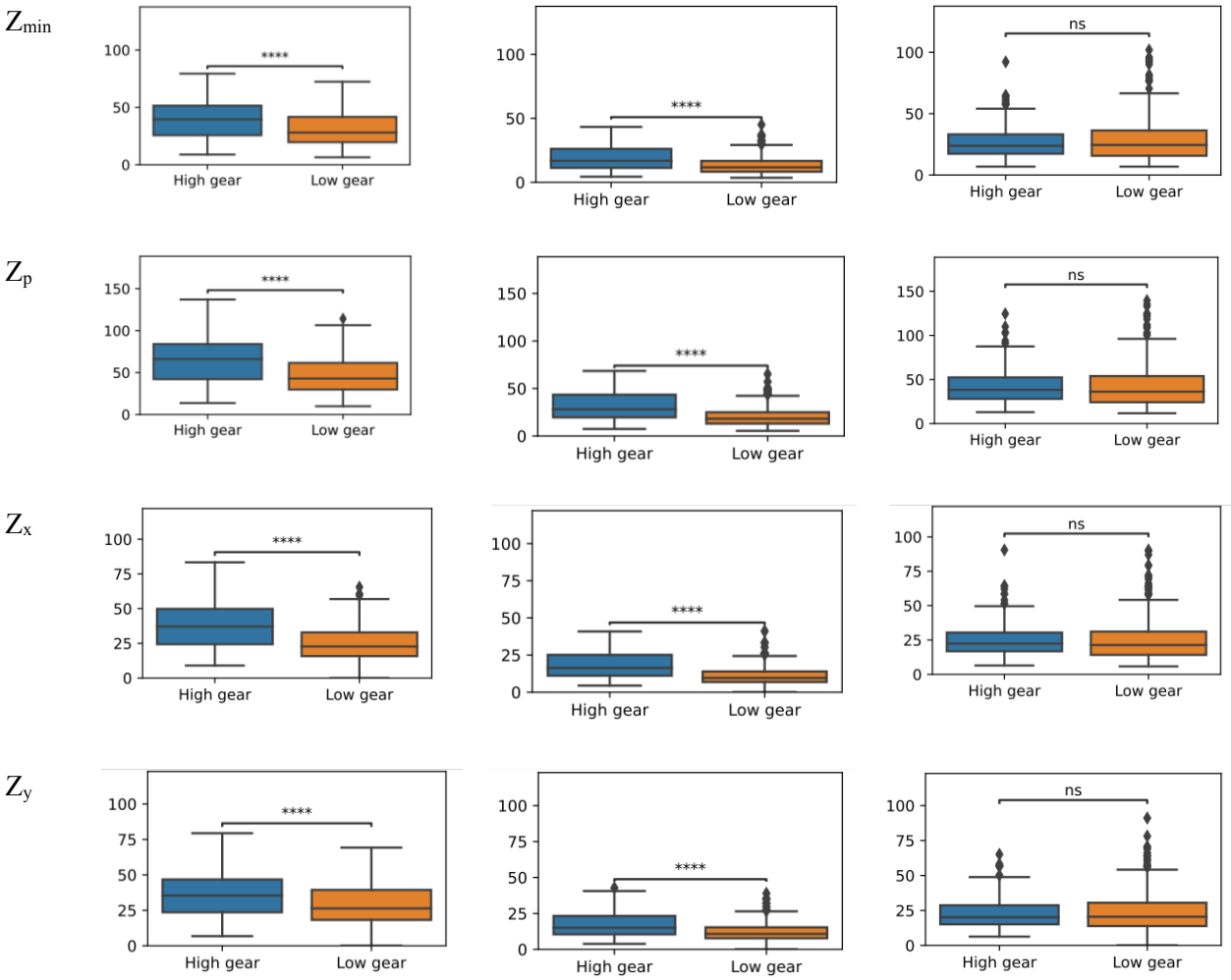


Figure 3.2. Boxplots (median, quartile, and range) of high gear (MT1 and 2) and low gear (MT2, 3, 4 and 5) mean MT CSGPs for the post-industrial individuals of South Africa, LSA foragers of South Africa and the Jomon of Japan. Variables displayed on the y-axis are dimensionless since they are standardised by bone length. Boxplot whiskers are based on an interquantile range value set to the default of 1.5. Diamond shaped points outside of boxplot whiskers represent outliers. Stars above brackets in the plots refer to statistically significant p-values associated with Mann-Whitney U test (two-sided) results. The number of stars corresponds to the following:

p-value >= 0.05: 'ns' (not significant), p-value < 0.05: '*', p-value < 0.01: '**', p-value < 0.001: '***', p-value < 0.0001: '****'CSA, cross sectional area; I_x ,Second moments of area about the x-axis; I_y , Second moments of area about the y-axis; I_{max} ,Maximum second moments of area; I_{min}, Minimum second moments of area; I_{max}/I_{min}, Shape Ratio; Z_x , Section modulus about the x-axis.

3.3 Individual metatarsal diaphyseal CSGPs

The mean CSGPs for MTs 1-5 of post-industrial individuals of South Africa, LSA Southern Africans and the Jomon of Japan are shown in Fig. 3.3. The CSGPs of MT5 differ far less from MT1 in the Jomon from Japan compared to the LSA Southern Africans and post-industrial individuals of South Africa who differ significantly, with the highest CSGPs for MT1. The difference in the CSGPs between MT1 and 2 is subtle in the Jomon of Japan yet very distinct in the LSA southern Africans and post-industrial individuals of South Africa.

3.3.1 Metatarsal diaphyseal rigidity

Dorso-plantar (D-P) rigidity (I_x) of Jomon of Japan MTs 1-5 were similar. By comparison, D-P rigidity of MT1 was higher than that of the other MTs in the Later Stone Age southern Africans and post-industrial individuals of South Africa. Specifically, D-P rigidity (I_x) of the LSA southern Africans and post-industrial individuals of South Africa displayed a similar pattern to one another in that their MT1 exhibited the highest D-P rigidity, MT5 the lowest, and MT 2, 3 and 4 were similar.

Jomon of Japan MT1 and 5 exhibited higher mediolateral rigidity (I_y) than MTs 2-4 with MT4 being the third highest. M-L rigidity of the LSA southern Africans and post-industrial individuals of South Africa displayed a similar pattern in that MT1 exhibited the highest M-L rigidity followed by MT5 and then MT4.

3.3.2 Metatarsal diaphyseal strength

D-P strength (Z_x) of Jomon of Japan MT1 and 4 were similar to each other, yet less than MT 2, 3 and 5, while MT 3 is the highest. D-P strength of MT1 is the highest, while MT5 is the lowest in the LSA southern Africans and post-industrial individuals of South Africa.

M-L strength (Zy) of MT5 is the highest amongst the Jomon of Japan MTs, while MT1 of the LSA southern Africans and post-industrial individuals of South Africa displayed the highest M-L strength.

The torsional and average bending strength (Z_p) of MT1 in the LSA southern Africans and post-industrial individuals of South Africa is significantly higher than those of the other MTs. However, in the Jomon of Japan, MT5 is the highest, followed by MT1 with MT 2-4 having similar strength values.

3.3.3 Metatarsal diaphyseal shape ratio

There is a general pattern of decrease in MT diaphyseal circularity from medial to lateral among the LSA southern Africans, post-industrial individuals of South Africa and Jomon of Japan. High gear MT1 and 2 are the most circular (closer to 1) while MT's 3-5 are more asymmetrical.

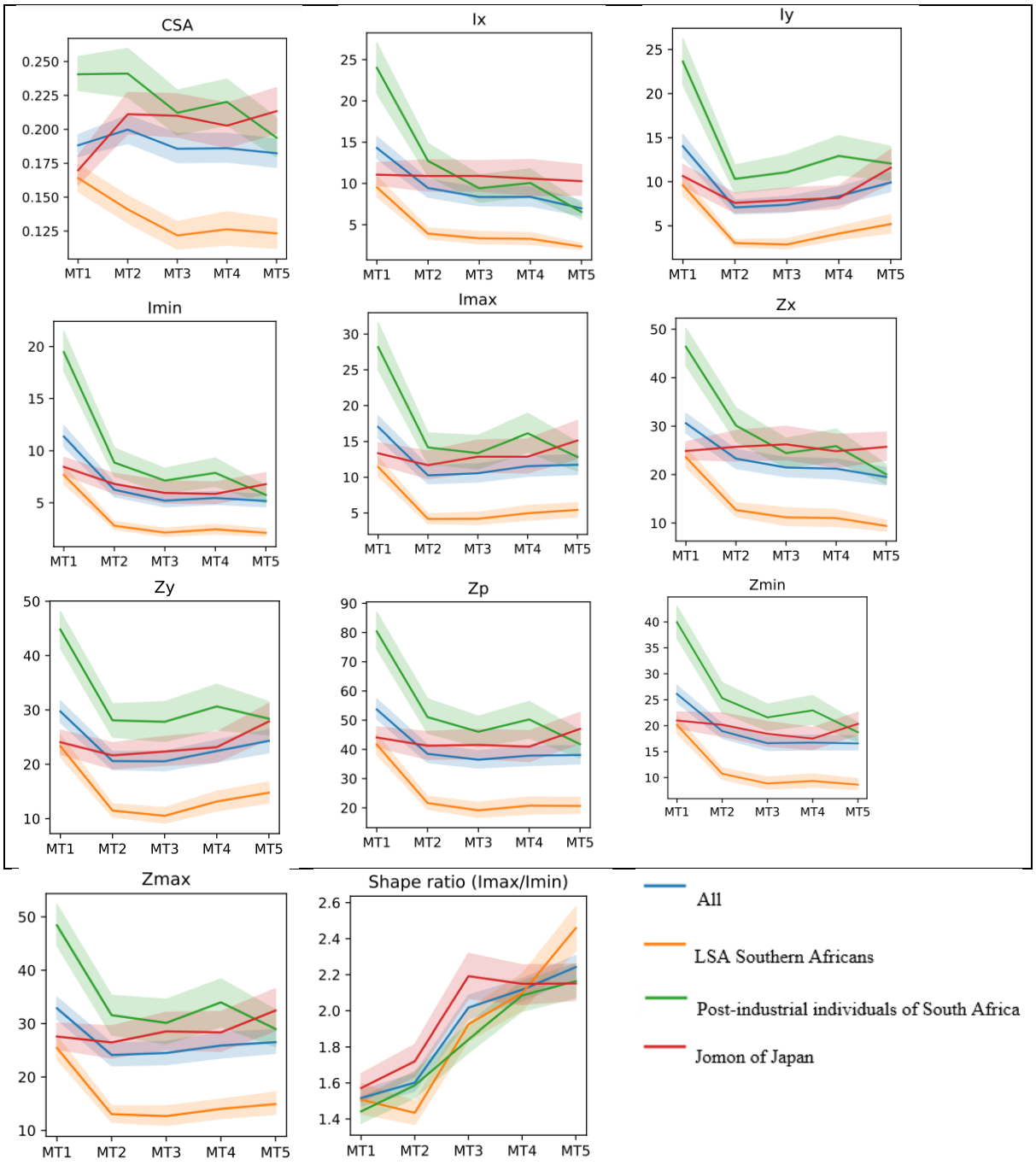


Figure 3.3. Line plots of the mean CSGPs for MTs 1-5 of the post-industrial individuals of South Africa, Later Stone Age southern Africans and the Jomon of Japan. Values displayed on the y-axis are after standardisation by bone length i.e.: CSA is standardised to bone length^2; I_{max}, I_{min}, I_x, I_y are standardised to bone length^4; and Z_{max}, Z_{min}, Z_p, Z_x, and Z_y are standardised to bone length^3. The shaded region surrounding each line represents a 95% confidence interval.

p-value >= 0.05: 'ns' (not significant), p-value < 0.05: '*', p-value < 0.01: '**', p-value < 0.001: '***', p-value < 0.0001: '****'CSA, cross sectional area; I_x ,Second moments of area about the x-axis; I_y , Second moments of area about the y-axis; I_{max} ,Maximum second moments of area; I_{min}, Minimum second moments of area; I_{max}/I_{min}, Shape Ratio; Z_x , Section modulus about the x-axis.

CHAPTER 4 – DISCUSSION AND CONCLUSION

4.1 Discussion

The aim of the current study was to investigate whether lateral forefoot loading, depicted by higher strength and rigidity of MT 2-5 (low gear MTs) in relation to MT 1-2 (high gear MTs), occurred at push-off in the selected human populations. The objective being to assess whether forefoot loading varies between individuals and population groups, or whether it consistently favours high gear as depicted in theoretical foot function models (Dananberg, 2000; Durrant and Chockalingam, 2009; Fuller, 2000; Harradine and Bevan, 2009; Hicks, 1954). As predicted, forefoot loading during the propulsion phase of gait is variable when considering the three samples investigated in the present study. The results indicate that the Jomon lateral forefoot is relatively more strongly reinforced against loading compared to their medial forefoot when assessing this pattern against those exhibited by the post-industrial individuals of South Africa and the LSA southern Africans. These latter groups appear to have loaded their medial forefoot relatively more frequently than their lateral forefoot given greater disparities in reinforcement observed between their sets of MTs.

The results obtained for the Jomon population agree with a recent study conducted by Hagihara and Nara (2018) who found the lateral forefoot of a prehistoric Jomon population to have high loading. The results obtained for the post-industrial individuals of South Africa and the LSA Southern Africans is in accordance with theoretical models of foot function that emphasise medial weight transfer mostly to the first metatarsal-phalangeal joint and hallucal phalangeal joints to stabilize the foot through the windlass mechanism. This variation supports studies that conclude that medial longitudinal arch stiffening that occurs during stance phase is not only reliant on the plantar fascia (through high gear push-off activating the windlass mechanism) but instead on a load sharing system comprised of the osseus elements of the arch, the achilles tendon, the plantar ligaments, and the intrinsic foot muscles (Kelly et al., 2014; Kelly et al., 2012; Kirby, 2017; Pataky et al., 2008). If the windlass mechanism is not required to stiffen the medial longitudinal arch, then forefoot lateral to medial weight transfer is not required either, since theoretical models state that one leads to the other (Hicks, 1953). The Jomon of Japan may have relied less on the windlass mechanism to stiffen the medial longitudinal

arch and more on the load sharing system of the foot for an energy efficient push-off. The Jomon of Japan's mobility may have required more direct central nervous system control of the plantar intrinsic and extrinsic muscles rather than the passive tension (non-central nervous system control) created by the plantar fascia and plantar ligaments (windlass mechanism), to stiffen the foot. This may have been a selective advantage to the Jomon of Japan as they navigated their uneven mountainous and coastal terrain.

Considering high gear push-off as typical and contemporary human-like (Aiello et al., 1990; Bojsen-Møller and Lamoreux, 1979; Haile-Selassie et al., 2012) is a conjecture that allows for a convenient interpretation of foot kinematics and evolution. For example, the "high gear paradigm" makes it convenient to explain why a non-divergent first ray is preferred for striding bipedalism. High gear push-off (only possible with an aligned first ray) activates the windlass mechanism, stiffening the foot resulting in energy efficient propulsion (Bojsen-Møller, 1979; Bojsen-Møller and Flagstad, 1976; Fauth et al., 2004; Hicks, 1954; Vogler and Bojsen-Møller, 2000). Using this reasoning, the presence of a divergent first ray suggests a non-striding bipedal gait when interpreting the fossil hominin foot record. The rationale being that a non-divergent first ray is required to activate the windlass mechanism to stiffen the foot for propulsion. However, BRT-VP-w/73 was a facultative biped yet had an abducted hallux (Haile-Selassie et al., 2012). *Ardipithecus ramidus* was a striding biped with an abducted first ray (Lovejoy et al., 2009). The "high gear paradigm" fails to explain how a foot becomes sufficiently stiffened for striding bipedalism in the presence of an abducted first ray.

Furthermore, the "high gear paradigm" makes it convenient to explain why MT1 in contemporary humans is relatively robust when compared to other apes. The reasoning being that higher strain magnitudes (caused by high gear push-off) stimulate deposition of new bone increasing its robusticity (Lieberman and Crompton, 1998; Lieberman et al., 2003, Ruff, 2018). However, forefoot loading at push-off in this study appeared to be lateral in the Jomon of Japan because MT5 had higher CSGP values relative to MT2-4 of the same population. Although this was the case, the Jomon of Japan's MT1 was still heavily built and reinforced analogous to that of the LSA Southern Africans who appeared to have medial forefoot loading at push-off. A robust MT1 can therefore be present in high gear or low gear push-off. Strength and rigidity of MT1 may not be due to high gear push-off and the windlass mechanism. This suggests that conclusions regarding push-off

patterns cannot be drawn from isolated fossil MTs. All five MTs are required to make accurate inferences on push-off patterns since MT robusticity is relative to other MTs of the same foot. Relative strengths and rigidities across all 5 MTs would be the minimum amount of information to determine the push-off pattern of a pedal fossil. Since hominin foot fossils are often fragmentary it is unlikely that all 5 MTs of the same foot will always be available. It would therefore be helpful, in a future study, to calculate the mean MT1, MT2, MT3, MT4, and MT5 strength and rigidities and then to add a standard deviation to create a threshold value for each MT. This threshold value could then be used to analyse isolated MTs to help interpret forefoot loading patterns at push-off.

Additionally, the "high gear paradigm" is used to describe why the contemporary human hallucal distal phalanx is robust compared to African apes, displays axial torsion in the coronal plane and is laterally angled proximo-distally (DeSilva et al., 2019). The author of the present study through personal observation as a clinical podiatrist has observed that the hallux, given its overall dimensions, invariably would be loaded to varying degrees, in both high and low gear push-off (Fig. 4.1). Similarly, Crompton and colleagues (2010) cited an example of a clinically normal individual displaying peak plantar pressures under the lateral mid-foot, and metatarsal head (MH) 2-4 and the hallux, with no lateral-to-medial movement of the centre of pressure. These pedography results suggest low gear push-off with the hallux loaded. High gear push-off may therefore not explain why the distal phalanx is robust since the distal phalanx is loaded during high or low gear. It also does not provide an explanation for the distal hallucal phalanx being laterally deviated since known bipedal distal phalanges of australopiths, Early Pleistocene *Homo* and the Middle Pleistocene Dinaledi sample exhibit minimal lateral deviation of the hallucal distal phalanx when compared to recent humans (Pastoors and Lenssen-Erz, 2021). Furthermore, the MT5 of *H. erectus* (D4058) *and H. naledi* (UW.101-1439, UW.101-518) exhibited a more African ape-like uniform rigidity along the diaphysis (Dowdeswell et al., 2017), suggesting the absence or less reliance on a windlass mechanism in these individuals due to analogy with African apes that do not have a lateral to medial forefoot weight transfer initiating the windlass mechanism during high gear push-off.

In conclusion, the "high gear paradigm" of which the windlass mechanism is a key component, fails as a model to explain why hominins have a non-divergent first ray, why MT1 in contemporary humans is relatively robust when compared to other apes, why

contemporary human hallucal distal phalanx is robust compared to African apes, displays axial torsion in the coronal plane and is laterally angled proximo-distally. Compounding its failure further, it is not even known as to when during hominin evolution the windlass mechanism emerged since “components that make up the windlass mechanism are poorly preserved in the fossil record” (Griffin et al.,2015). In essence, the windlass mechanism activated by high gear push-off, as described by Hicks (1954), is too narrowly attributed.

Forefoot loading during push-off is variable. Sufficient stiffening of the foot for push-off does not only rely on the windlass mechanism. Striding bipedalism does not necessarily require lateral to medial forefoot loading in preparation for push-off.

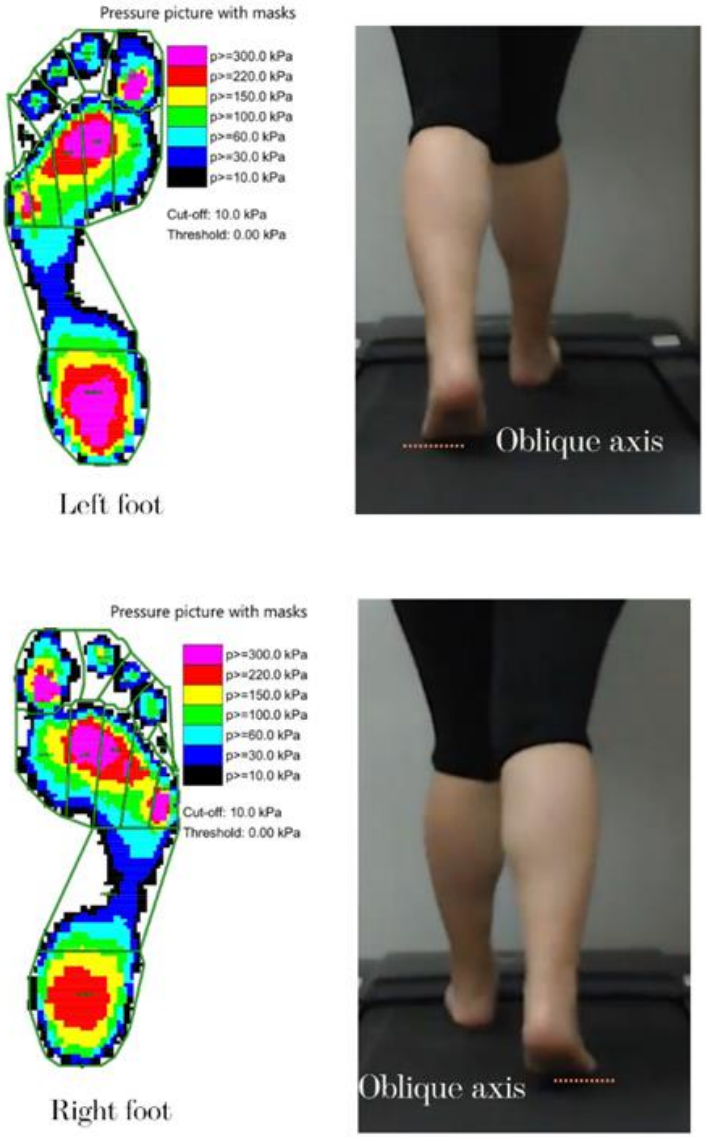


Figure 4.1. Pedography using the Novel-emed ® system and kinematic video gait analyses of a contemporary human's unshod feet displaying low gear push-off. The Novel-emed scanner is a common way to measure plantar pressures and is repeatable (Bryant et al., 2000; Hayafune et al., 1999; Putti et al., 2008; Maetzler et al.,2010; Jacob, 2001) The individual was asymptomatic and attended the Family Podiatry Centre in Singapore for a general check-up. The image is an average of three scans per foot taken using the repeatable two-step technique (McPoil et al., 1999). Plantar peak pressures of 220 kPa (red) to 300 kPa (pink) during push-off occurred on MH 2, 3, 4 and 5 indicating low gear push-off. At the same time, the halluces also display a plantar peak pressure of 300 kPa (pink) whereas the first metatarso-phalangeal joint do not.

This study has limitations. While "CSGP's are strongly related to relative rigidity and strength *in vivo*" (Ruff et al., 2006), there are many other factors that can affect bone form (Bae et al., 2012; Carlson and Marchi, 2014; Duncan et al., 2002; Ferretti et al., 1996; Groll et al., 1999; Högler et al., 2003; Laskey et al., 2010; Martin et al., 1998; Pathria et al., 2016; van Rietbergen et al., 2002; Wehrli et al., 2006;). One of these factors are non-

mobility habitual activities (Carlson and Marchi, 2014). Modern Japanese people frequently sit on the floor in a position known as Seiza or Japanese style kneel sitting (Fukuichi and Sugamura, 2022; Moon et al., 2018). Both legs are flexed at the knee at a 180-degree angle so that both femurs lay on both lower legs and is frequently used in daily Japanese life (Demura and Uchiyama, 2005). This habitual activity is presumed to cause internal tibial torsion (Mullaji et al., 2008) which leads to an intoe'd gait. Internal tibial torsion with the resultant intoe'd gait loads the lateral column of the foot more relative to a normal out-toe'd gait and sitting on the feet loads the lateral forefoot directly. This could be another reason why this study and that of Hagihara and Nara (2018) found the Jomon of Japan to have higher robustness of the lateral forefoot. Further investigation, incorporating larger contemporaneous population groups from different geographical locations, with known cultural non-mobility activities affecting the lower limb, is needed to confirm this.

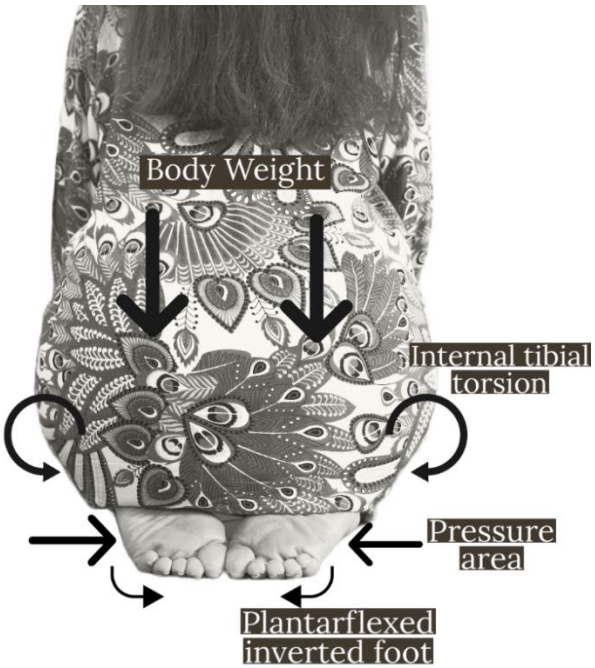


Figure 4.2. Seiza or Japanese style kneel sitting (Fukuichi and Sugamura, 2022; Moon et al., 2018). A habitual non-mobility activity that plantarflexes and forcefully adducts the foot under the individual's body weight causing internal tibial torsion.

Furthermore, CSGP were standardized to bone length to various powers (Ruff, 2018). It is preferable to control for differences in body size since it affects mechanical loads and influences factors like muscle size that in turn create mechanical loads (Ruff, 2018). This study did not account for sexual dimorphism as did Hagihara and Nara (2018), who found Jomon women to have higher lateral forefoot loading than men. Whole shaft means for CSGPs were used as the basis of interindividual comparisons instead of comparing each slice across MTs. The latter may be useful to explore in future studies since it addresses different questions. Whole shaft means were chosen in this study so that comparisons could be made between entire MT diaphysis. Comparing each slice across MTs was beyond the scope of this study's objectives. The sample size only included 3 populations. It would be beneficial for future studies to include additional population groups to investigate whether they possibly display evidence for low gear push-off similar to the Jomon from Japan. The LSA population was from one rock shelter site and may not be representative of the whole LSA population of southern Africa.

4.2 Conclusions

Push-off is variable and can occur in either high or low gear. In this study, high gear push-off occurred more frequently (both LSA southern Africans and Post-industrial individuals from South African) than low gear push-off (Jomon of Japan). Nonetheless, low gear push-off, indicated by relative strength and rigidity of MT2-5, still occurred in one population. The theoretical model of foot function is not in agreement with this study, with the current pedal fossil record or with anecdotal clinical pedography scans. It is probable that the foot is a highly adaptable structure that responds to different substrates and conditions to maintain a level of mobility that is energy efficient and minimises tissue stress.

REFERENCE LIST

Aiello, R.A. in E.A., Aiello, L., Dean, C. (1990). *An Introduction to Human Evolutionary Anatomy*. Academic Press.

Akazawa T. (1999). "Regional variation in Jomon hunting-fishing-gathering societies", in Omoto K, (eds), *Interdisciplinary perspectives on the origins of the Japanese*. Kyoto: International Research Center for Japanese Studies, pp. 223–231.

Akins, J.S., Keenan, K.A., Sell, T.C., Abt, J.P., Lephart, S.M. (2012), "Test–retest reliability and descriptive statistics of geometric measurements based on plantar pressure measurements in a healthy population during gait", *Gait & Posture* **35**, 167–169.

Aquino, A., Payne, C. (2001), "Function of the windlass mechanism in excessively pronated feet". *Journal of the American Podiatric Medical Association* **91**, 245–250.

Bae, W.C., Chen, P.C., Chung, C.B., Masuda, K., D'Lima, D., Du, J. (2012), "Quantitative ultrashort echo time (UTE) MRI of human cortical bone: correlation with porosity and biomechanical properties". *Journal of Bone and Mineral Research* **27**, 848–857.

Barak, M.M. (2019), "Bone modeling or bone remodeling: That is the question". *American journal of physical anthropology* **172**, 153–155.

Bass, S.L., Saxon, L., Daly, R.M., Turner, C.H., Robling, A.G., Seeman, E., Stuckey, S. (2002), "The Effect of Mechanical Loading on the Size and Shape of Bone in Pre-, Peri-, and Postpubertal Girls: A Study in Tennis Players". *Journal of Bone and Mineral Research* **17**, 2274–2280.

Bates, K.T., Collins, D., Savage, R., McClymont, J., Webster, E., Pataky, T.C., D'Aout, K., Sellers, W.I., Bennett, M.R., Crompton, R.H. (2013), "The evolution of compliance in the human lateral mid-foot". *Proceedings of the Royal Society B: Biological Sciences*, **280**(1769), 20131818.

Bojsen-Møller, F., (1979), "Calcaneo-cuboid joint and stability of the longitudinal arch of the foot at high and low gear push off". *Journal of Anatomy* **129**(Pt1), 165–176.

Bojsen-Moller, F., Flagstad, K.E., (1976), “Plantar aponeurosis and internal architecture of the ball of the foot”. *Journal of Anatomy* **121**, 599–611.

Bojsen-Møller, F., Lamoreux, L., (1979), Significance of Free Dorsiflexion of the Toes in Walking. *Acta Orthopaedica Scandinavica* **50**(4), 471–479.

Bondioli, L., Bayle, P., Dean, C., Mazurier, A., Puymerail, L., Ruff, C., Stock, J.T., Volpato, V., Zanolli, C., Macchiarelli, R. (2010), “Technical note: Morphometric maps of long bone shafts and dental roots for imaging topographic thickness variation”. *American Journal of Physical Anthropology: The Official Publication of the American Association of Physical Anthropologists* **142**(2), 328-334.

Bryant, A., Tinley, P., Singer, K., (2000), “Normal values of plantar pressure measurements determined using the EMED-SF system”. *Journal of the American Podiatric Medical Association* **90**(6), 295–299.

Carlson, K.J. (2005), “Investigating the form-function interface in African apes: Relationships between principal moments of area and positional behaviors in femoral and humeral diaphyses”. *American Journal of Physical Anthropology: The Official Publication of the American Association of Physical Anthropologists* **127**(3), 312-334.

Carlson, K.J. (2014), “Linearity in the Real World: An Experimental Assessment of Nonlinearity in Terrestrial Locomotion”, *Reconstructing mobility: environmental, behavioral, and morphological determinants*, pp.253-271.

Carlson, K.J., Grine, F.E., Pearson, O.M. (2007), “Robusticity and sexual dimorphism in the postcranium of modern hunter-gatherers from Australia”. *American Journal of Physical Anthropology: The Official Publication of the American Association of Physical Anthropologists*, **134**(1), 9-23.

Carlson, K.J., Judex, S. (2007), “Increased non-linear locomotion alters diaphyseal bone shape”. *Journal of Experimental Biology* **210**(17), 3117–3125.

Carlson, K.J., Marchi, D. (2014), “Introduction: Towards Refining the Concept of Mobility”, in Carlson, K.J., Marchi, D. (eds.), *Reconstructing Mobility*: *Environmental, behavioral, and morphological determinants*, Springer US, pp. 1–11.

Chirchir, H., Kivell, T.L., Ruff, C.B., Hublin, J.-J., Carlson, K.J., Zipfel, B., Richmond, B.G. (2015), "Recent origin of low trabecular bone density in modern humans". *Proceedings of the National Academy of Sciences*, **112**(2), 366-371.

Clough, J.G. (2005) "Functional hallux limitus and lesser-metatarsal overload". *Journal of the American Podiatric Medical Association* **95**(6), 593–601.

Collier, S. (1989), "The influence of economic behaviour and environment upon robusticity of the post-cranial skeleton: a comparison of Australian Aborigines and other populations". *Archaeology in Oceania* **24**(1), 17–30.

Crompton, R.H., Pataky, T.C., Savage, R., D'Août, K., Bennett, M.R., Day, M.H., Bates, K., Morse, S., Sellers, W.I. (2012), "Human-like external function of the foot, and fully upright gait, confirmed in the 3.66 million year old Laetoli hominin footprints by topographic statistics, experimental footprint-formation and computer simulation". *Journal of the Royal Society Interface* **9**(69), 707–719.

Crompton, R.H., Sellers, W.I., Thorpe, S.K. (2010) "Arboreality, terrestriality and bipedalism". *Philosophical Transactions of the Royal Society of London B: Biological Sciences* **365**(1556), 3301–3314.

D'Aout, K., Pataky, T., De Clercq, D., Aerts, P. (2009), "The effects of habitual footwear use: Foot shape and function in native barefoot walkers". *Footwear Science* **1**(2), 81-94.

D'Août, K., Vereecke, E., Schoonaert, K., De Clercq, D., Van Elsacker, L., Aerts, P. (2004), "Locomotion in bonobos (Pan paniscus): differences and similarities between bipedal and quadrupedal terrestrial walking, and a comparison with other locomotor modes". *Journal of Anatomy* **204**(5), 353–361.

Dananberg, H. (2000), "Sagittal plane biomechanics". American Diabetes Association. *Journal of the American Podiatric Medical Association* **90**(1), 47–50.

Davies, T.G. and Stock, J.T. (2014), "Human Variation in the Periosteal Geometry of the Lower Limb: Signatures of Behaviour Among Human Holocene Populations", in K.J. Carlson and D. Marchi (eds) *Reconstructing Mobility*. Springer US, pp. 67–90.

Dayal, M.R., Kegley, A.D.T., Štrkalj, G., Bidmos, M.A., Kuykendall, K.L. (2009), "The history and composition of the Raymond A. Dart Collection of Human Skeletons at the

University of the Witwatersrand, Johannesburg, South Africa", *American Journal of Physical Anthropology: The Official Publication of the American Association of Physical Anthropologists* **140**(2), 324-335.

Dayal, M.R., Spocter, M.A., Bidmos, M.A. (2008), "An assessment of sex using the skull of black South Africans by discriminant function analysis", *HOMO* **59**(3), 209–221.

Demura, S. and Uchiyama, M. (2005), "Effect of Japanese sitting style (seiza) on the center of foot pressure after standing", *Journal of physiological anthropology and applied human science*, **24**(2), 167-173.

DeSilva, J., McNutt, E., Benoit, J., Zipfel, B. (2019), "One small step: a review of Plio-Pleistocene hominin foot evolution", *American journal of physical anthropology* **168**, 63–140.

DeSilva, J.M. (2010), "Revisiting the "midtarsal break".", *American Journal of Physical Anthropology: The Official Publication of the American Association of Physical Anthropologists* **141**(2), 245-258.

DeSilva, J.M., Holt, K.G., Churchill, S.E., Carlson, K.J., Walker, C.S., Zipfel, B., Berger, L.R., (2013), "The Lower Limb and Mechanics of Walking in Australopithecus sediba", *Science* **340**(6129), 1232999.

Dingwell, J.B., Cusumano, J.P., Cavanagh, P.R., Sternad, D. (2000), "Local Dynamic Stability Versus Kinematic Variability of Continuous Overground and Treadmill Walking". *Journal of Biomechanical Engineering* **123**(1), 27–32.

Doube, M., Kłosowski, M.M., Arganda-Carreras, I., Cordelières, F.P., Dougherty, R.P., Jackson, J.S., Schmid, B., Hutchinson, J.R., Shefelbine, S.J. (2010), "BoneJ: free and extensible bone image analysis in ImageJ", *Bone* **47**(6), 1076–1079.

Dowdeswell, M.R., Jashashvili, T., Patel, B.A., Lebrun, R., Susman, R.L., Lordkipanidze, D., Carlson, K.J. (2017), "Adaptation to bipedal gait and fifth metatarsal structural properties in Australopithecus, Paranthropus, and Homo". *Comptes Rendus Palevol* **16**(5-6), 585–599.

Ducher, G., Courteix, D., Même, S., Magni, C., Viala, J.F., Benhamou, C.L. (2005), "Bone geometry in response to long-term tennis playing and its relationship with muscle

volume: A quantitative magnetic resonance imaging study in tennis players", *Bone* **37**(4), 457–466.

Duncan, C.S., R. Blimkie, C.J., Kemp, A., Higgs, W., Cowell, C.T., Woodhead, H., Briody, J.N., Howman-Giles, R. (2002), "Mid-femur geometry and biomechanical properties in 15- to 18-yr-old female athletes", *Medicine & Science in Sports & Exercise* **34**(4), 673–681.

Durrant, B., Chockalingam, N. (2009), "Functional Hallux Limitus", *Journal of the American Podiatric Medical Association* **99**(3), 236–243.

Ericksen, M.F. (1976), "Cortical bone loss with age in three Native American populations", *American Journal of Physical Anthropology*, **45**(3), 443–452.

Fauth, A.R., Hamel, A.J., Sharkey, N.A. (2004), "In vitro measurements of first and second tarsometatarsal joint stiffness", *Journal of applied biomechanics* **20**(1), 14–24.

Ferretti, J.L., Capozza, R.F. and Zanchetta, J.R. (1996), "Mechanical validation of a tomographic (pQCT) index for noninvasive estimation of rat femur bending strength", *Bone*, **18**(2), 97–102.

Fukuichi, A. and Sugamura, G. (2022), "Sitting posture and moral impression formation: a focus on traditional Japanese sitting posture (Seiza)", *Journal of Physical Education and Sport*, ***2*** (2), 503-511.

Fuller, E.A. (2000), "The windlass mechanism of the foot. A mechanical model to explain pathology", *Journal of the American Podiatric Medical Association* **90**(1), 35–46.

Gomberg, B.R., Saha, P.K., Wehrli, F.W. (2005), "Method for Cortical Bone Structural Analysis from Magnetic Resonance Images1*". Academic Radiology* **12**(10), 1320–1332.

Griffin, N.L., Gordon, A.D., Richmond, B.G., Antón, S.C. (2008), "Cross-sectional geometric analysis of a foot bone assemblage from Mangaia, Cook Islands". *HOMO - Journal of Comparative Human Biology* **59**(1), 27–40.

Griffin, N.L., Miller, C.E., Schmitt, D., D'Août, K. (2015), "Understanding the evolution of the windlass mechanism of the human foot from comparative anatomy: Insights,

obstacles, and future directions", *American journal of physical anthropology*, **156**(1), 1-10.

Griffin, N.L. and Richmond, B.G. (2005), 'Cross-sectional geometry of the human forefoot', *Bone*, **37**(2), 253–260.

Groll, O., Lochmüller, E.-M., Bachmeier, M., Willnecker, J., Eckstein, F. (1999), "Precision and intersite correlation of bone densitometry at the radius, tibia and femur with peripheral quantitative CT", *Skeletal radiology* **28**, 696–702.

Habu, J. (1996), "Jomon Sedentism and Intersite Variability: Collectors of the Early Jomon Moroiso Phase in Japan", *Arctic Anthropology* **33**, 38–49.

Habu, J., Junko, H. (2004), *Ancient Jomon of Japan*, Cambridge University Press.

Hagihara, Y., Nara, T. (2018), "Diaphyseal cross-sectional geometry of the metatarsal bones in the Jomon population". *American Journal of Physical Anthropology* **166**(3), 745–752.

Haile-Selassie, Y., Saylor, B.Z., Deino, A., Levin, N.E., Alene, M., Latimer, B.M. (2012), "A new hominin foot from Ethiopia shows multiple Pliocene bipedal adaptations", *Nature* **483**(7391), 565–569.

Harcourt-Smith, W.E.H., Aiello, L.C. (2004), "Fossils, feet and the evolution of human bipedal locomotion", *Journal of Anatomy* **204**(5), 403–416.

Harcourt-Smith, W.E.H., Throckmorton, Z., Congdon, K.A., Zipfel, B., Deane, A.S., Drapeau, M.S.M., Churchill, S.E., Berger, L.R., DeSilva, J.M. (2015), "The foot of Homo naledi. *Nature Communications* **6**(1), 1-8.

Harradine, P., Bevan, L. (2009), "A Review of the Theoretical Unified Approach to Podiatric Biomechanics in Relation to Foot Orthoses Therapy", *Journal of the American Podiatric Medical Association* **99**(4), 317–325.

Hayafune, N., Hayafune, Y., Jacob, H.A.C (1999), "Pressure and force distribution characteristics under the normal foot during the push-off phase in gait". *The Foot* **9**(2), 88–92.

Hicks, J.H. (1954), "The mechanics of the foot: II. The plantar aponeurosis and the arch", *Journal of Anatomy*, **88**(Pt 1), 25

Högler, W., Blimkie, C.J.R., Cowell, C.T., Kemp, A.F., Briody, J., Wiebe, P., Farpour-Lambert, N., Duncan, C.S., Woodhead, H.J. (2003), "A comparison of bone geometry and cortical density at the mid-femur between prepuberty and young adulthood using magnetic resonance imaging". *Bone*, **33**(5), 771–778.

Hughes, J., Clark, P., Klenerman, L. (1990), "The importance of the toes in walking", *The Journal of bone and joint surgery. British volume*, **72**(2), 245-251.

Jacob, H.A.C. (2001), "Forces acting in the forefoot during normal gait – an estimate", *Clinical Biomechanics* **16**(9), 783–792.

Jashashvili, T., Dowdeswell, M.R., Lebrun, R., Carlson, K.J. (2015) "Cortical Structure of Hallucal Metatarsals and Locomotor Adaptations in Hominoids", *PLOS one* **10**(1), e0117905.

Jenkins, T., Bonner, P., Esterhuysen, A. (2007), *A Search for Origins: Science, history and South Africa's "Cradle of Humankind*". NYU Press.

Kallet, R.H. (2004), "How to Write the Methods Section of a Research Paper". *Respiratory care*, **49**(10), 1229-1232.

Kelikian, A.S., Sarrafian, S.K. (2011), *Sarrafian's anatomy of the foot and ankle: descriptive, topographic, functional*. Lippincott Williams & Wilkins.

Kelly, L.A., Cresswell, A.G., Racinais, S., Whiteley, R., Lichtwark, G. (2014), "Intrinsic foot muscles have the capacity to control deformation of the longitudinal arch". *Journal of The Royal Society Interface* **11**(93), 20131188.

Kelly, L.A., Kuitunen, S., Racinais, S., Cresswell, A.G. (2012) "Recruitment of the plantar intrinsic foot muscles with increasing postural demand". *Clinical biomechanics* **27**(1), 46–51.

Kirby, K.A. (2017), "Longitudinal arch load-sharing system of the foot". *Revista Española de Podología* **28**(1), e18–e26.

Kontulainen, S.A., Johnston, J.D., Liu, D., Leung, C., Oxland, T.R., McKay, H.A. (2008), "Strength indices from pQCT imaging predict up to 85% of variance in bone failure properties at tibial epiphysis and diaphysis", *Journal of Musculoskeletal Neuronal Interactions* **8**(4), 401–9.

L'Abbé, E.N., Loots, M., Keough, N. (2008), "The Matjes river rock shelter: A description of the skeletal assemblage", *South African Archaeological Bulletin* **63**(187) 61-68

Laskey, M.A., de Bono, S., Zhu, D., Shaw, C.N., Laskey, P.J., Ward, K.A., Prentice, A., (2010), "Evidence for enhanced characterization of cortical bone using novel pQCT shape software", *Journal of Clinical Densitometry* **13**(3), 247–255.

Latimer, B., Lovejoy, C.O. (1989), "The calcaneus of Australopithecus afarensis and its implications for the evolution of bipedality", *American Journal of Physical Anthropology*, **78**(3), 369-386.

Latimer, B. and Lovejoy, C.O. (1990) 'Metatarsophalangeal joints of Australopithecus afarensis', *American Journal of Physical Anthropology*, **83**(1), 13–23.

Lazenby, R.A. (1990) 'Continuing periosteal apposition II: The significance of peak bone mass, strain equilibrium, and age-related activity differentials for mechanical compensation in human tubular bones', *American Journal of Physical Anthropology*, **82**(4), 473–484.

Lieberman, D.E., Crompton, A.W. (1998), "Responses of bone to stress: constraints on symmorphosis", in Weibel, E.R., Weibel, E.F., Taylor, C.R., Bolis, L. (eds), *Principles of Animal Design: The Optimization and Symmorphosis Debate*, Cambridge University Press, pp.78.

Lieberman, D.E., Devlin, M.J., Pearson, O.M. (2001), "Articular area responses to mechanical loading: effects of exercise, age, and skeletal location", *American Journal of Physical Anthropology: The Official Publication of the American Association of Physical Anthropologists,* **116**(4), 266–277.

Lieberman, D.E., Pearson, O.M., Polk, J.D., Demes, B. and Crompton, A.W. (2003), Optimization of bone growth and remodeling in response to loading in tapered mammalian limbs. *Journal of Experimental Biology*, **206**(18), 3125-3138.

Louis, O., Fierens, Y., Strantza, M., Luypaert, R., de Mey, J., Cattrysse, E. (2015), "Using Magnetic Resonance for Predicting Femoral Strength: Added Value with respect to Bone Densitometry", *BioMed Research International* **2015**, 1–5.

Lovejoy, C.O., 2005. The natural history of human gait and posture: Part 1. Spine and pelvis. Gait & Posture **21**, 95–112.

Lovejoy, C.O., Burstein, A.H., Heiple, K.G. (1976), "The biomechanical analysis of bone strength: A method and its application to platycnemia", *American journal of physical anthropology*, ***44***(3), 489-505.

Lovejoy, C.O., Latimer, B., Suwa, G., Asfaw, B., White, T.D. (2009) "Combining Prehension and Propulsion: The Foot of Ardipithecus ramidus". *Science* **326**(5949), 72–72e8.

Maetzler, M., Bochdansky, T., Abboud, R.J. (2010), "Normal pressure values and repeatability of the Emed® ST2 system". *Gait & Posture* **32**(3), 391–394.

Manske, S.L., Liu-Ambrose, T., de Bakker, P.M., Liu, D., Kontulainen, S., Guy, P., Oxland, T.R., McKay, H.A. (2006), "Femoral neck cortical geometry measured with magnetic resonance imaging is associated with proximal femur strength", *Osteoporosis International*, **17**(10), 1539–1545.

Marchi, D. (2005), "The cross-sectional geometry of the hand and foot bones of the Hominoidea and its relationship to locomotor behavior". *Journal of Human Evolution* **49**(6), 743–761.

Marchi, D. (2010), "Articular to diaphyseal proportions of human and great ape metatarsals", *American journal of physical anthropology*, ***143***(2), 198–207.

Martin R.B., Burr D.B., Sharkey N.A., Fyhrie D.P. (2015), "Mechanical Properties of Bone", *Skeletal Tissue Mechanics,* Springer, New York, NY

McGee-Lawrence, M.E., Stoll, D.M., Mantila, E.R., Fahrner, B.K., Carey, H.V., Donahue, S.W. (2011), "Thirteen-lined ground squirrels (Ictidomys tridecemlineatus) show microstructural bone loss during hibernation but preserve bone macrostructural geometry and strength". *Journal of Experimental Biology* **214**(8), 1240–1247.

McPoil, T., Cornwall, M., Dupuis, L., Cornwell, M., (1999), "Variability of plantar pressure data. A comparison of the two-step and midgait methods". *Journal of the American Podiatric Medical Association* **89**(10), 495–501.

Moon, M.S., Lee, H., Kim, S.T., Kim, S.J., Kim, M.S. and Kim, D.S. (2018), "Spinopelvic orientation on radiographs in various body postures: upright standing, chair sitting, Japanese style kneel sitting, and Korean style cross-legged sitting". *Clinics in orthopedic surgery*, **10**(3), 322-327.

Morag, E., Cavanagh, P.R. (1999), "Structural and functional predictors of regional peak pressures under the foot during walking", *Journal of Biomechanics* **32**(4), 359–370.

Morris, A.G. (1992), *A master catalogue: Holocene human skeletons from South Africa,* Witwatersrand University Press.

Mullaji, A.B., Sharma, A.K., Marawar, S.V. and Kohli, A.F. (2008), "Tibial torsion in non-arthritic Indian adults: a computer tomography study of 100 limbs" *Indian journal of orthopaedics*, **42**(3), 309.

Nester, C.J. (2009), "Lessons from dynamic cadaver and invasive bone pin studies: do we know how the foot really moves during gait?", *Journal of Foot and Ankle Research* **2**, 1-7.

Pakendorf, B., Stoneking, M., (2021), "The genomic prehistory of peoples speaking Khoisan languages". *Human Molecular Genetics* **30**(R1), R49–R55.

Pataky, T.C., Caravaggi, P., Savage, R., Parker, D., Goulermas, J.Y., Sellers, W.I. and Crompton, R.H. (2008), "New insights into the plantar pressure correlates of walking speed using pedobarographic statistical parametric mapping (pSPM)". *Journal of biomechanics*, **41**(9), 1987-1994.

Pathria, M.N., Chung, C.B., Resnick, D.L. (2016), "Acute and stress-related injuries of bone and cartilage: pertinent anatomy, basic biomechanics, and imaging perspective". *Radiology* **280**(1), 21–38.

Payne, C., Chuter, V. and Miller, K. (2002), "Sensitivity and specificity of the functional hallux limitus test to predict foot function", *Journal of the American Podiatric Medical Association*, **92**(5), 269–271.

Pearson, O.M. (2000), "Activity, Climate, and Postcranial Robusticity: Implications for Modern Human Origins and Scenarios of Adaptive Change". *Current Anthropology* **41**(4), 569–607.

Pearson, O.M., Lieberman, D.E. (2004), "The aging of Wolff's law? Ontogeny and responses to mechanical loading in cortical bone". *American Journal of Physical Anthropology* **125**(S39), 63–99.

Perri, A.R. (2016), "Hunting dogs as environmental adaptations in Jōmon Japan", *Antiquity* **90**(353), 1166–1180.

Phillips, R.D., Law, E.A., Ward, E.D. (1996), "Functional motion of the medial column joints of the foot during propulsion". *Journal of the American Podiatric Medical Association*, **86(**10), 474–486.

Pontzer, H., Rolian, C., Rightmire, G.P., Jashashvili, T., Ponce de León, M.S., Lordkipanidze, D., Zollikofer, C.P.E. (2010), "Locomotor anatomy and biomechanics of the Dmanisi hominins", *Journal of Human Evolution* **58**(6), 492–504.

Prang, T.C. (2015), "Rearfoot posture of Australopithecus sediba and the evolution of the hominin longitudinal arch" *Scientific Reports*, **5**(1), 17677.

Putti, A.B., Arnold, G.P., Cochrane, L.A., Abboud, R.J. (2008), "Normal pressure values and repeatability of the Emed® ST4 system", *Gait & Posture* **27**(3), 501–505.

Rightmire, G.P. (1978), "Human skeletal remains from the southern Cape Province and their bearing on the stone age prehistory of South Africa", *Quaternary Research* **9**(2), 219–230.

Ruff, C. (1987), “Sexual dimorphism in human lower limb bone structure: relationship to subsistence strategy and sexual division of labor”, *Journal of Human Evolution* **16**(5), 391–416.

Ruff, C. (2009), “Relative limb strength and locomotion in Homo habilis”, *American Journal of Physical Anthropology*, **138**(1), 90–100.

Ruff, C., Holt, B., Trinkaus, E. (2006), “Who’s afraid of the big bad Wolff?: “Wolff’s law” and bone functional adaptation”, *American Journal of Physical Anthropology: The Official Publication of the American Association of Physical Anthropologists*, **129**(4), 484–498.

Ruff, C.B. (2000), “Body size, body shape, and long bone strength in modern humans”, *Journal of human evolution* **38**(2), 269–290.

Ruff, C.B. (2018), “Biomechanical Analyses of Archaeological Human Skeletons”, in Katzenberg M.A., Grauer A.L. (eds), *Biological Anthropology of the Human Skeleton*, John Wiley & Sons, Ltd, pp. 189–224.

Ruff, C.B., Higgins, R.W. and Carlson, K.J. (2020), “Long bone cross-sectional geometry”, in Zipfel, B., Richmond, B.G., Ward, C.V. (eds), *Hominin Postcranial Remains from Sterkfontein, South Africa, 1936-1995*. Oxford University Press, pp. 307–320.

Ruff, C.B., Larsen, C.S. (2014), “Long Bone Structural Analyses and the Reconstruction of Past Mobility: A Historical Review”, in Carlson, K.J., Marchi, D. (eds*), Reconstructing Mobility*, Springer US, pp. 13–29.

Ruff, C.B., Trinkaus, E., Walker, A., Larsen, C.S. (1993), “Postcranial robusticity in Homo. I: Temporal trends and mechanical interpretation”. *American Journal of Physical Anthropology* **91**(1), 21–53.

Manske, S.L., Liu-Ambrose, T., De Bakker, P.M., Liu, D., Kontulainen, S., Guy, P., Oxland, T.R. and McKay, H.A. (2006), “Femoral neck cortical geometry measured with magnetic resonance imaging is associated with proximal femur strength”, *Osteoporosis international*, **17**, 1539-1545.

Saers, J.P.P., DeMars, L.J., Stephens, N.B., Jashashvili, T., Carlson, K.J., Gordon, A.D., Shaw, C.N., Ryan, T.M., Stock, J.T. (2021), "Combinations of trabecular and cortical bone properties distinguish various loading modalities between athletes and controls", *American Journal of Physical Anthropology* **174**(3), 434–450.

Schindelin, J., Arganda-Carreras, I., Frise, E., Kaynig, V., Longair, M., Pietzsch, T., Preibisch, S., Rueden, C., Saalfeld, S., Schmid, B., Tinevez, J.-Y., White, D.J., Hartenstein, V., Eliceiri, K., Tomancak, P., Cardona, A. (2012), "Fiji: an open-source platform for biological-image analysis", *Nature Methods* **9**(7), 676–682.

Schindelin, J., Rueden, C.T., Hiner, M.C., Eliceiri, K.W. (2015), "The ImageJ ecosystem: An open platform for biomedical image analysis", *Molecular Reproduction and Development* **82**(7-8), 518–529.

Schuster, S.C., Miller, W., Ratan, A., Tomsho, L.P., Giardine, B., Kasson, L.R., Harris, R.S., Petersen, D.C., Zhao, F., Qi, J., Alkan, C., Kidd, J.M., Sun, Y., Drautz, D.I., Bouffard, P., Muzny, D.M., Reid, J.G., Nazareth, L.V., Wang, Q., Burhans, R., Riemer, C., Wittekindt, N.E., Moorjani, P., Tindall, E.A., Danko, C.G., Teo, W.S., Buboltz, A.M., Zhang, Z., Ma, Q., Oosthuysen, A., Steenkamp, A.W., Oostuisen, H., Venter, P., Gajewski, J., Zhang, Y., Pugh, B.F., Makova, K.D., Nekrutenko, A., Mardis, E.R., Patterson, N., Pringle, T.H., Chiaromonte, F., Mullikin, J.C., Eichler, E.E., Hardison, R.C., Gibbs, R.A., Harkins, T.T., Hayes, V.M. (2010) "Complete Khoisan and Bantu genomes from southern Africa", *Nature* **463**(7283), 943–947.

Sealy, J., Ludwig, B., Henderson, Z. (2006), "New radiocarbon dates for Matjes River Rock Shelter", *South African Archaeological Bulletin* **61**(183), 98-101

Sealy, J., Pfeiffer, S. (2000), "Diet, Body Size, and Landscape Use among Holocene People in the Southern Cape, South Africa", *Current Anthropology* **41**(4), 642–655.

Sharir, A., Barak, M.M. and Shahar, R. (2008), "Whole bone mechanics and mechanical testing", *The Veterinary Journal*, **177**(1), 8–17.

Shaw, C.N., Stock, J.T. (2009), "Intensity, repetitiveness, and directionality of habitual adolescent mobility patterns influence the tibial diaphysis morphology of athletes", *American Journal of Physical Anthropology: The Official Publication of the American Association of Physical Anthropologists,* 140(1), 149–159.

Shaw, C.N., Stock, J.T., Davies, T.G., Ryan, T.M. (2014), "Does the Distribution and Variation in Cortical Bone Along Lower Limb Diaphysis Reflect Selection for Locomotor Economy?", in Carlson, K.J., Marchi, D. (eds), *Reconstructing Mobility*, Springer US, pp. 49–66.

Smith-Bindman, R., Lipson, J., Marcus, R., KwangPyo, K., Mahesh, M., Gould, R., González, A.B. de, Miglioretti, D.L. (2009), "Radiation dose associated with common computed tomography examinations and the associated lifetime attributable risk of cancer", *Archives of Internal Medicine* **169**(22), 2078–2086.

Song, S., Geyer, H. (2011), "The energetic cost of adaptive feet in walking", *IEEE International Conference on Robotics and Biomimetics (ROBIO)*, Phuket, Thailand, pp. 1597–1602.

Stock, J., Pfeiffer, S. (2001), "Linking structural variability in long bone diaphyses to habitual behaviors: Foragers from the southern African Later Stone Age and the Andaman Islands", *American Journal of Physical Anthropology* **115**(4), 337–348.

Stokes, I.A., Hutton, W.C., Stott, J.R. (1979), "Forces acting on the metatarsals during normal walking. Journal of Anatomy" **129**(Pt3), 579–590.

Su, A., Carlson, K.J. (2017), "Comparative analysis of trabecular bone structure and orientation in South African hominin tali. *Journal of Human Evolution* **106**, 1–18.

Susman, R.L., Brain, T.M. (1988), "New first metatarsal (SKX 5017) from Swartkrans and the gait of Paranthropus robustus". *American Journal of Physical Anthropology*, **77**(1), 7-15.

Tal, H., Tau S. (1983), "Statistical survey of the human skulls in the Raymond Dart collection of skeletons" *South African Journal of Science* **79**(6), 215–217.

Tea Jashashvili, M.R.D. (2015), "Cortical Structure of Hallucal Metatarsals and Locomotor Adaptations in Hominoids", *PloS one*, **10**(1), p.e0117905.

The Python Software Foundation (2023), "The Python Standard Library - Python 3.10.7 documentation", [online at https://docs.python.org/3/library/index.html, accessed 10 February 2022).

Thompson, A.L.T., Zipfel, B. (2005), "The unshod child into womanhood—forefoot morphology in two populations" *The Foot* **15**(1), 22–28.

Tobias, P. (2005), *Into the past: a memoir.* Johannesburg: Picador Africa and Witwatersrand University Press.

Trinkaus E., Jashashvili T., Patel B.A. (2021), "Perspectives on the Pliocene and Pleistocene Pedal Patterns and Protection", in Pastoors, A., Lenssen-Erz, T. (eds), *Reading Prehistoric Human Tracks: Methods & Material*, Springer International Publishing, Cham, pp. 121-132

Tweed, J.L., Barnes, M.R., Allen, M.J. and Campbell, J.A. (2009), "Biomechanical consequences of total plantar fasciotomy: a review of the literature", *Journal of the American Podiatric Medical Association*, **99**(5), 422-430.

Underhill, A.P., Habu, J. (2006), "Early communities in East Asia: economic and sociopolitical organization at the local and regional levels", in Stark M.T (eds) *Archaeology of Asia*, Blackwell Malden, MA, pp.121–148.

Van Gheluwe, B., Dananberg, H.J., Hagman, F. and Vanstaen, K. (2006), "Effects of hallux limitus on plantar foot pressure and foot kinematics during walking," *Journal of the American Podiatric Medical Association*, **96**(5), 428-436.

van Rietbergen, B., Majumdar, S., Newitt, D., MacDonald, B. (2002) "High-resolution MRI and micro-FE for the evaluation of changes in bone mechanical properties during longitudinal clinical trials: application to calcaneal bone in postmenopausal women after one year of idoxifene treatment" *Clinical Biomechanics* **17**(2), 81–88.

Vogler, H.W., Bojsen-Møller, F., (2000) "Tarsal functions, movement, and stabilization mechanisms in foot, ankle, and leg performance" *Journal of the American Podiatric Medical Association* **90**(3), 112–125.

Waskom, M.L. (2021) "Seaborn: statistical data visualization", *Journal of Open Source Software*, **6**(60), 3021.

Wehrli, F.W., Song, H.K., Saha, P.K., Wright, A.C. (2006) "Quantitative MRI for the assessment of bone structure and function", *NMR in Biomedicine: An International*

Journal Devoted to the Development and Application of Magnetic Resonance In vivo **19**(7), 731–764.

Wei, P., Wallace, I.J., Jashashvili, T., Musiba, C.M., Liu, W. (2017), "Structural analysis of the femoral diaphyses of an early modern human from Tianyuan Cave, China", *Quaternary International* **434**, 48–56.

Welte, L., Kelly, L.A., Lichtwark, G.A. and Rainbow, M.J. (2018), "Influence of the windlass mechanism on arch-spring mechanics during dynamic foot arch deformation", *Journal of the Royal Society Interface*, ***15***(145), p.20180270.

Wescott, D.J. (2014), "The Relationship Between Femur Shape and Terrestrial Mobility Patterns, in: Carlson, K.J., Marchi, D. (eds), *Reconstructing Mobility*. Springer US, pp. 111–132.

White, T.D., Black, M.T., Folkens, P.A. (2011) *Human Osteology*. Academic Press.

Whittle, M.W. (2014) *Gait analysis: an introduction*. Butterworth-Heinemann.

Wollmann, J.S., Cameron, M.E. (2022), "Intraindividual variation in the cross-sectional geometry of the first metatarsal, femur, and tibia", *American Journal of Biological Anthropology* **179**(2), 229-239.

Woodhead, H.J., Kemp, A.F., Blimkie, C.J., Briody, J.N., Duncan, C.S., Thompson, M., Lam, A., Howman-Giles, R. and Cowell, C.T. (2001) "Measurement of midfemoral shaft geometry: Repeatability and accuracy using magnetic resonance imaging and dual-energy X-ray absorptiometry", *Journal of bone and mineral research* **16(**12), 2251-2259.

Xing, S., Carlson, K.J., Wei, P., He, J., Liu, W. (2018) "Morphology and structure of Homo erectus humeri from Zhoukoudian, Locality 1" *PeerJ* **6**, e4279.

Yamaguchi, B. (1982), "A Review of the Osteological Characteristics of the Jomon Population in Prehistoric Japan. *The Journal of Anthropological Society of Nippon* **90**(Supplement), 77–90.

Zipfel, B., Berger, L.R. (2007), "Shod versus unshod: The emergence of forefoot pathology in modern humans?" *The Foot* **17**(4), 205–213.

Zipfel, B., DeSilva, J.M., Kidd, R.S., Carlson, K.J., Churchill, S.E., Berger, L.R. (2011) "The Foot and Ankle of Australopithecus sediba", *Science* **333**(6048), 1417–1420.

Zipfel, B. and Kidd, R.S. (2008) "Size and shape of a human foot bone from Klasies River main site, South Africa", *Palaeontologica Africana*, **43**, 51-56.

Zipfel, B., Richmond, B.G., Ward, C.V. (eds) (2020), "Hominin Postcranial Remains from Sterkfontein, South Africa, 1936-1995", Oxford University Press.

APPENDIX A – METATARSAL SAMPLE BIOMECHANICAL LENGTHS

Table A.1: Metatarsal biomechanical lengths of the post-industrial individuals of South Africa, the Later Stone Age (LSA) Foragers of South Africa and the Jomon.

Population Sample	Collection Accession Number	MT Sample	MT Length (mm)
Post-Industrial Individuals from South Africa			
	A8	MT1	64.04
		MT2	78.74
		MT3	79.98
		MT4	75.94
		MT5	68.47
	A9	MT1	64.04
		MT2	78.74
		MT3	79.98
		MT4	75.94
		MT5	68.47
	A13	MT1	57.66
		MT2	72.24
		MT3	69.86
		MT4	70.6
		MT5	66.39
	A14	MT1	61.33
		MT2	74.56
		MT3	71.05
		MT4	67.62
		MT5	65.17
	A17	MT1	64.65
		MT2	77.51
		MT3	75.01
		MT4	73.77
		MT5	65.84
	A163	MT1	65.52
		MT2	76.74
		MT3	73.25
		MT4	72.09
		MT5	66.78
	A170	MT1	64.43
		MT2	76.28
		MT3	76.29
		MT4	74.31
		MT5	66.14
	A22	MT1	60.72
		MT2	70.97
		MT3	70.41
		MT4	67.44
		MT5	65.11
	A209	MT1	70.25
		MT2	80.52
		MT3	78.16
		MT4	76.08
		MT5	71.88
	A218	MT1	61.13
		MT2	70.27
		MT3	68.12

		MT4	66.52
		MT5	61.15
	A458	MT1	59.99
		MT2	69.07
		MT3	66.05
		MT4	62.55
		MT5	57.28
	A883	MT1	61.95
		MT2	75.48
		MT3	71.85
		MT4	70.17
		MT5	61.95
	A1285	MT1	54.86
		MT2	67.93
		MT3	64.57
		MT4	60.34
		MT5	55.17
	A3060	MT1	54.86
		MT2	75.53
		MT3	73.33
		MT4	72.26
		MT5	64.28
LSA Foragers of South Africa			
	MRN4Wilton	MT1	54.63
		MT2	66.36
		MT3	61.53
		MT4	60.29
		MT5	56.56
	NMB not acc MSk2	MT1	47.59
		MT2	61.88
		MT3	59.18
		MT4	55.82
		MT5	52.2
	NMB not acc SS2	MT1	48.58
		MT2	53.3
		MT3	55.71
		MT4	52.97
		MT5	50.95
	NMB not acc SS1	MT1	52.99
		MT2	57.47
		MT3	61.51
		MT4	59.97
		MT5	54.96
	NMB not acc SS3	MT1	56.41
		MT2	66.66
		MT3	62.17
		MT4	60.08
		MT5	55.83
	NMB MSk5	MT1	52.53
		MT2	62.22
		MT3	60.3
		MT4	59.95
		MT5	55.03
	NMB 1231 - 1	MT1	55.27
		MT2	65.37
		MT3	62.79
		MT4	60.68

		MT5	52.71
	NMB 1231 - 2	MT1	57.71
		MT2	66.12
		MT3	66.89
		MT4	63.9
		MT5	58.96
	NMB 1231 - 4	MT1	61.01
		MT2	64.14
		MT3	65.72
		MT4	66.84
		MT5	58.42
	NMB 1231 - 5	MT1	58.39
		MT2	67.6
		MT3	62.63
		MT4	65.6
		MT5	59.88
	NMB 1231 - 9	MT1	59.57
		MT2	67.93
		MT3	67.73
		MT4	62.58
		MT5	59.23
	NMB 1231 - 11	MT1	56.02
		MT2	63.7
		MT3	60
		MT4	60.04
		MT5	58.66
	NMB 1231 - 12	MT1	55.36
		MT2	63.92
		MT3	65.83
		MT4	61.26
		MT5	54.97
	NMB 1231 - 14	MT1	58.43
		MT2	69.1
		MT3	63.09
		MT4	63.17
		MT5	55.96
	NMB 1420	MT1	56.13
		MT2	66.3
		MT3	64.59
		MT4	61.49
		MT5	57.04
The Jomon			
	UMUT130145	MT1	56.32
		MT2	71.46
		MT3	75.33
		MT4	65.34
		MT5	70.2
	UMUT130152	MT1	56.29
		MT2	78.48
		MT3	75.33
		MT4	72.54
		MT5	69.12
	UMUT130195	MT1	55.22
		MT2	76.77
		MT3	71.64
		MT4	69.57
		MT5	69.93

UMUT131086-1	MT1	58.4
	MT2	77
	MT3	74.34
	MT4	72
	MT5	72.63
UMUT131086-2	MT1	52.67
	MT2	72.63
	MT3	71.1
	MT4	67.32
	MT5	70.56
UMUT13138-G1	MT1	55.53
	MT2	76.23
	MT3	72.72
	MT4	69.84
	MT5	72
UMUT131380-G2	MT1	58.33
	MT2	76.32
	MT3	75.06
	MT4	70.2
	MT5	69.93
UMUT131376	MT1	52.93
	MT2	74.25
	MT3	70.02
	MT4	67.86
	MT5	66.33
UMUT131067	MT1	57.73
	MT2	80.6
	MT3	75.51
	MT4	74.97
	MT5	73.08
UMUT130166	MT1	55.88
	MT2	66.33
	MT3	68.4
	MT4	67.59
	MT5	68.85
UMUT130242	MT1	56.05
	MT2	69.9
	MT3	73.08
	MT4	70.56
	MT5	71.91
UMUT130849	MT1	52.12
	MT2	61.23
	MT3	65.16
	MT4	69.57
	MT5	74.52
UMUT130850	MT1	59.32
	MT2	72.76
	MT3	76.95
	MT4	74.88
	MT5	76.14
UMUT130857-2	MT1	52.86
	MT2	70
	MT3	75.69
	MT4	71.82
	MT5	74.79
UMUT130860	MT1	56.23
	MT2	72
	MT3	70.11

	MT4	66.78
	MT5	63.54
UMUT130861	MT1	54.58
	MT2	61.2
	MT3	73.62
	MT4	76.14
	MT5	71.28
UMUT130867	MT1	53.38
	MT2	72.3
	MT3	65.97
	MT4	66.06
	MT5	67.41
UMUT130868	MT1	53.92
	MT2	66.6
	MT3	67.05
	MT4	66.15
	MT5	67.77
UMUT131061	MT1	59.01
	MT2	79.56
	MT3	78.3
	MT4	75.51
	MT5	76.05
UMUT131085-1	MT1	53.67
	MT2	70.47
	MT3	68.13
	MT4	66.96
	MT5	65.07
UMUT131096	MT1	58.12
	MT2	76.9
	MT3	75.69
	MT4	66.96
	MT5	70.02
UMUT131098	MT1	64.68
	MT2	84.15
	MT3	77.13
	MT4	77.04
	MT5	81
UMUT131377	MT1	58.66
	MT2	79.83
	MT3	72.99
	MT4	70.29
	MT5	71.19
UMUT131719	MT1	55.24
	MT2	74.07
	MT3	70.92
	MT4	68.85
	MT5	68.85
UMUT131729	MT1	59.84
	MT2	80.55
	MT3	75.6
	MT4	74.97
	MT5	78.12
UMUT131737	MT1	61.64
	MT2	79.74
	MT3	76.77
	MT4	74.25
	MT5	78.3

APPENDIX B – METATARSAL CROSS-SECTIONAL GEOMETRIC PROPERTY SOURCE DATA

Table B.1: FIJI/Bone J results. Non-standardised metatarsal diaphyseal CSGPs followed by standardised metatarsal diaphyseal CSGPs.

group		LSA SA	LSA SA	LSA SA	LSA SA	LSA SA	PI SA	PI SA	PI SA	PI SA	PI SA	Jomon	Jomon	Jomon	Jomon	Jomon
slice		MT1	MT2	MT3	MT4	MT5	MT1	MT2	MT3	MT4	MT5	MT1	MT2	MT3	MT4	MT5
metric	prc															
CSA	0.25	157768.6524	171617.7189	145663.219	160649.5231	154574.483	233586.6338	289170.2139	254825.0832	276009.1837	241164.8	147823.8	274853.6	296784.7	294544	291175.6
CSA	0.3	160567.1784	161720.8901	142516.217	145002.3827	145103.362	243153.9909	268905.5368	242427.5361	253124.7757	223768.3	150168.2	235273.1	232640.5	223848	249637
CSA	0.5	166760.0218	129950.2141	112926.325	113692.5695	111972.525	249860.3904	227183.0349	198653.1555	201035.0311	177060	173646.2	186592.5	177184.3	167729.9	185228.5
CSA	0.65	171204.7361	100723.3241	86113.5631	86034.04327	81716.4831	235960.2177	179239.7363	152981.2504	150916.5058	133234.5	207659.8	147989.5	133351	124800.1	127653.3
Imax	0.25	8887568544	4110393340	3620750352	4608915000	3350157414	21723444357	13753658027	12211899849	13969455898	8.8E+09	9.13E+09	1.15E+10	1.17E+10	1.16E+10	1.18E+10
Imax	0.3	7915811111	3125186584	2351838780	2480716463	2210565154	20154953011	9963585610	7841748233	8448774807	6.43E+09	8.37E+09	7.49E+09	5.69E+09	5.28E+09	6.81E+09
Imax	0.5	6953940318	2213130611	1496703116	1582550199	1611135241	18550307367	6857734176	5093068987	5464241297	4.46E+09	8.03E+09	4.91E+09	3.71E+09	3.61E+09	4.77E+09
Imax	0.65	6935286658	1729987235	1066478034	1114441172	1276285295	17461730264	4913681918	3393859340	3632080318	3.36E+09	8.31E+09	3.39E+09	2.72E+09	2.9E+09	3.76E+09
Imin	0.25	15532483335	6929956309	7328896398	9114942399	9738547332	36841561665	23735175265	23413222952	28513998589	2.17E+10	1.81E+10	2.2E+10	2.52E+10	2.7E+10	2.87E+10
Imin	0.3	10858631468	4628011621	4658692493	5528727934	5983024701	27186707635	15440575764	15078560232	18494806541	1.46E+10	1.16E+10	1.19E+10	1.37E+10	1.3E+10	1.64E+10
Imin	0.5	8650090179	2946311600	2830507502	3197112585	3526606087	22603582913	10240445607	8951671585	10739774030	9.03E+09	9.58E+09	7.47E+09	7.7E+09	7.05E+09	9.35E+09
Imin	0.65	10766418602	2141441925	1910066332	2007616158	2478160310	26056610248	7276849597	6032044967	6698692983	6.02E+09	1.42E+10	5.44E+09	4.91E+09	4.41E+09	6.12E+09
Ix	0.25	13776738291	6523771607	6035302224	6328425926	3742112320	33943750015	21265655317	16497854828	16868515580	1E+10	1.65E+10	2.06E+10	2.16E+10	2.29E+10	1.84E+10
Ix	0.3	9991993499	4273581079	3426640367	3298002969	2446852723	25355610177	13516510861	10008696690	11598288812	7.3E+09	1.12E+10	1.09E+10	1.09E+10	9.9E+09	1.11E+10
Ix	0.5	7234425883	2797873795	2319722211	2061672735	1739533281	19040682794	9405383854	6565007072	6754674338	5.02E+09	8.22E+09	7.01E+09	6.58E+09	5.5E+09	6.84E+09
Ix	0.65	7118431157	2061380063	1620143377	1473671405	1471852956	17707046503	6717765117	4613171120	4985749009	3.82E+09	8.43E+09	5.11E+09	4.56E+09	4.07E+09	4.76E+09
Iy	0.25	10643315997	4516582148	4914345786	7395431137	9346593953	24621253125	16223176455	19127270249	22042972112	2.05E+10	1.03E+10	1.28E+10	1.53E+10	1.58E+10	2.21E+10
Iy	0.3	8782449202	3479615998	3249324959	4711444815	5746738390	21986048389	11887658868	12911610707	15345294880	1.38E+10	8.81E+09	8.47E+09	8.5E+09	8.4E+09	1.21E+10
Iy	0.5	8369603302	2361563226	2007489978	2717988842	3398208901	22113205069	7692793821	7479728407	8979762242	8.47E+09	9.38E+09	5.37E+09	4.84E+09	5.16E+09	7.28E+09
Iy	0.65	10583275444	1810045865	1356401805	1648388116	2282590707	25811290323	5472764232	4812724904	5345030445	5.55E+09	1.41E+10	3.73E+09	3.07E+09	3.24E+09	4.82E+09
Zmax	0.25	20455338.54	14454671.06	12712559.2	14179908.01	11600153	39728384.84	34692196.6	30825577.37	33538530.75	25392562	19607134	30587689	30897703	29683555	30286213
Zmax	0.3	19738865.87	11964488.7	10049545.4	10288501.63	9572038.75	39249946.42	28419628.15	24582161.03	26075178.1	20931893	19322584	21959475	18981827	17697648	21951893
Zmax	0.5	19814407.05	9229717.985	7245682.67	7401792.974	7420613.05	40905505.23	21610870.46	18044404.83	18789824.83	16256565	21039813	15805468	13376895	12327071	16731021
Zmax	0.65	20675846.19	7332650.984	5489297.76	5543839.525	5998083.48	39913391.85	16569247.81	12945778.17	13420259.47	12369121	24041384	12356296	10539768	10387375	12479418
Zmin	0.25	29901285.95	18736010.35	19308533.4	22127076.14	22943887.8	54231985.38	46013483.55	46138621.88	52537908.78	43701009	31044373	43098523	49105145	50795056	52529288
Zmin	0.3	24152690.99	14657635.48	14240994	15980880.19	16721593.2	47510835.92	34962720.4	34147235.78	39452076.86	32354138	23523595	28122095	31198113	30132359	36395242
Zmin	0.5	22225608.12	10530490.41	9881876.59	10668475.65	11604417.2	44809263.77	25751946.16	23210152.93	26126062.43	23098086	23710381	19461308	19645573	19133668	24141095
Zmin	0.65	25470912.71	8238791.673	7267914.38	7344847.342	8443257.68	47089579.59	19592226.96	17034544.93	17787738.93	16823385	32034697	15209341	14217820	13326730	16762764
Zp	0.25	46250858.37	29479689.22	28768506.6	32835639.34	30600041.9	85479833.39	72078592.69	69781981.51	77414284.44	60562986	45410242	65066577	71180203	71874819	73763550
Zp	0.3	40879289.63	24251453.06	21398753.5	22975456.39	22612503.5	80838839.79	57294573	51486687.33	57289934.7	46313463	39693976	44439864	44123724	42229720	51490184
Zp	0.5	38945009.13	18226201.57	15100202.5	15832955.53	16826513.2	78849540.88	42651350.12	36420631.24	38610991.2	34305739	41539493	31337561	29060872	28825189	36214118
Zp	0.65	40651555.75	14600046.57	11289232.3	11382884.22	12563323.8	76454817.94	32209486.87	26454008.8	27722022.17	25950747	49728969	24208223	21774208	20830129	26650632
Zx	0.25	28338419.9	18042305.99	17425661.3	18145310.62	13259491.9	55230749.84	43333739.13	36943623.76	38584811.52	27956379	28967733	41525343	44976806	44634730	40306163
Zx	0.3	24338734.34	14172847.07	11865087.2	11832350.57	10126534.6	48229942.37	32593751.02	26858053.43	29752939.86	22183410	24328560	27027298	27658502	25848937	29094797
Zx	0.5	20810133.63	10420519.34	8868957.86	8059496.542	7789871.25	42100460.42	25261977.71	19473166.55	20350178.4	16893452	22045851	19197843	18538932	16585989	19526654
Zx	0.65	20872955.83	8164190.394	6568266.1	6093299.739	6473683.86	39907795.34	19325541.23	14485506.43	14875246.8	13162513	24182520	15205546	13821939	12241515	14024738
Zy	0.25	23664889.72	15407918.97	15604932.9	20758484.23	22425035.5	44235632.75	39144927.11	42013210.08	45899500.11	42063305	20738389	32698239	37716568	39579177	44502544
Zy	0.3	21777814.8	12789914.2	11705198.2	14956711.63	16713280	42537116.19	31615888.25	32140553.45	36442285.34	32130060	19973561	23886947	24093457	24426087	31408026
Zy	0.5	22559600.8	9808667.334	8445069.83	10013508.03	11515186.7	45187592.32	23319013.95	21624594.65	24063515.96	22768741	23482562	16896117	15943958	16607561	21068150
Zy	0.65	25309197.82	7947255.941	6296848.57	6888965.224	8448344.82	47199619.28	18262594.46	15482291.31	16182609.16	16576639	32034814	13079751	11604226	11989080	14563761

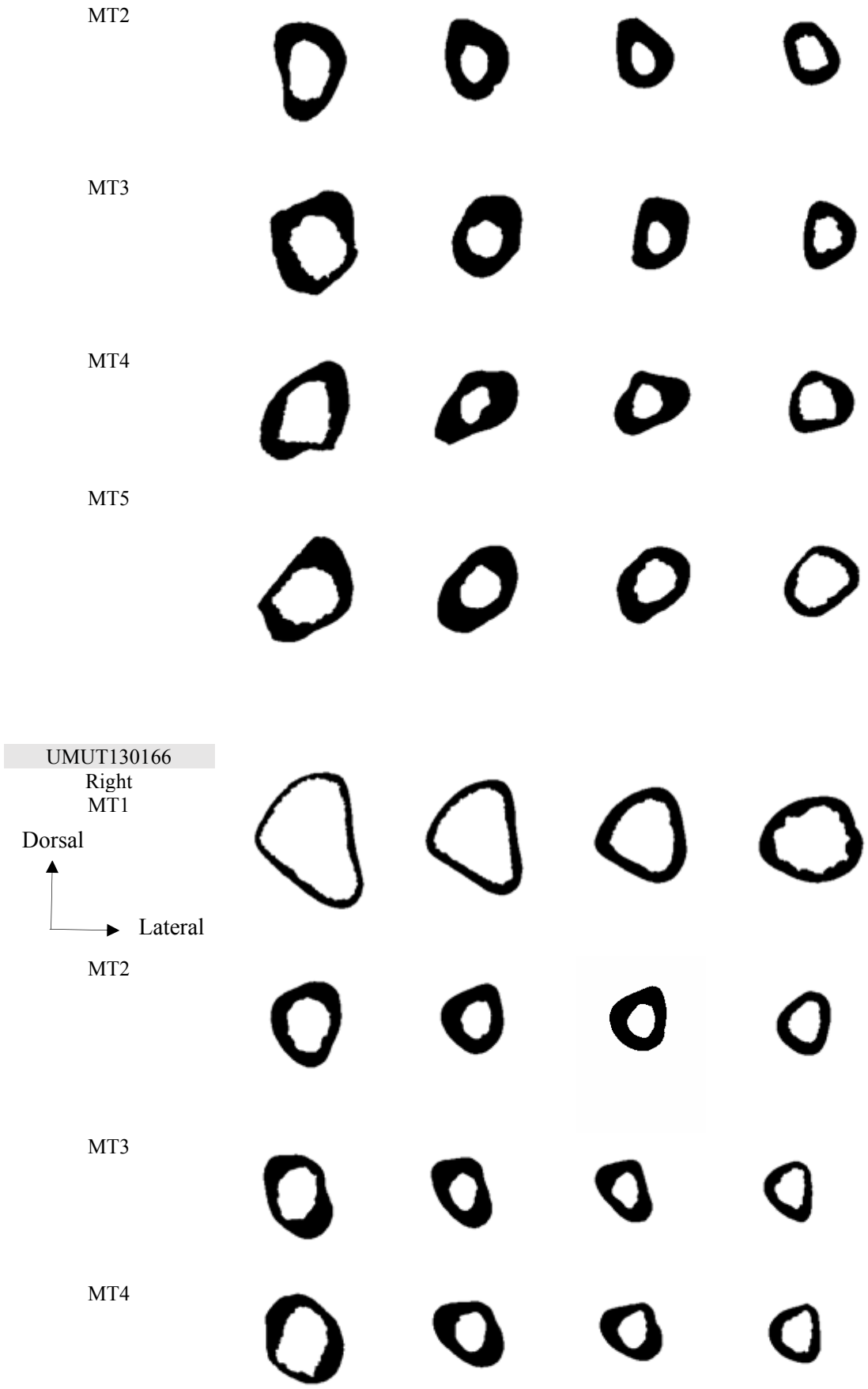
group		LSA SA	LSA SA	LSA SA	LSA SA	LSA SA	PI SA	PI SA	PI SA	PI SA	PI SA	Jomon	Jomon	Jomon	Jomon	Jomon
slice		MT1	MT2	MT3	MT4	MT5	MT1	MT2	MT3	MT4	MT5	MT1	MT2	MT3	MT4	MT5
metric	prc															
CSA	0.25	0.157769	0.171618	0.145663	0.16065	0.154574	0.233587	0.28917	0.254825	0.276009	0.241165	0.147824	0.274854	0.296785	0.294544	0.291176
CSA	0.3	0.160567	0.161721	0.142516	0.145002	0.145103	0.243154	0.268906	0.242428	0.253125	0.223768	0.150168	0.235273	0.23264	0.223848	0.249637
CSA	0.5	0.16676	0.12995	0.112926	0.113693	0.111973	0.24986	0.227183	0.198653	0.201035	0.17706	0.173646	0.186592	0.177184	0.16773	0.185228
CSA	0.65	0.171205	0.100723	0.086114	0.086034	0.081716	0.23596	0.17924	0.152981	0.150917	0.133234	0.20766	0.14799	0.133351	0.1248	0.127653
Imax	0.25	8.887569	4.110393	3.62075	4.608915	3.350157	21.72344	13.75366	12.2119	13.96946	8.796855	9.129976	11.46247	11.6836	11.63597	11.83371
Imax	0.3	7.915811	3.125187	2.351839	2.480716	2.210565	20.15495	9.963586	7.841748	8.448775	6.429869	8.369313	7.486157	5.687805	5.283667	6.807237
Imax	0.5	6.95394	2.213131	1.496703	1.58255	1.611135	18.55031	6.857734	5.093069	5.464241	4.459527	8.025494	4.906501	3.709141	3.605231	4.773746
Imax	0.65	6.935287	1.729987	1.066478	1.114441	1.276285	17.46173	4.913682	3.393859	3.63208	3.356501	8.311619	3.391006	2.719524	2.899807	3.759309
Imin	0.25	15.53248	6.929956	7.328896	9.114942	9.738547	36.84156	23.73518	23.41322	28.514	21.70411	18.05171	21.95824	25.17788	27.04769	28.71328
Imin	0.3	10.85863	4.628012	4.658692	5.528728	5.983025	27.18671	15.44058	15.07856	18.49481	14.63057	11.58909	11.9044	13.73351	13.02055	16.39986
Imin	0.5	8.65009	2.946312	2.830508	3.197113	3.526606	22.60358	10.24045	8.951672	10.73977	9.031538	9.575574	7.469763	7.70485	7.047153	9.352911
Imin	0.65	10.76642	2.141442	1.910066	2.007616	2.47816	26.05661	7.27685	6.032045	6.698693	6.016679	14.20551	5.439965	4.912153	4.409861	6.12246
Ix	0.25	13.77674	6.523772	6.035302	6.328426	3.742112	33.94375	21.26566	16.49785	16.86852	10.02249	16.45177	20.59283	21.59812	22.89142	18.42705
Ix	0.3	9.991993	4.273581	3.42664	3.298003	2.446853	25.35561	13.51651	10.0087	11.59829	7.299233	11.15202	10.92051	10.9262	9.90352	11.08303
Ix	0.5	7.234426	2.797874	2.319722	2.061673	1.739533	19.04068	9.405384	6.565007	6.754674	5.024414	8.221688	7.005084	6.575092	5.495049	6.844892
Ix	0.65	7.118431	2.06138	1.620143	1.473671	1.471853	17.70705	6.717765	4.613171	4.985749	3.82058	8.427985	5.105286	4.561847	4.068639	4.758568
Iy	0.25	10.64332	4.516582	4.914346	7.395431	9.346594	24.62125	16.22318	19.12727	22.04297	20.47848	10.30182	12.82789	15.26336	15.79224	22.11995
Iy	0.3	8.782449	3.479616	3.249325	4.711445	5.746738	21.98605	11.88766	12.91161	15.34529	13.76121	8.806377	8.470045	8.495116	8.400699	12.12407
Iy	0.5	8.369603	2.361563	2.00749	2.717989	3.398209	22.11321	7.692794	7.479728	8.979762	8.466655	9.379382	5.371171	4.838901	5.157335	7.281766
Iy	0.65	10.58328	1.810046	1.356402	1.648388	2.282591	25.81129	5.472764	4.812725	5.34503	5.552604	14.08914	3.725687	3.069831	3.241029	4.824964
Zmax	0.25	20.45534	14.45467	12.71256	14.17991	11.60015	39.72838	34.6922	30.82558	33.53853	25.39256	19.60713	30.58769	30.8977	29.68355	30.28621
Zmax	0.3	19.73887	11.96449	10.04955	10.2885	9.572039	39.24995	28.41963	24.58216	26.07518	20.93189	19.32258	21.95947	18.98183	17.69765	21.95189
Zmax	0.5	19.81441	9.229718	7.245683	7.401793	7.420613	40.90551	21.61087	18.0444	18.78982	16.25657	21.03981	15.80547	13.3769	12.32707	16.73102
Zmax	0.65	20.67585	7.332651	5.489298	5.54384	5.998083	39.91339	16.56925	12.94578	13.42026	12.36912	24.04138	12.3563	10.53977	10.38738	12.47942
Zmin	0.25	29.90129	18.73601	19.30853	22.12708	22.94389	54.23199	46.01348	46.13862	52.53791	43.70101	31.04437	43.09852	49.10515	50.79506	52.52929
Zmin	0.3	24.15269	14.65764	14.24099	15.98088	16.72159	47.51084	34.96272	34.14724	39.45208	32.35414	23.5236	28.12209	31.19811	30.13236	36.39524
Zmin	0.5	22.22561	10.53049	9.881877	10.66848	11.60442	44.80926	25.75195	23.21015	26.12606	23.09809	23.71038	19.46131	19.64557	19.13367	24.14109
Zmin	0.65	25.47091	8.238792	7.267914	7.344847	8.443258	47.08958	19.59223	17.03454	17.78774	16.82338	32.0347	15.20934	14.21782	13.32673	16.76276
Zp	0.25	46.25086	29.47969	28.76851	32.83564	30.60004	85.47983	72.07859	69.78198	77.41428	60.56299	45.41024	65.06658	71.1802	71.87482	73.76355
Zp	0.3	40.87929	24.25145	21.39875	22.97546	22.6125	80.83884	57.29457	51.48669	57.28993	46.31346	39.69398	44.43986	44.12372	42.22972	51.49018
Zp	0.5	38.94501	18.2262	15.1002	15.83296	16.82651	78.84954	42.65135	36.42063	38.61099	34.30574	41.53949	31.33756	29.06087	28.82519	36.21412
Zp	0.65	40.65156	14.60005	11.28923	11.38288	12.56332	76.45482	32.20949	26.45401	27.72202	25.95075	49.72897	24.20822	21.77421	20.83013	26.65063
Zx	0.25	28.33842	18.04231	17.42566	18.14531	13.25949	55.23075	43.33374	36.94362	38.58481	27.95638	28.96773	41.52534	44.97681	44.63473	40.30616
Zx	0.3	24.33873	14.17285	11.86509	11.83235	10.12653	48.22994	32.59375	26.85805	29.75294	22.18341	24.32856	27.0273	27.6585	25.84894	29.0948
Zx	0.5	20.81013	10.42052	8.868958	8.059497	7.789871	42.10046	25.26198	19.47317	20.35018	16.89345	22.04585	19.19784	18.53893	16.58599	19.52665
Zx	0.65	20.87296	8.16419	6.568266	6.0933	6.473684	39.9078	19.32554	14.48551	14.87525	13.16251	24.18252	15.20555	13.82194	12.24152	14.02474
Zy	0.25	23.66489	15.40792	15.60493	20.75848	22.42504	44.23563	39.14493	42.01321	45.8995	42.0633	20.73839	32.69824	37.71657	39.57918	44.50254
Zy	0.3	21.77781	12.78991	11.7052	14.95671	16.71328	42.53712	31.61589	32.14055	36.44229	32.13006	19.97356	23.88695	24.09346	24.42609	31.40803
Zy	0.5	22.5596	9.808667	8.44507	10.01351	11.51519	45.18759	23.31901	21.62459	24.06352	22.76874	23.48256	16.89612	15.94396	16.60756	21.06815
Zy	0.65	25.3092	7.947256	6.296849	6.888965	8.448345	47.19962	18.26259	15.48229	16.18261	16.57664	32.03481	13.07975	11.60423	11.98908	14.56376

CSA, cross-sectional area; I_x, Second moments of area about the x-axis; I_y Second moments of area about the y-axis; I_{max} Maximum second moments of area; I_{min} Minimum second moments of area; I_{max}/I_{min}, Shape Ratio; Z_x , Section modulus about the x-axis.

APPENDIX C – METATARSAL SAMPLE CROSS-SECTIONAL OUTLINES

Table C.1: Metatarsal (MT) cross-sectional outlines at location 25%, 35%, 50% and 65% of MT shaft biomechanical length for the Jomon, the post-industrial individuals of South Africa and the Later Stone Age individuals from South Africa. Diaphyseal slices were derived from CT scans and followed the process described in the methodology. Cross-sectional outlines are orientated with dorsal above, plantar below, medial to the right for left sided MT's and medial to the left for right sided MT's. Images are approximately to the same scale.

The Jomon	25%	35%	50%	65%
UMUT130145 Left MT1 Dorsal Medial				
MT2				
MT3				
MT4				
MT5				
UMUT130152 Left MT1 Dorsal Medial				


MT2
MT3
MT4
MT5
UMUT130166
Right
MT1
Dorsal
Lateral
MT2
MT3
MT4

MT5



UMUT130850
Right
MT1

Dorsal

Lateral



MT2



MT3



MT4



MT5

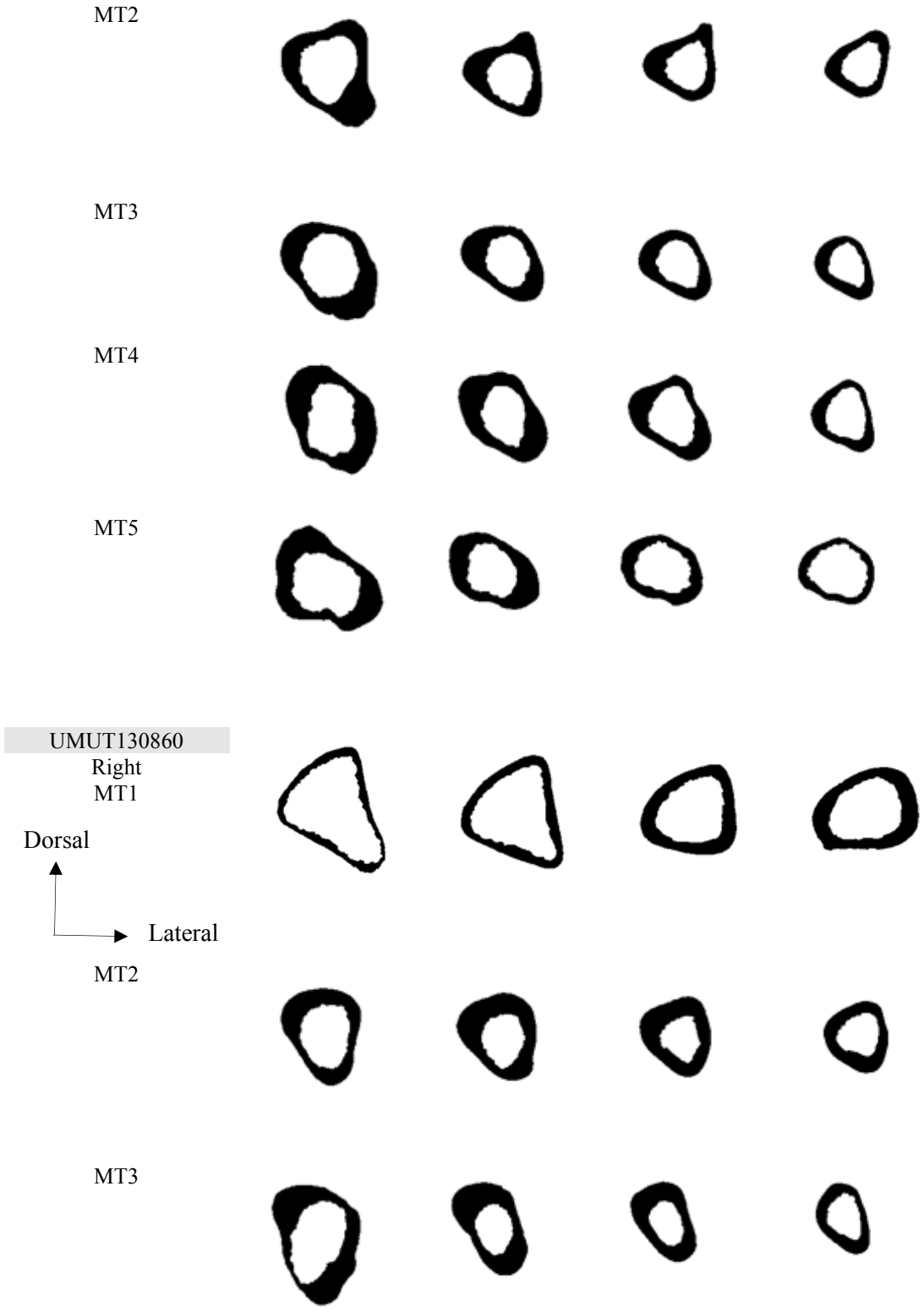


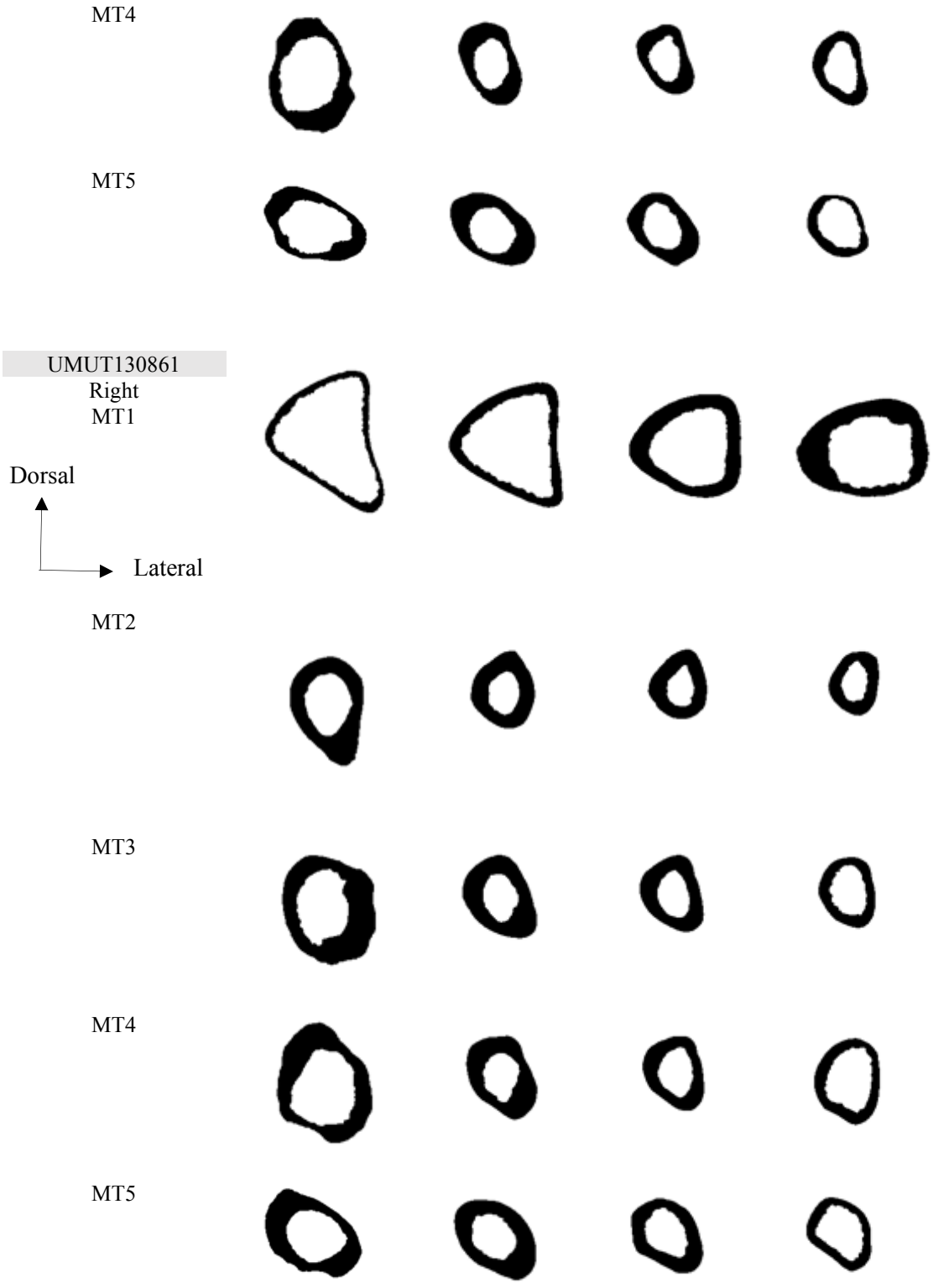
UMUT130857-2
Right
MT1

Dorsal

Lateral




MT2
MT3
MT4
MT5
UMUT130860
Right
MT1
Dorsal
Lateral
MT2
MT3


MT4
MT5
UMUT130861
Right
MT1
Dorsal
Lateral
MT2
MT3
MT4
MT5

UMUT130867

Right

MT1

Dorsal

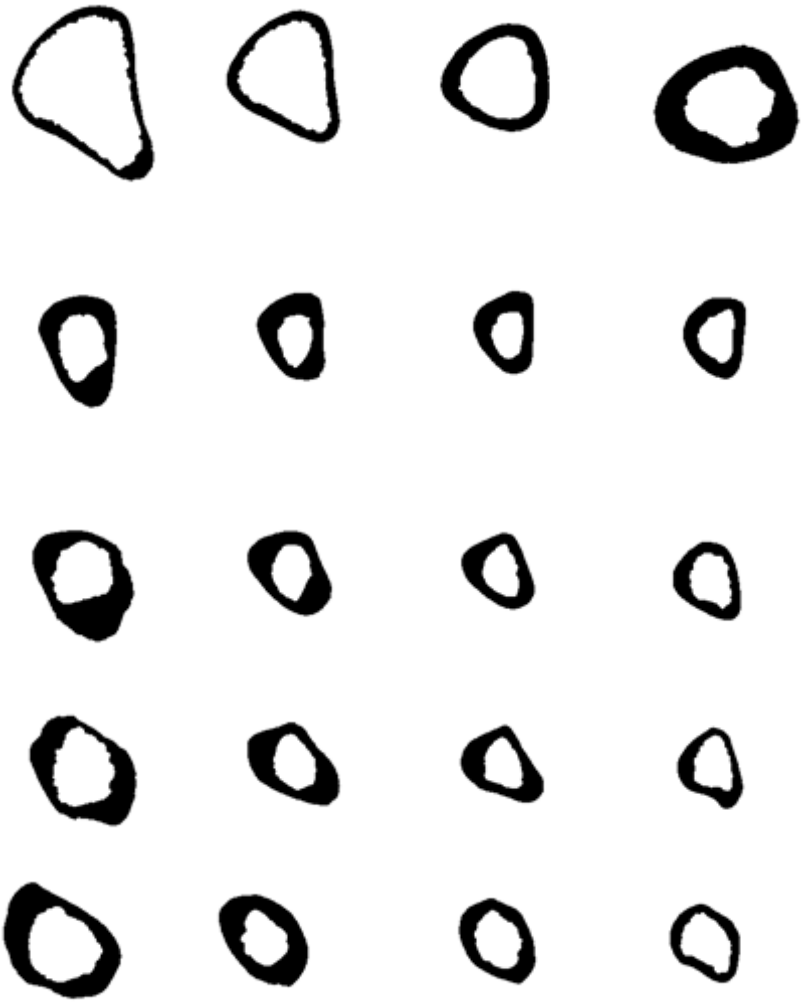
Lateral

MT2

MT3

MT4

MT5



UMUT130868

Right

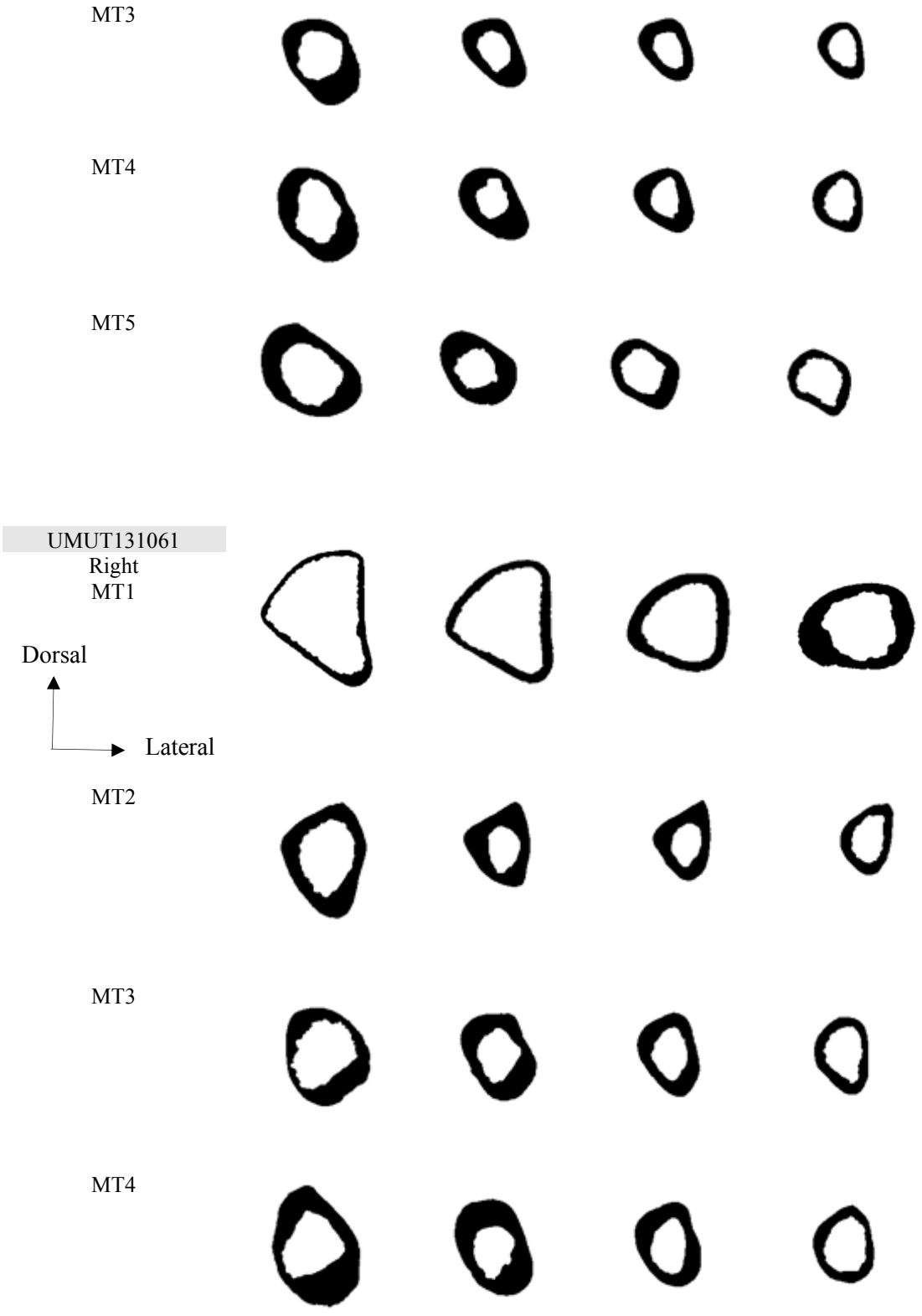
MT1

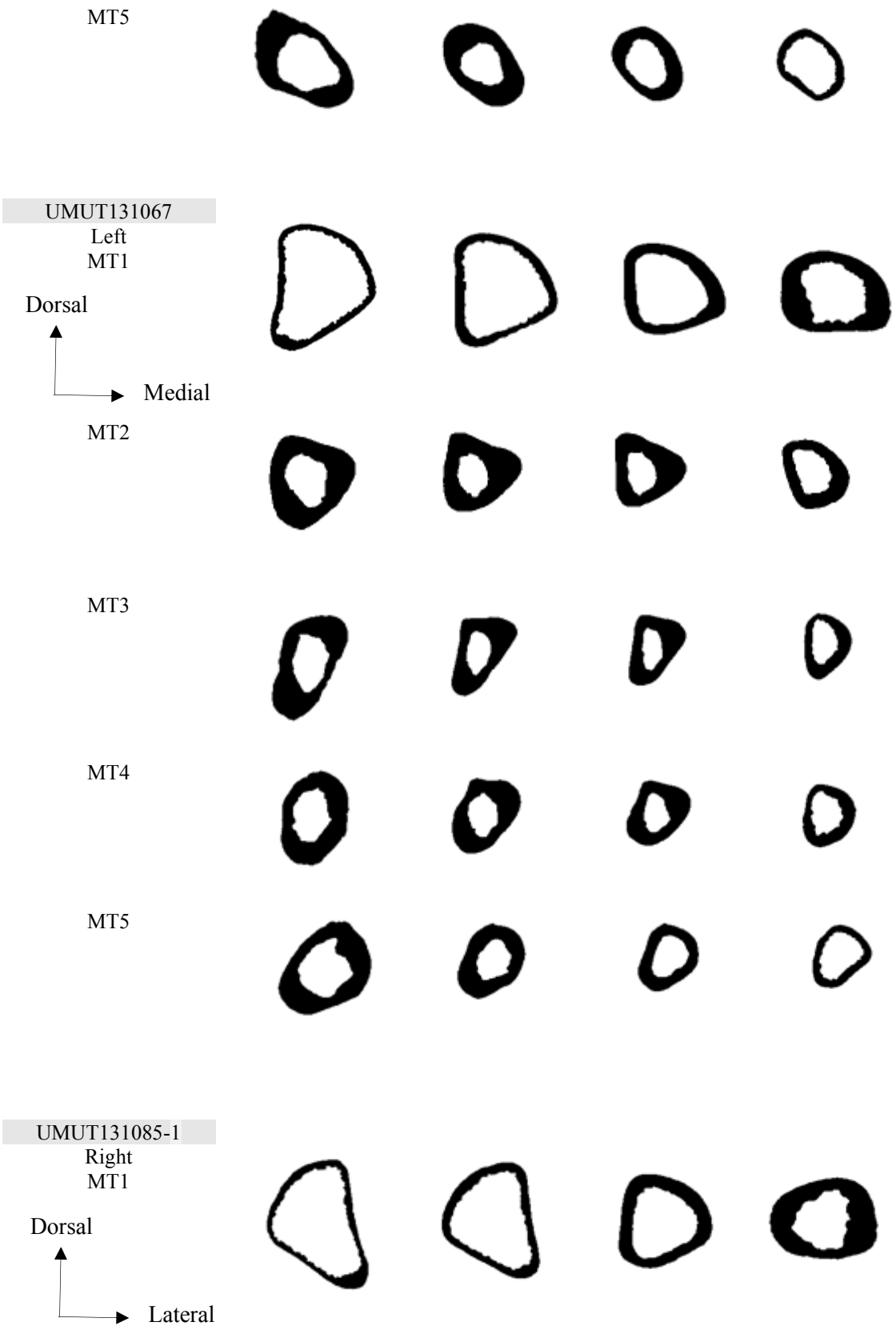
Dorsal

Lateral

MT2




MT3
MT4
MT5
UMUT131061
Right
MT1
Dorsal
Lateral
MT2
MT3
MT4

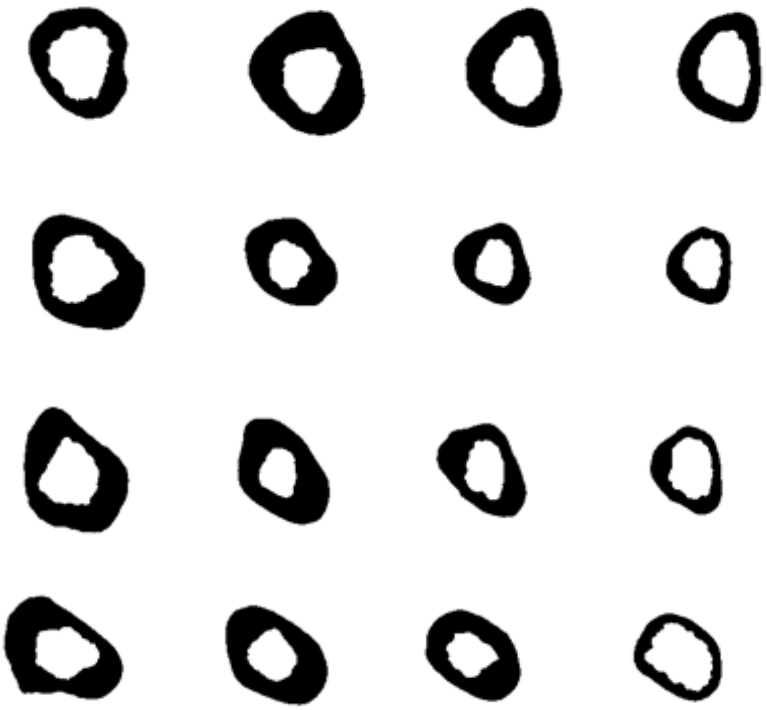

MT5
UMUT131067
Left
MT1
Dorsal
Medial
MT2
MT3
MT4
MT5
UMUT131085-1
Right
MT1
Dorsal
Lateral

MT2

MT3

MT4

MT5



UMUT131086-1

Left

MT1

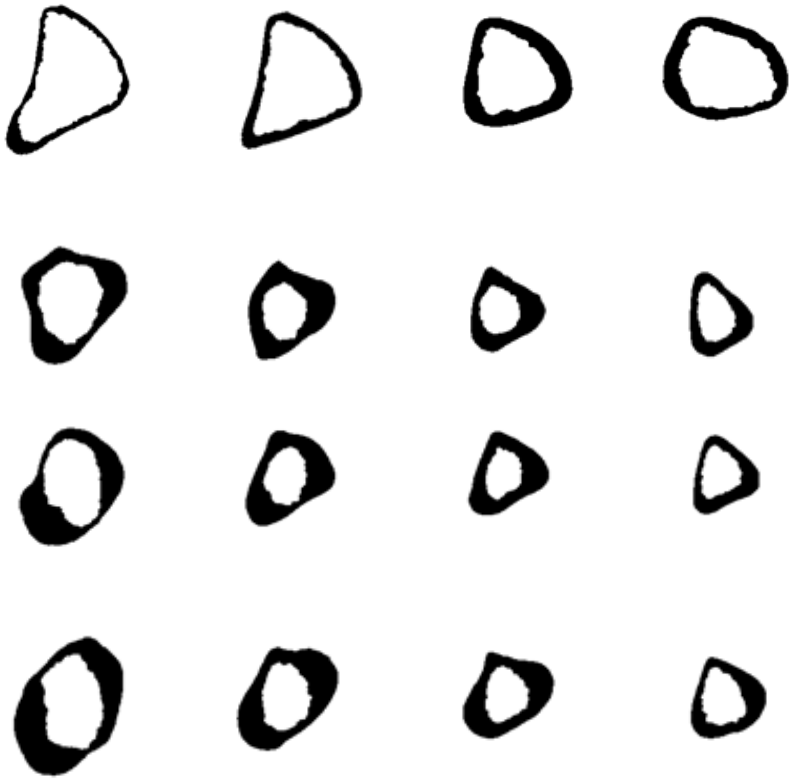
Dorsal

Medial

MT2

MT3

MT4



MT5



UMUT131086-2
Left
MT1

Dorsal

Medial



MT2



MT3



MT4



MT5



UMUT130195
Left
MT1

Dorsal

Medial



MT2



MT3



MT4



MT5



UMUT130242
Right
MT1

Dorsal

Lateral



MT2



MT3

MT4

MT5

UMUT130849
Right
MT1

Dorsal

Lateral



MT2

MT3

MT4

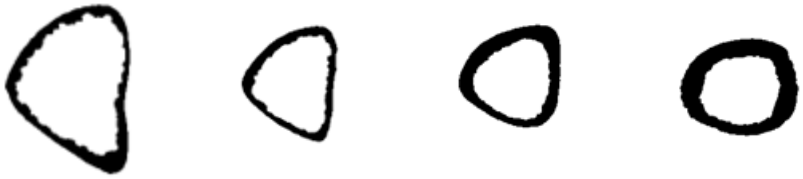
MT5



UMUT131096
Right
MT1

Dorsal

Lateral



MT2



MT3



MT4



MT5



UMUT131098
Right
MT1

Dorsal

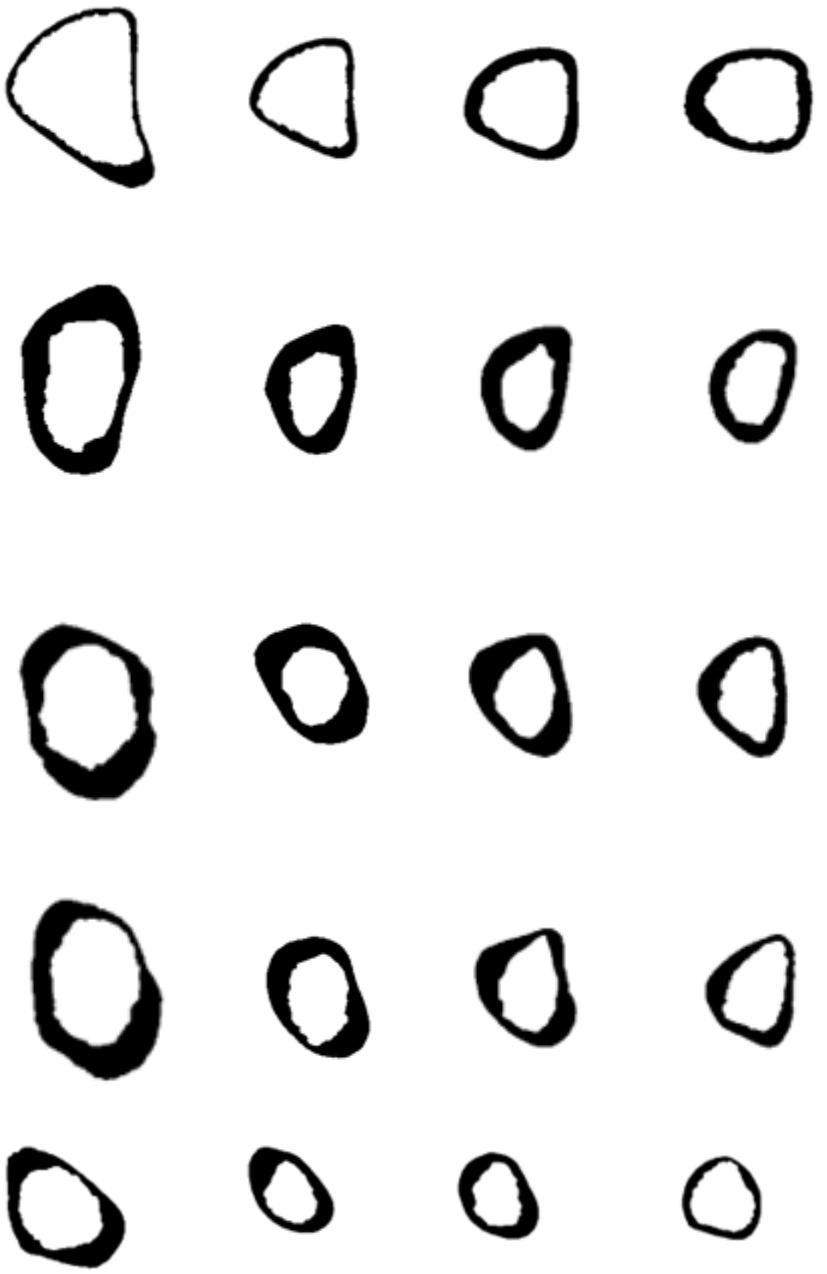
Lateral

MT2

MT3

MT4

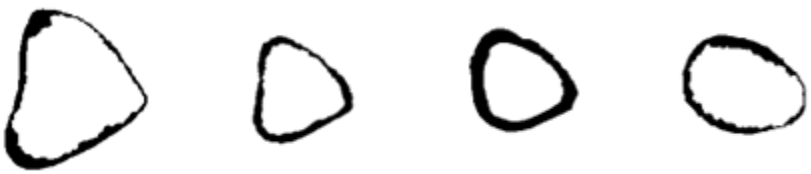
MT5



UMUT131376
Left
MT1

Dorsal

Medial



MT2



MT3



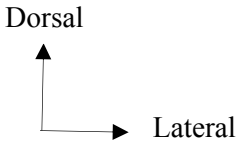
MT4



MT5



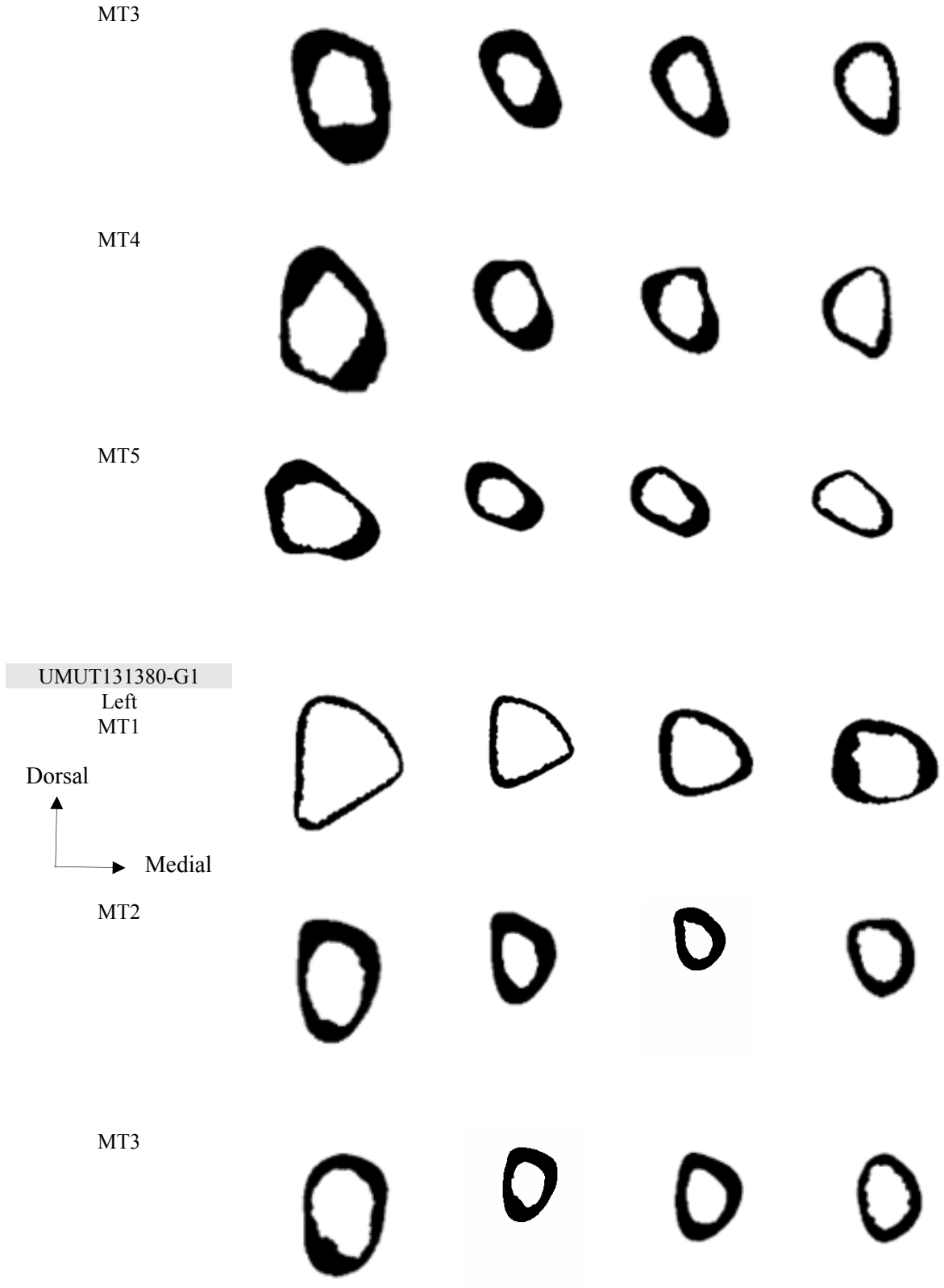
UMUT131377
Right
MT1





MT2




MT3
MT4
MT5
UMUT131380-G1
Left
MT1
Dorsal
Medial
MT2
MT3

MT4



MT5

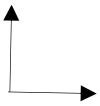


\

UMUT131380-G2
Left
MT1



Dorsal

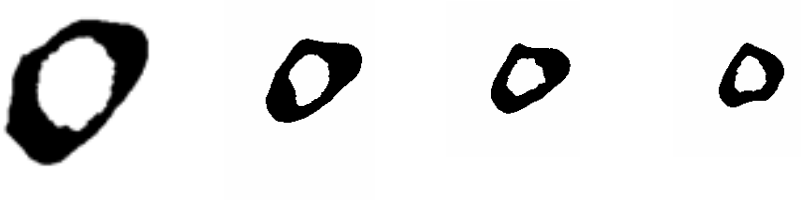


Medial

MT2



MT3



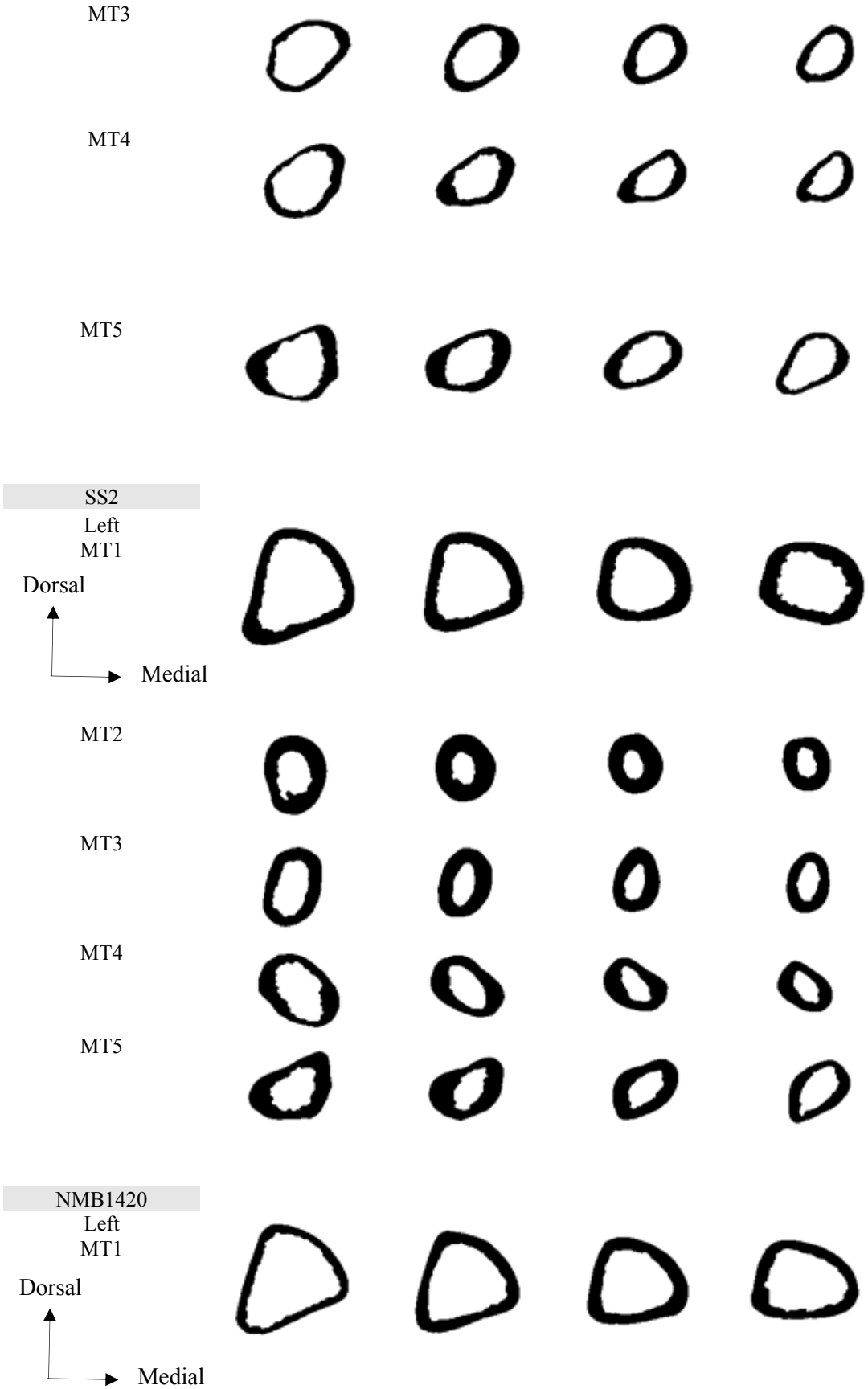
MT4

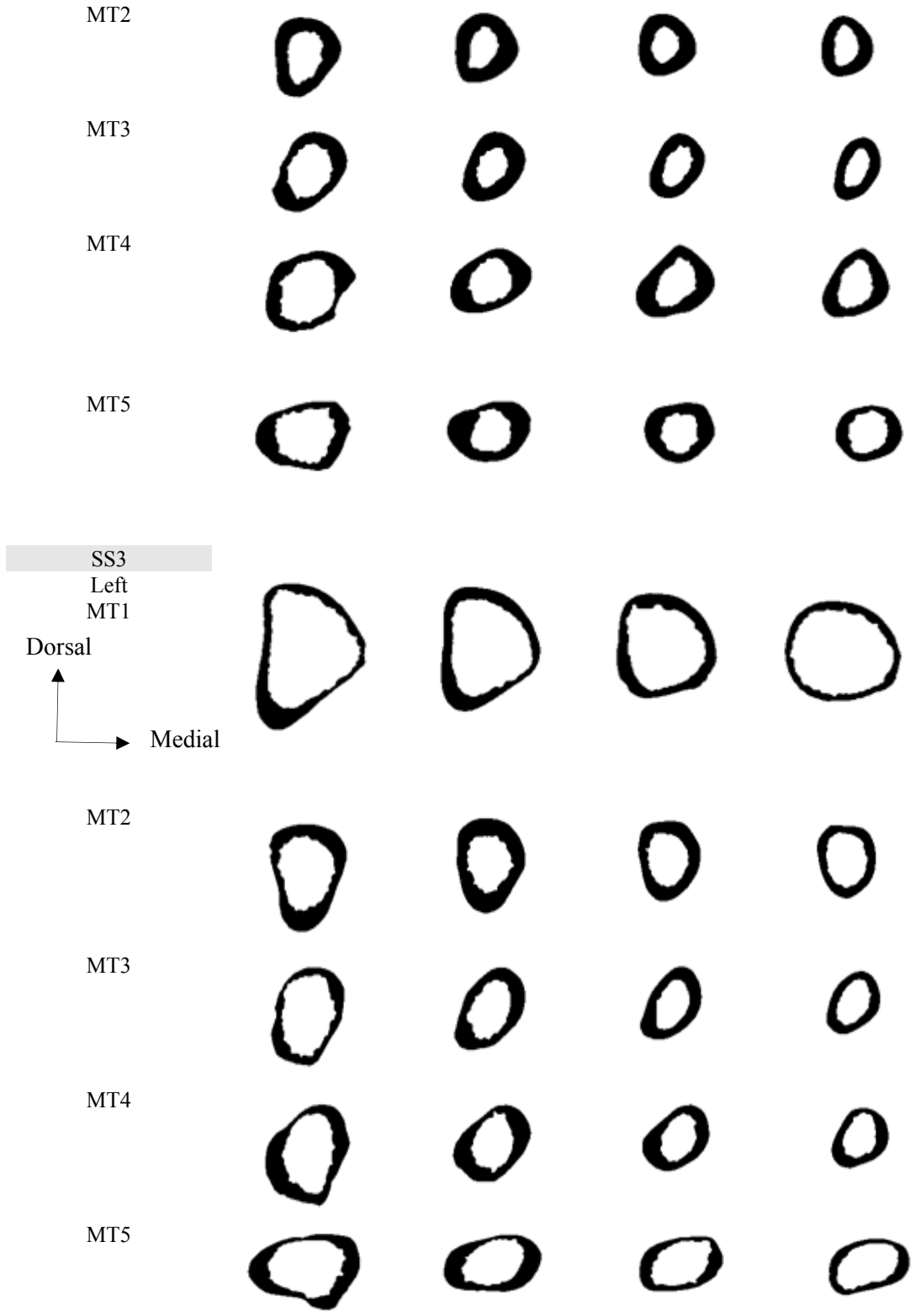


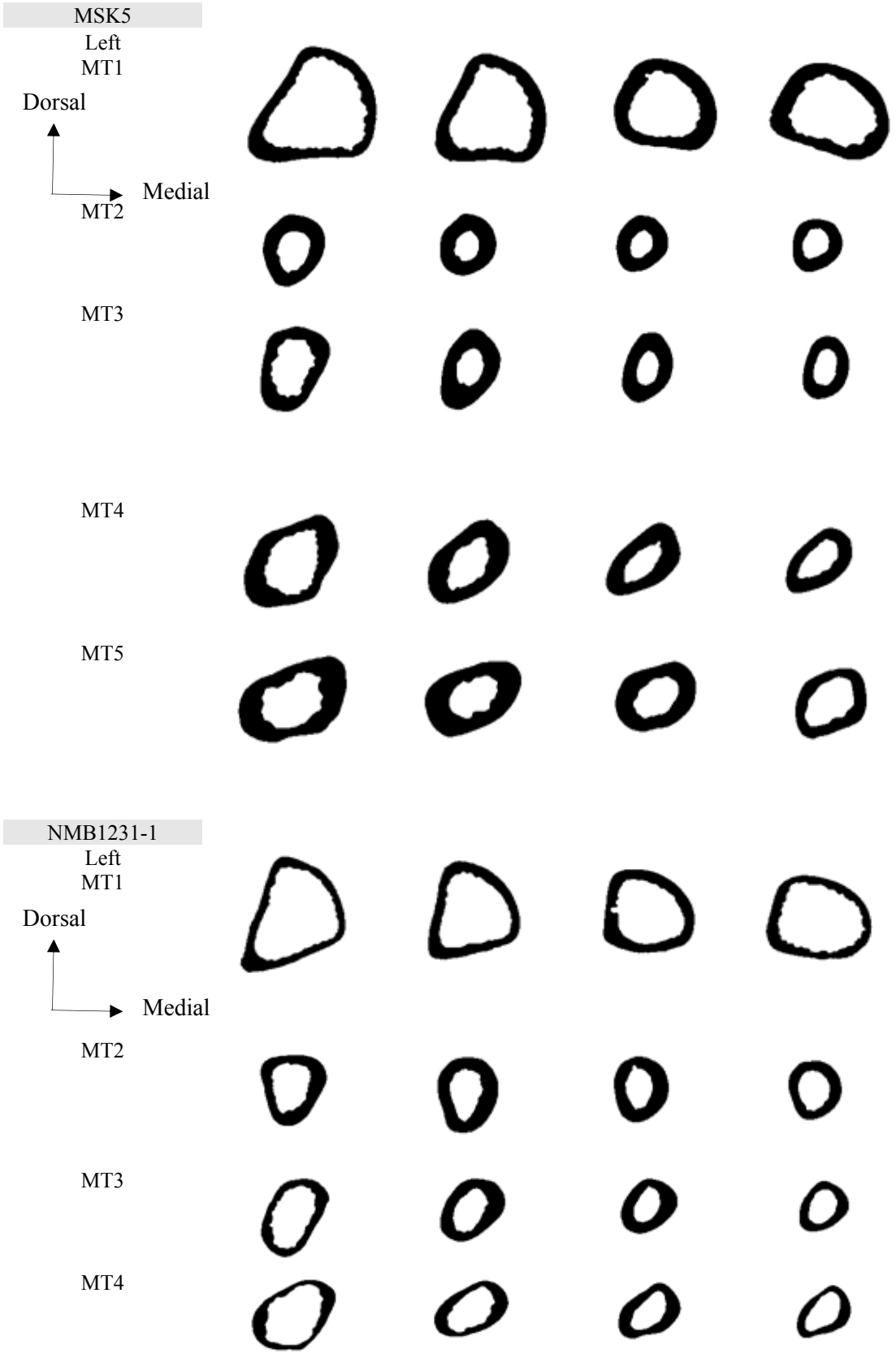
MT5

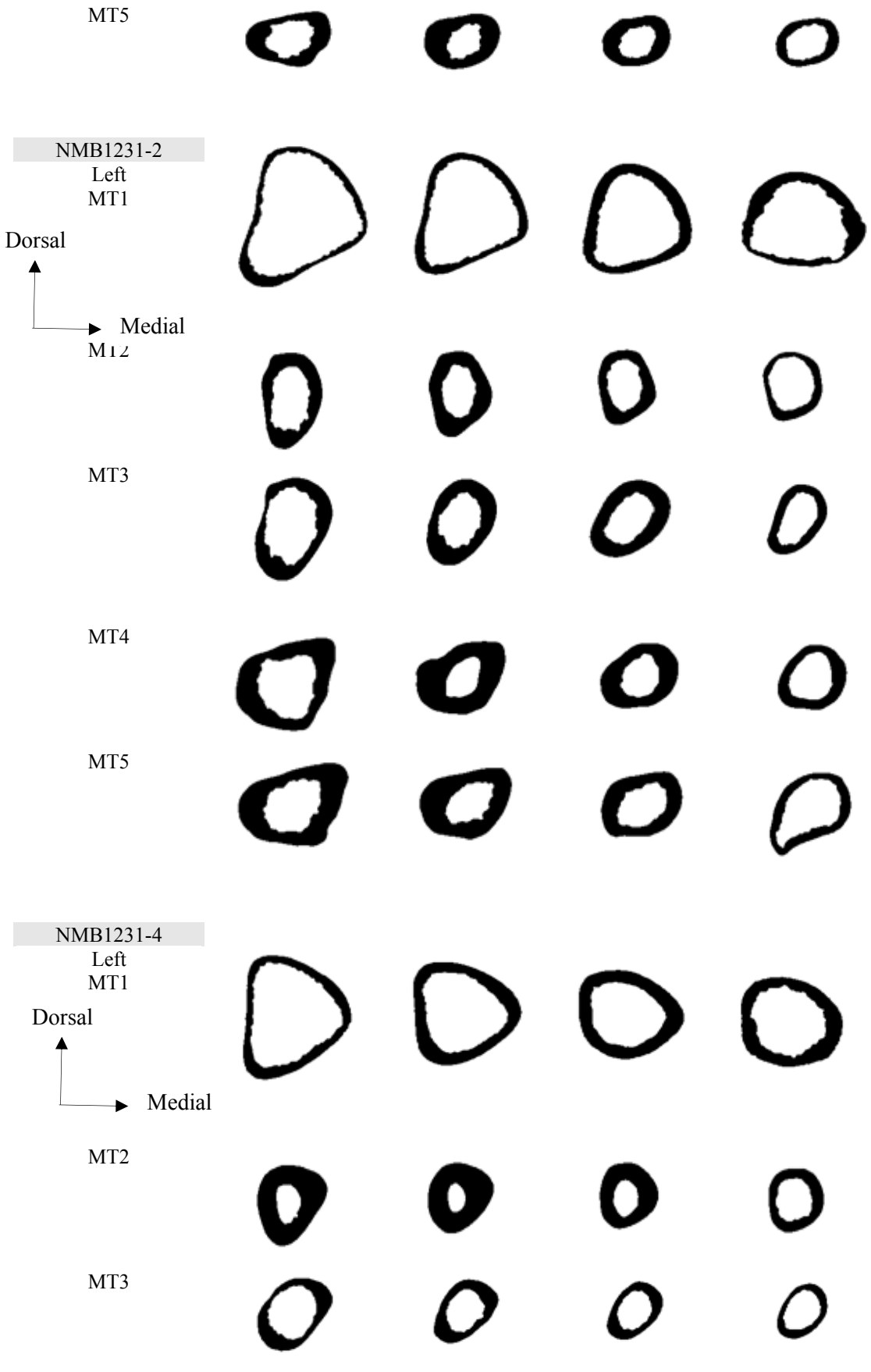


LSA Foragers from South Africa	25%	35%	50%	65%
MRN4Wilton Left MT1 Dorsal Medial M1				
MT3				
MT4				
MT5				
MSK2 Left MT1 Dorsal Medial				
MT2				


MT3
MT4
MT5
SS2
Left
MT1
Dorsal
Medial
MT2
MT3
MT4
MT5
NMB1420
Left
MT1
Dorsal
Medial

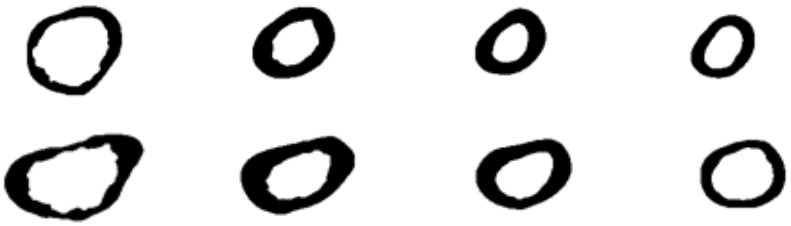

MT2
MT3
MT4
MT5
SS3
Left
MT1
Dorsal
Medial
MT2
MT3
MT4
MT5


MSK5
Left
MT1
Dorsal
Medial
MT2
MT3
MT4
MT5
NMB1231-1
Left
MT1
Dorsal
Medial
MT2
MT3
MT4


MT5
NMB1231-2
Left
MT1
Dorsal
Medial
MT2
MT3
MT4
MT5
NMB1231-4
Left
MT1
Dorsal
Medial
MT2
MT3

MT4

MT5



NMB1231-5
Left
MT1

Dorsal

Medial



MT2



MT3



MT4



MT5

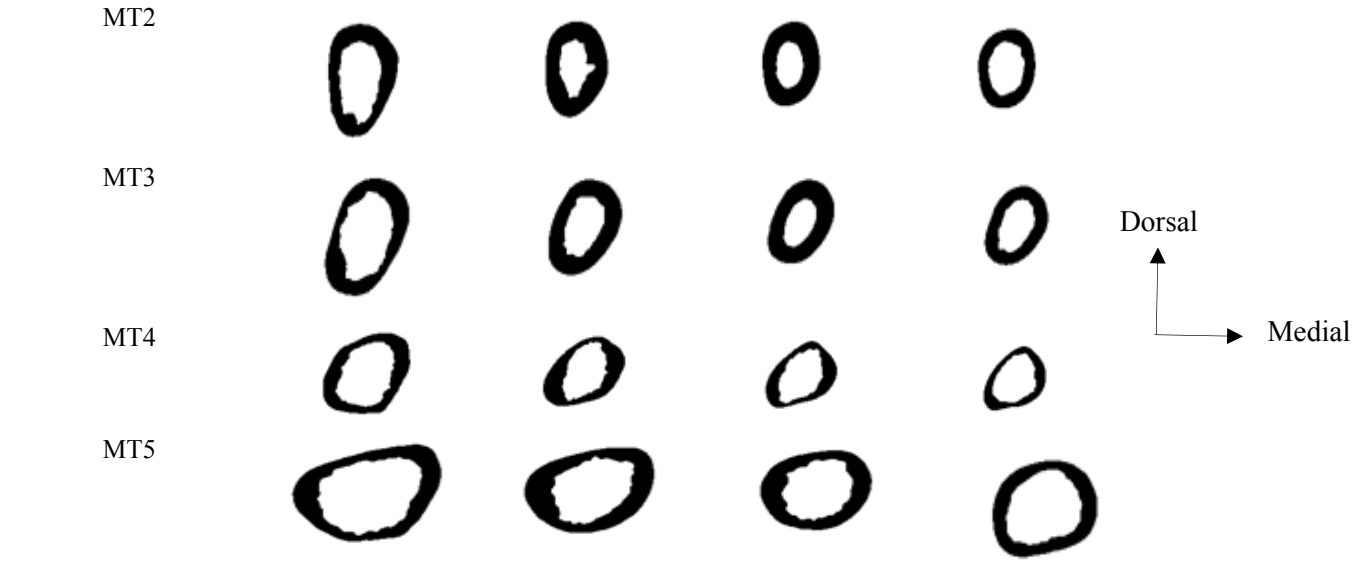


NMB1231-9
Left
MT1

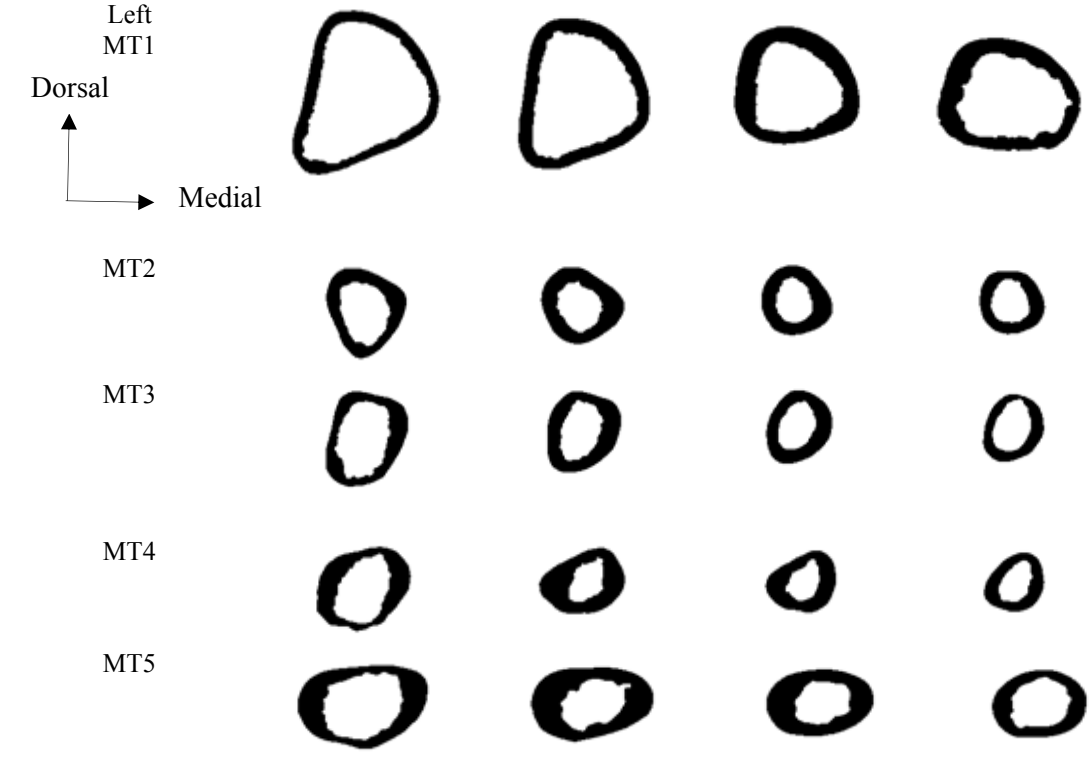
Dorsal

Medial



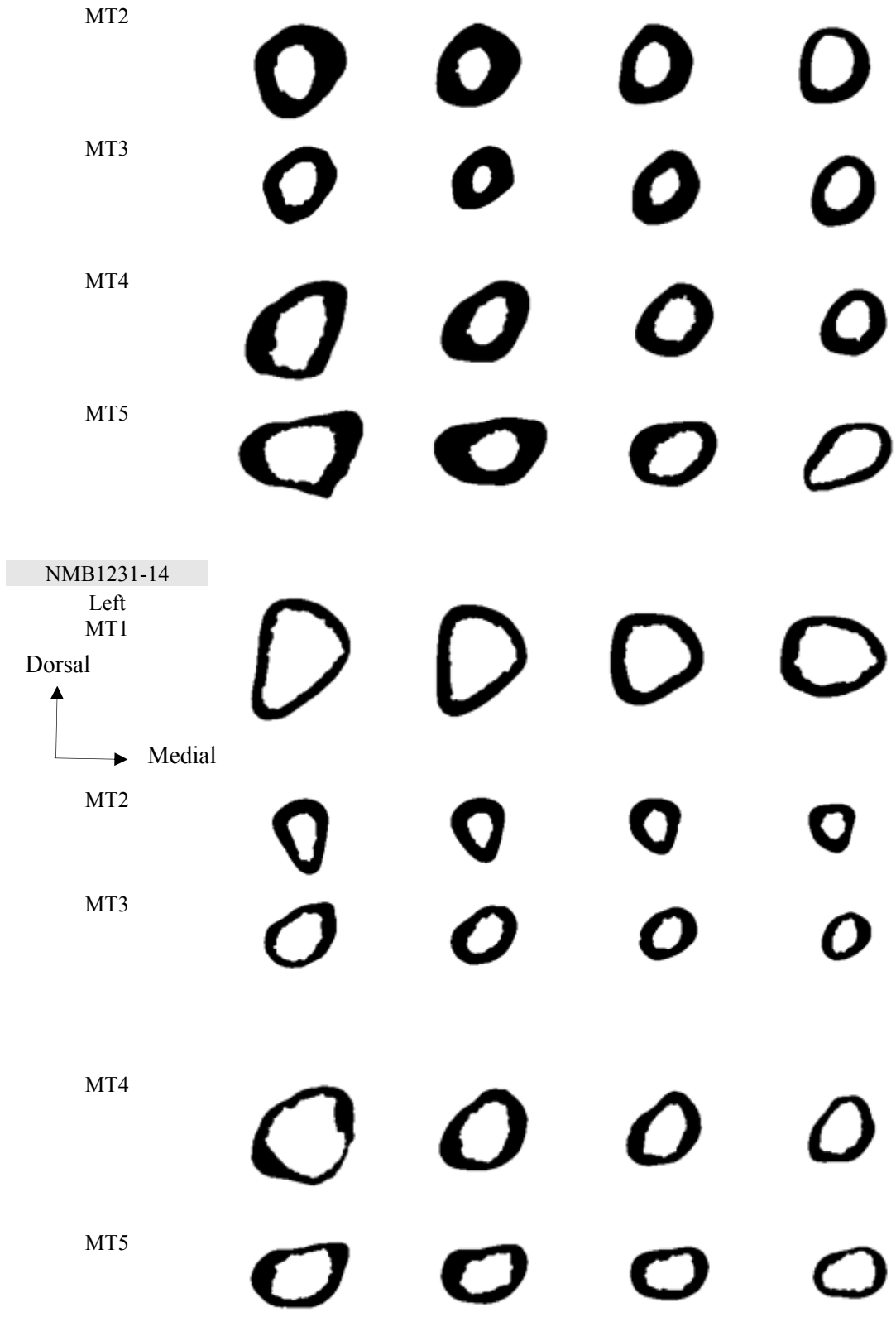


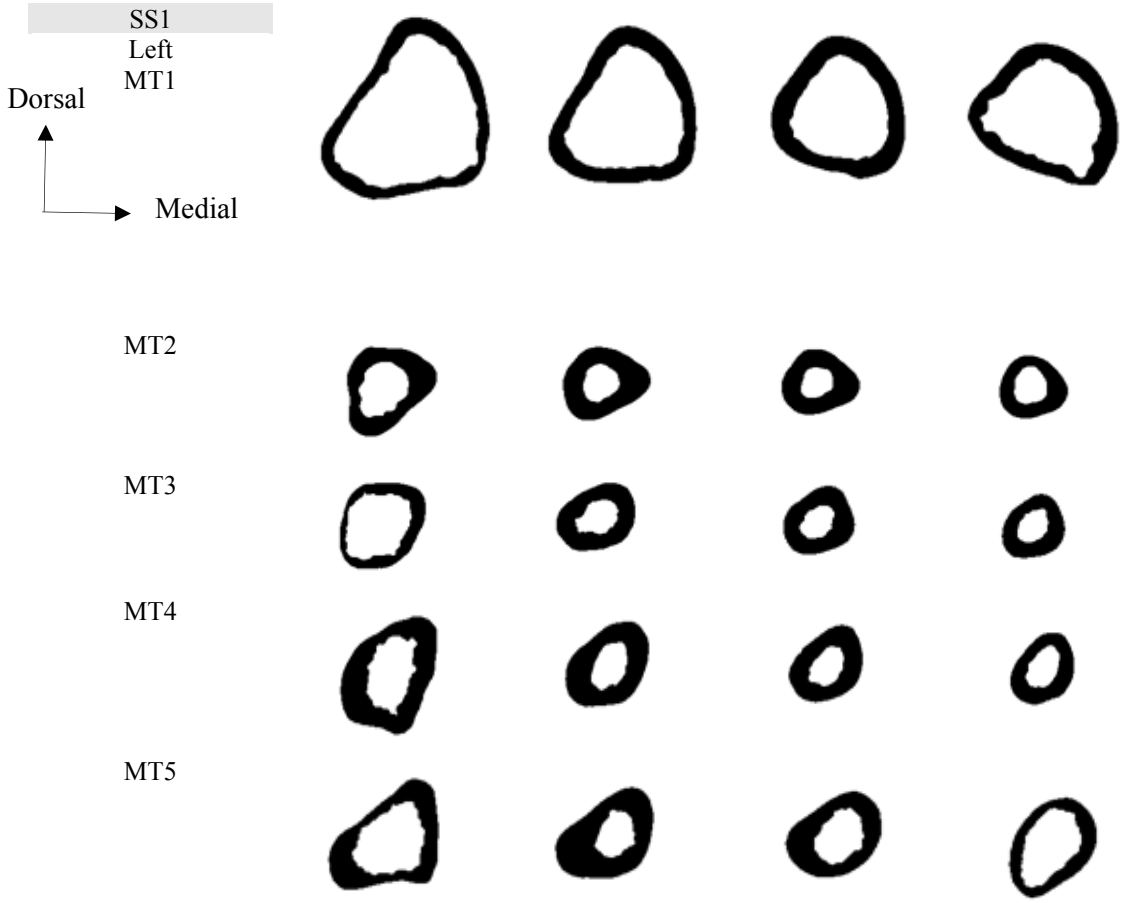
NMB1231-11
Left
MT1



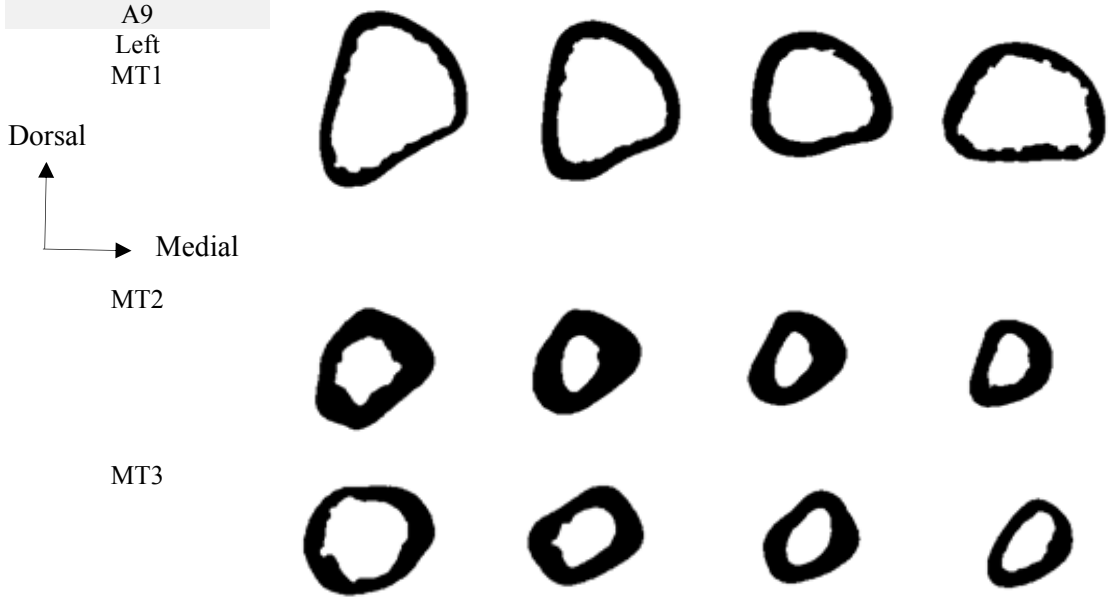
NMB1231-12
Left
MT1




MT2
MT3
MT4
MT5
NMB1231-14
Left
MT1
Dorsal
Medial
MT2
MT3
MT4
MT5



Post- Industrial individuals from South Africa	25%	35%	50%	65%



MT4

MT5

A458
Left
MT1

Dorsal

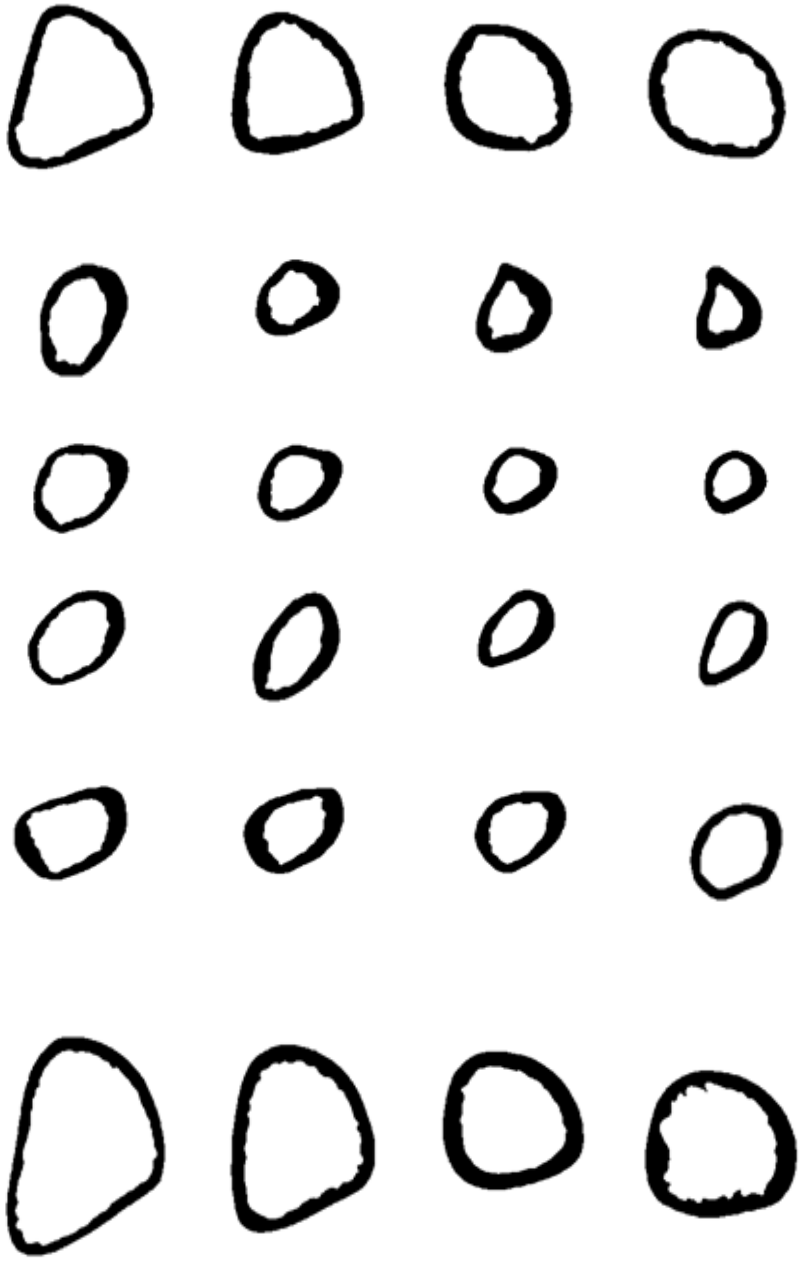
Medial

MT2

MT3

MT4

MT5



A209
Left
MT1

Dorsal

Medial

MT2

MT3

MT4

MT5

A218
Left
MT1

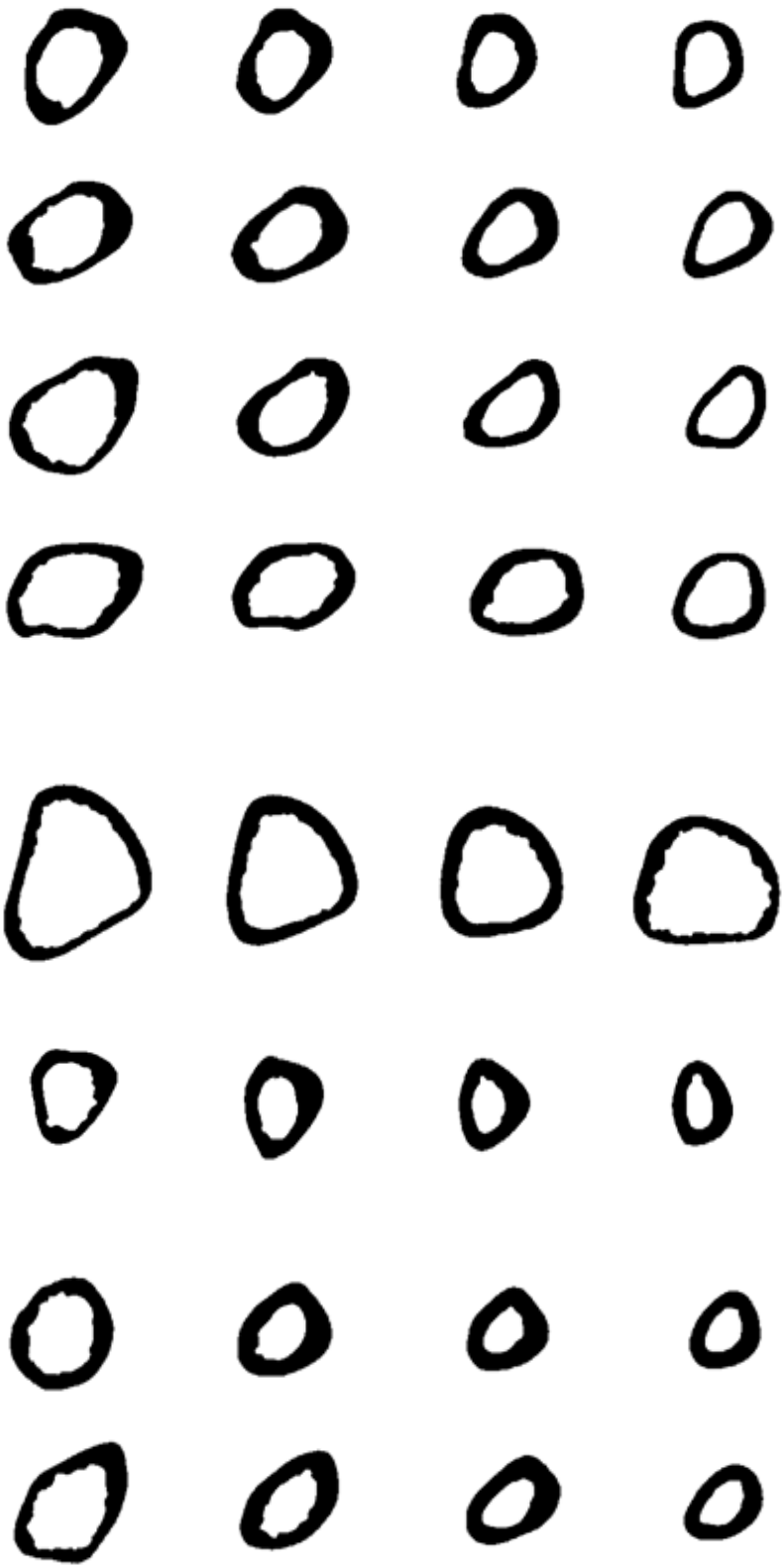
Dorsal

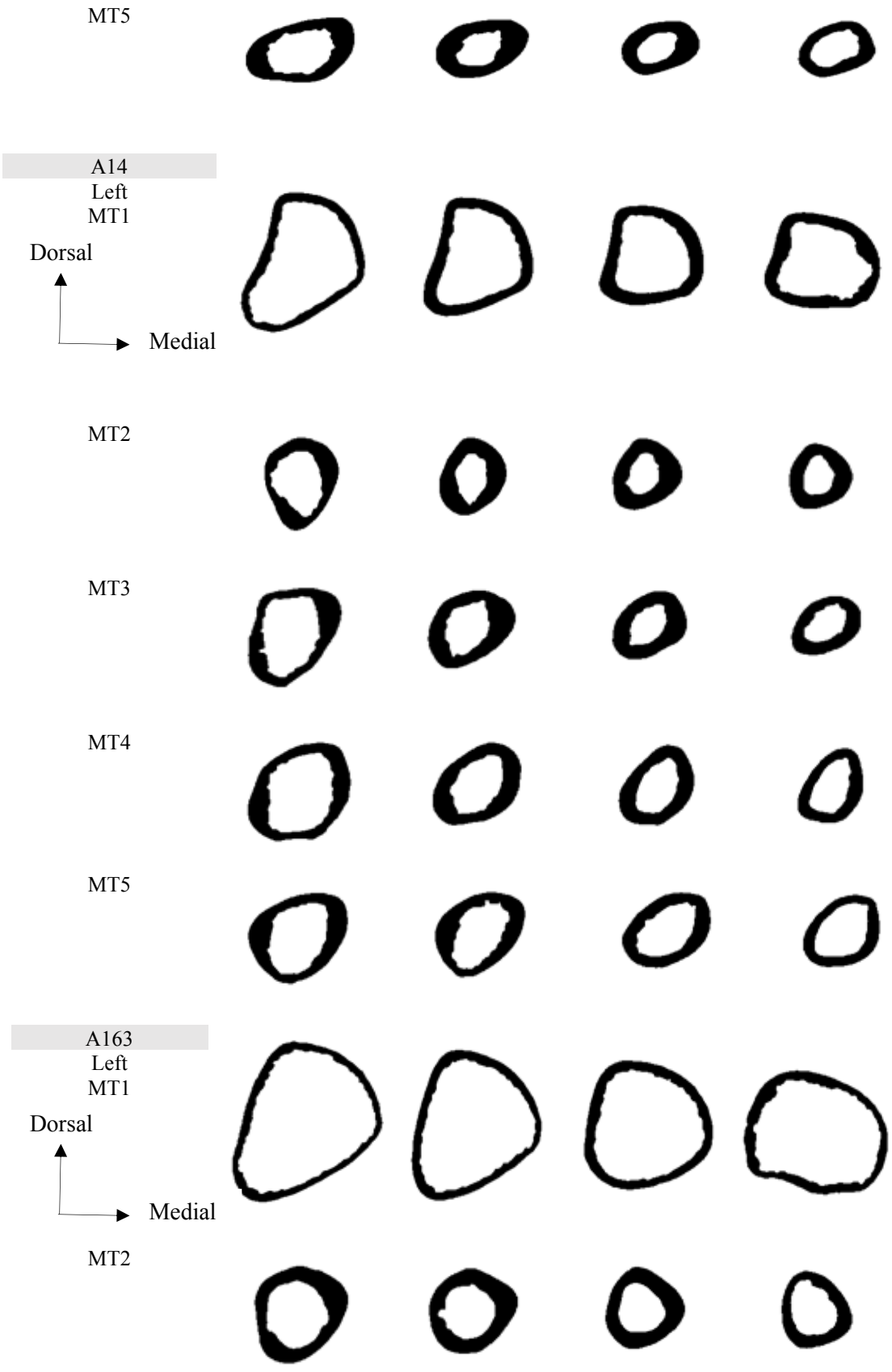
Medial

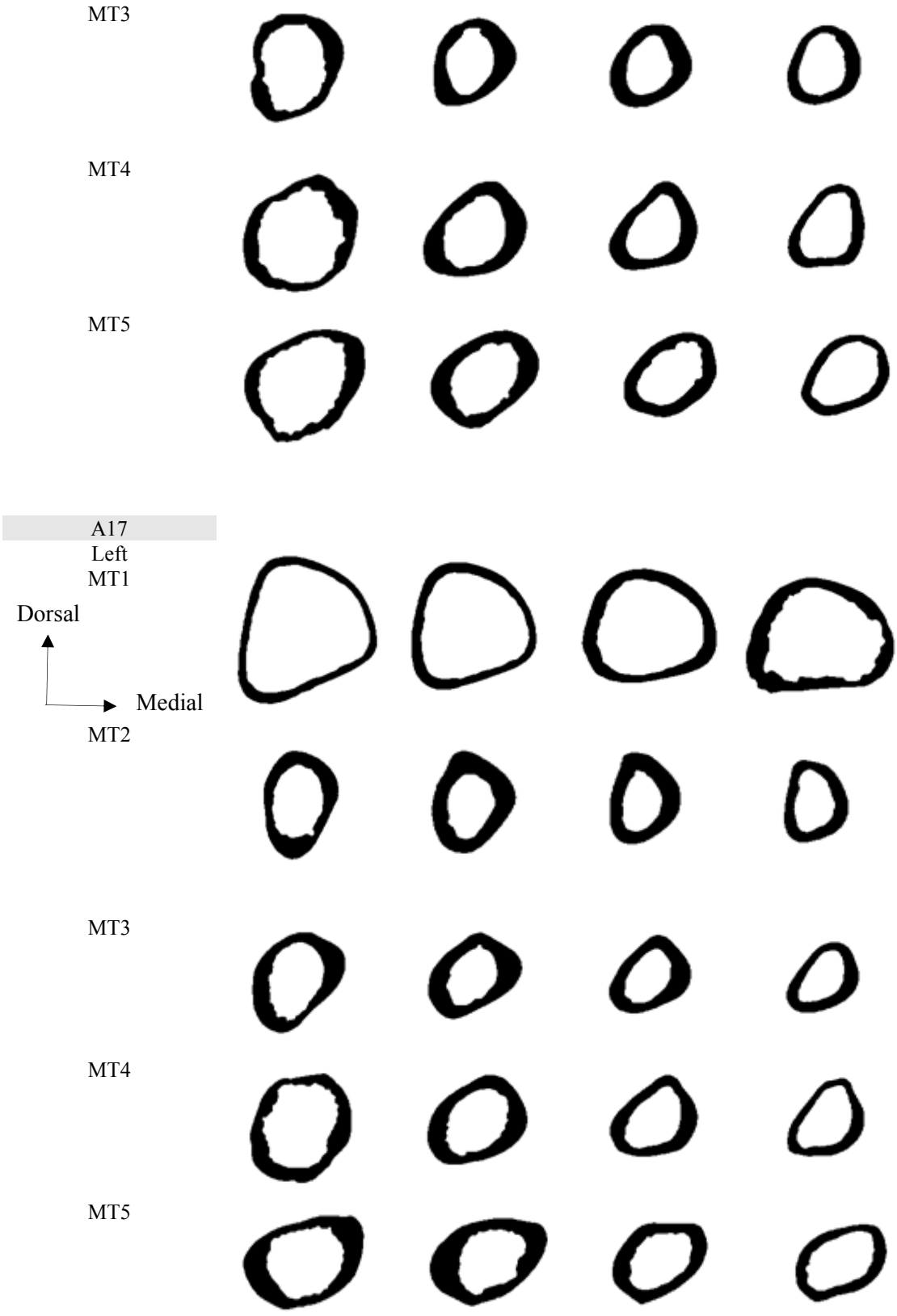
MT2

MT3

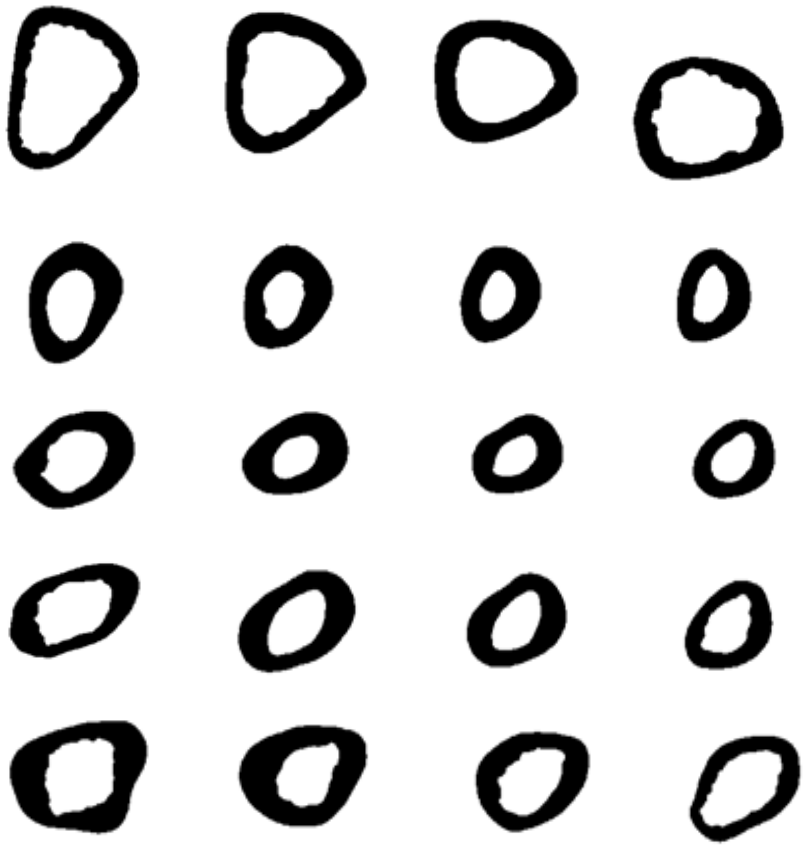
MT4



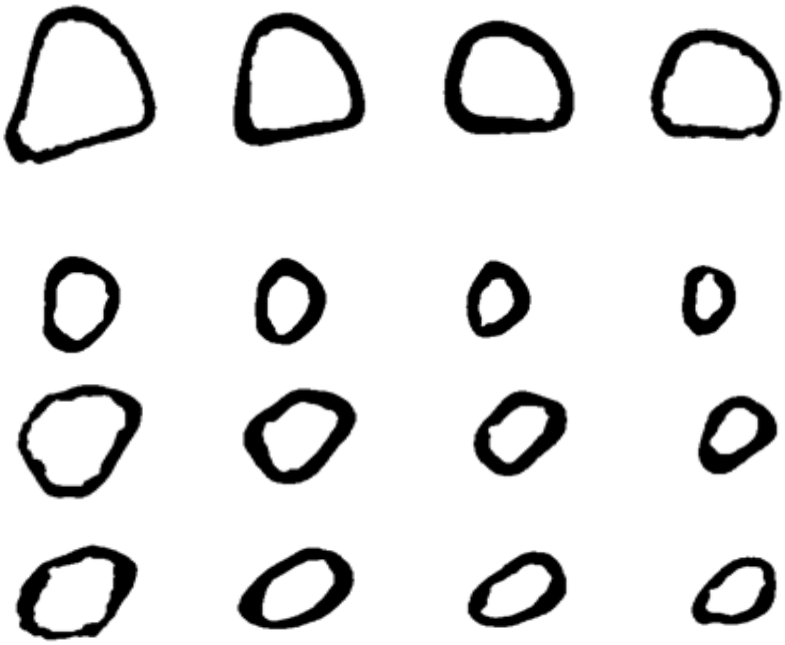

MT5
A14
Left
MT1
Dorsal
Medial
MT2
MT3
MT4
MT5
A163
Left
MT1
Dorsal
Medial
MT2


MT3
MT4
MT5
A17
Left
MT1
Dorsal
Medial
MT2
MT3
MT4
MT5

A883
Left
MT1
Dorsal
Medial
MT2
MT3
MT4
MT5



A1285
Left
MT1
Dorsal
Medial
MT2
MT3
MT4



MT5



A3060
Left
MT1

Dorsal

Medial



MT2



MT3



MT4



MT5



A170
Left
MT1

Dorsal

Medial



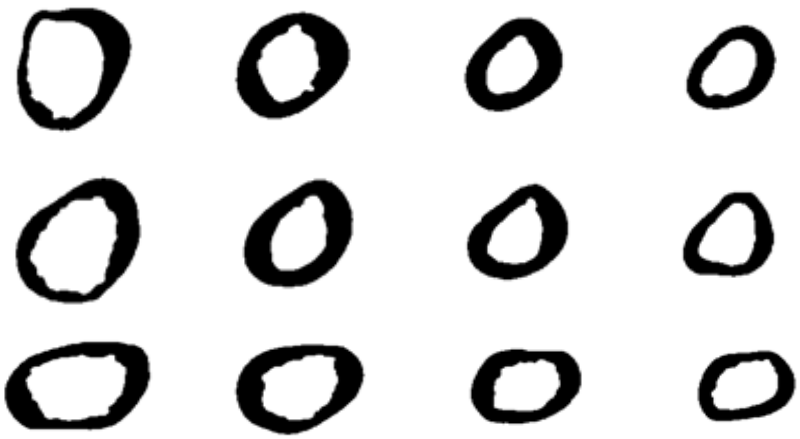
MT2



MT3

MT4

MT5



A22
Left
MT1

Dorsal

Medial

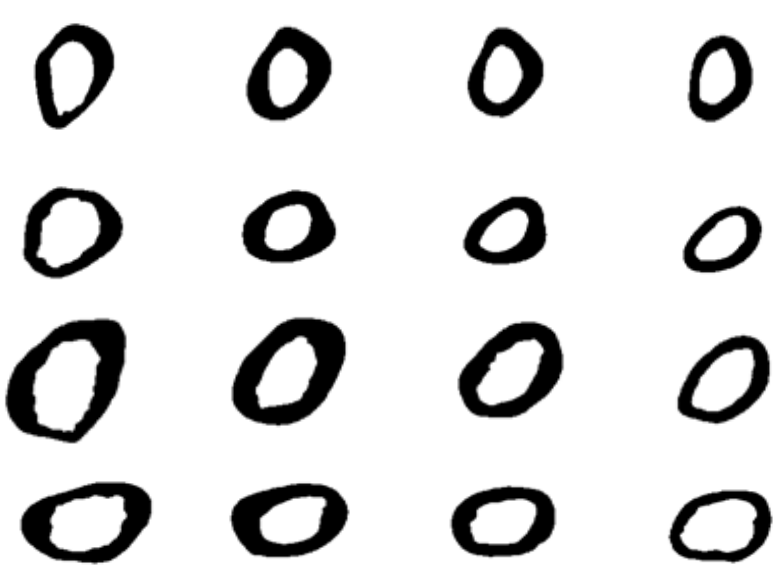


MT2

MT3

MT4

MT5

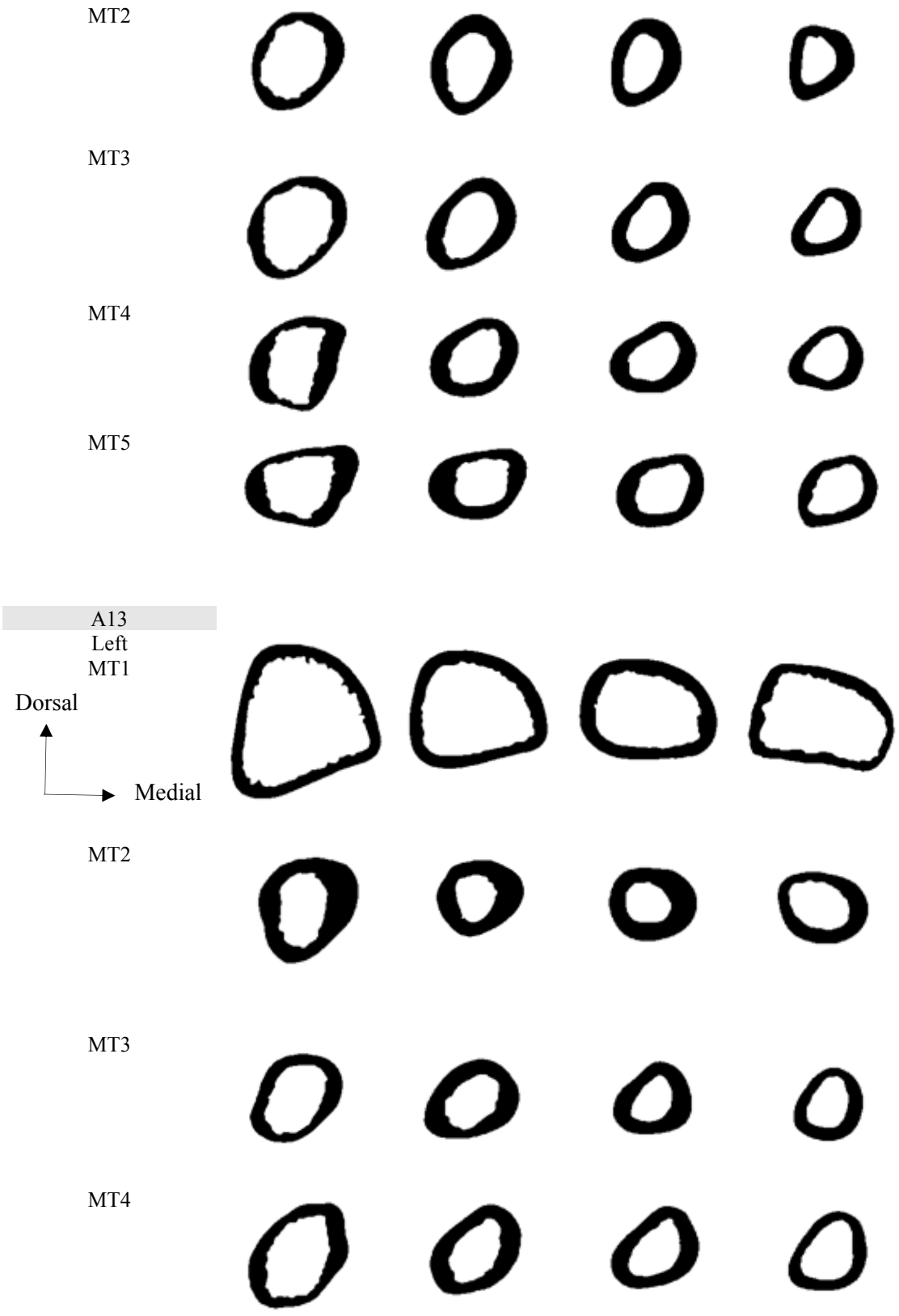


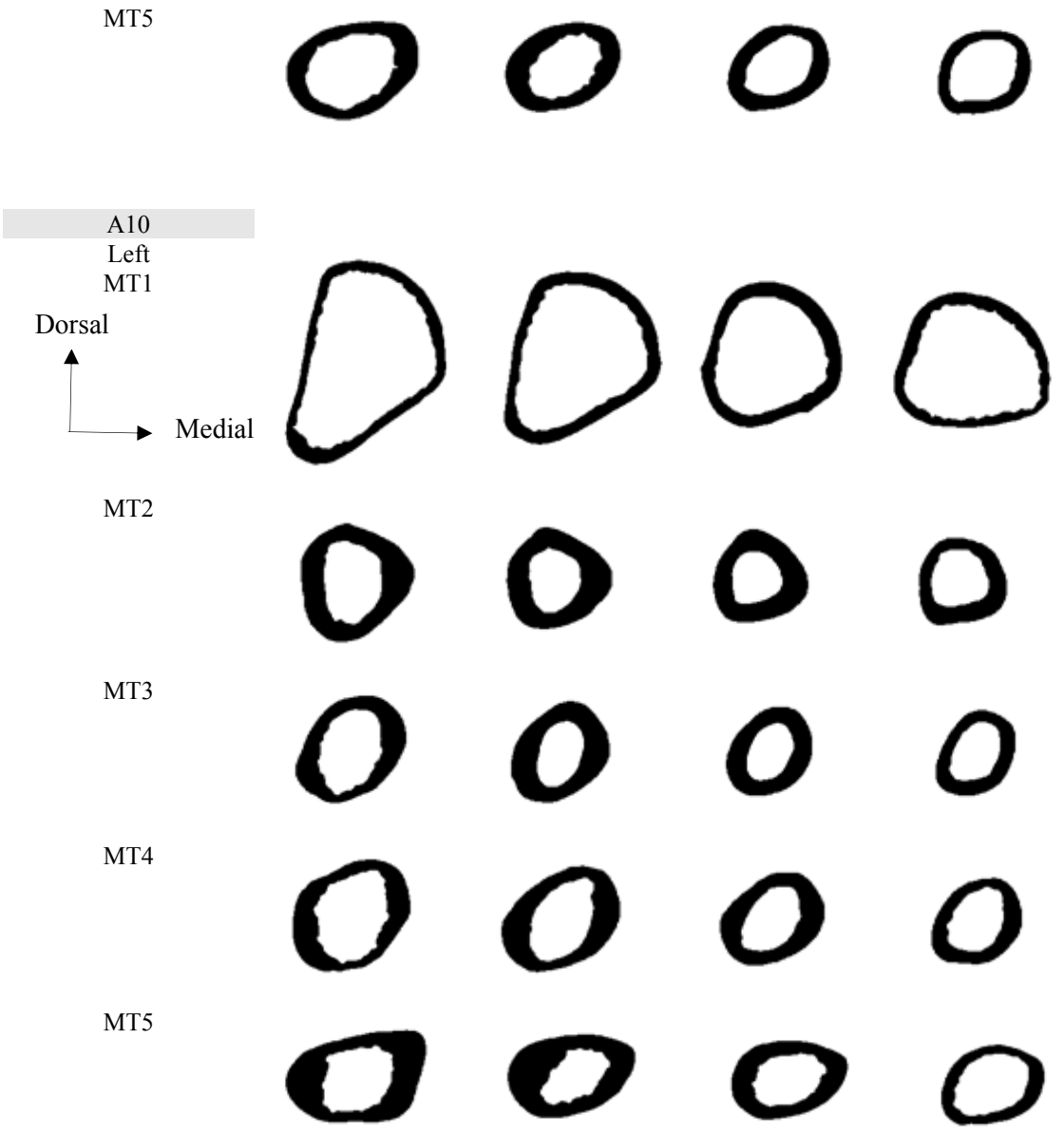
A8
Left
MT1

Dorsal

Medial




MT2
MT3
MT4
MT5
A13
Left
MT1
Dorsal
Medial
MT2
MT3
MT4



MT, Metatarsal.